# USE OF ENGINEERED CEMENTITIOUS COMPOSITE PANELS
# FOR SEISMIC STRENGTHENING

A THESIS SUBMITTED TO
THE GRADUATE SCHOOL OF NATURAL AND APPLIED SCIENCES
OF
MIDDLE EAST TECHNICAL UNIVERSITY

BY
MEHMET ENGİN AYATAR

IN PARTIAL FULFILLMENT OF THE REQUIREMENTS
FOR
THE DEGREE OF DOCTOR OF PHILOSOPHY
IN
CIVIL ENGINEERING

JUNE 2018

Approval of thesis:

**USE OF ENGINEERED CEMENTITIOUS COMPOSITE PANELS FOR SEISMIC STRENGTHENING**

submitted by MEHMET ENGİN AYATAR in partial fulfillment of the requirements for the degree of **Doctor of Philosophy in Civil Engineering Department, Middle East Technical University** by,

Prof. Dr. Halil Kalıpçılar ____________________
Dean, Graduate School of **Natural and Applied Sciences**

Prof. Dr. İsmail Özgür Yaman ____________________
Head of Department, **Civil Engineering**

Prof. Dr. Erdem Canbay ____________________
Supervisor, **Civil Engineering Dept., METU**

**Examining Committee Members:**

Prof. Dr. Barış Binici ____________________
Civil Engineering Dept., METU

Prof. Dr. Erdem Canbay ____________________
Civil Engineering Dept., METU

Assoc. Prof. Dr. Burcu Burak Bakır ____________________
Civil Engineering Dept., METU

Assoc. Prof. Dr. Sabahattin Aykaç ____________________
Civil Engineering Dept., Gazi University

Asst. Prof. Dr. Halit Cenan Mertol ____________________
Civil Engineering Dept., Atılım University

Date: …/06/2018

**I hereby declare that all information in this document has been obtained and presented in accordance with academic rules and ethical conduct. I also declare that, as required by these rules and conduct, I have fully cited and referenced all material and results that are not original to this work.**

Name, Surname: MEHMET ENGİN AYATAR

Signature :

# ABSTRACT

## USE OF ENGINEERED CEMENTITIOUS COMPOSITE PANELS FOR SEISMIC STRENGTHENING



Mehmet Ayatar, Engin
PhD., Department of Civil Engineering
Supervisor: Prof. Dr. Erdem Canbay



June 2018, 138 Pages



Due to the massive number of deficient buildings in seismically active zones, the demolition and rebuilding of such structures is not a viable option. Instead, rehabilitation of seismically deficient buildings is commonly employed. Although, the most preferred rehabilitation approach has been the application of RC infills to the frames, this technique inevitably causes the evacuation of the structure. Therefore, there have been many studies on new occupant-friendly strengthening techniques. The aim of this study is to contribute to such retrofit alternatives, and to strengthen the masonry infill walls by means of Engineered Cementitious Composite (ECC) panels. ECC is a mortar based composite reinforced with fibers. The main components of ECC are Portland cement, fly ash, water, silica sand, PolyVinyl Alcohol (PVA) fiber, and superplasticizer. In this study, a strengthening technique with implementing engineered cementitious composite (ECC) panels bonded to hollow brick infill walls was investigated experimentally and analytically. Three test frames noncompliant according to the Turkish Seismic Resistant Design Code (2007), were constructed and tested during the course of the study. The test specimens were composed of three story, three bay, and ½ scaled frames. The first specimen was a bare frame, whereas the other two frames had hollow brick walls at the central bay. The third frame was strengthened with ECC panels on the infill walls. Specimens were tested by using a Pseudo Dynamic (PsD) loading scheme. Synthetic ground motions compatible with the Düzce city center response spectrum were used for the three PsD tests. The performance of the proposed strengthening technique was evaluated based on the comparison of experimental results and nonlinear time history analyses of frames.



Keywords: Pseudo-Dynamic Testing, Engineered Cementitious Composites (ECC), Structural Performance Evaluation.

# ÖZ

## TASARLANMIŞ ÇİMENTO BAĞLAYICILI KOMPOZİT PANELLERİN SİSMİK GÜÇLENDİRME İÇİN KULLANIMI

Mehmet Ayatar, Engin
Doktora, İnşaat Mühendisliği Bölümü
Tez yöneticisi: Prof. Dr. Erdem CANBAY

Haziran 2018, 138 Sayfa

Deprem bölgelerindeki sismik açıdan yetersiz binaların yıkılıp yeniden inşa edilmesi yüksek sayıda olmalarından dolayı ekonomik bir çözüm olamamaktadır. Bunun yerine yetersiz binaların depreme karşı güçlendirilmeleri gerekli olabilmektedir. Betonarme duvarlar ile güçlendirme en çok tercih edilen yapı iyileştirme yöntemi olmasına rağmen, bu yöntem kaçınılmaz olarak yapının boşaltılmasını gerektirmektedir. Sonuç olarak, kullanıcı dostu yeni güçlendirme yöntemleri ile ilgili araştırmalar ortaya çıkmaktadır. Bu çalışmanın amacı, Tasarlanmış Çimento Bağlayıcılı Kompozit (TÇK) panel uygulamasıyla dolgu duvarların güçlendirilmesidir. TÇK, fiber ile güçlendirilmiş bağlayıcı özellikte harç bazlı bir malzemedir. TÇK malzemenin ana bileşenleri çimento, uçucu kül, su, silis kumu ile PVA fiber ve süper akışkanlaştırıcıdır. Bu çalışma kapsamında, boşluklu tuğla duvarlar üzerine tasarlanmış çimento bağlayıcılı kompozit panellerin yerleştirilmesiyle uygulanan güçlendirme yöntemi deneysel ve analitik olarak araştırılmıştır. Test numuneleri Türk Deprem Yönetmeliği ile uyumsuz tasarlanmış üç adet, üç katlı, üç açıklıklı ve ½ ölçekli betonarme çerçevelerdir. İlk deney numunesi boş çerçevedir. İkinci ve üçüncü numunelerde her katın orta açıklığında boşluklu dolgu duvar yer almaktadır. Bununla birlikte üçüncü numune TÇK panellerle güçlendirilmiştir. Bütün deney numuneler dinamik benzeri yükleme yöntemi kullanılarak test edilmiştir. Her numuneye Düzce Depremi ivme spektrumu kullanılarak oluşturulan sentetik yer hareketleri uygulanarak dinamik benzeri deneyler gerçekleştirilmiştir. Deney sonuçları ve dinamik analiz sonuçları karşılaştırılarak önerilen güçlendirme yöntemi değerlendirilmiştir.

Anahtar Kelimeler: Dinamik-Benzeri Deney, Tasarlanmış Çimento Bağlayıcılı Kompozit, Performans Değerlendirmesi.

***Eşime ve kızıma…***

# ACKNOWLEDGEMENT

This study was conducted under the supervision of Prof. Dr. Erdem CANBAY. I would like to acknowledge gratefully the expert guidance and support that he has provided me throughout my study. The guidance provided by Prof. Dr. Barış Binici and Prof. Dr. S. Tanvir Wasti is also equally appreciated.

I would like to express my sincere gratitude to my wife Eylem Ulutaş AYATAR, my parents and my sister for their patience, understanding, encouragement, and full support not only during my PhD study but also throughout my life.

I owe special thanks to the METU Structural Mechanics Laboratory staff; Murat Demirel, Hasan Metin, Osman Keskin and Barış Esen. I would also like to thank my esteemed friends Mehran Ghasabeh and Salim Azak

The financial support by the Scientific and Technological Research Council of Turkey (TÜBİTAK – 108G034) is acknowledged.

# TABLE OF CONTENTS

# LIST OF FIGURES

# LIST OF TABLES

# CHAPTER 1

# INTRODUCTION

## 1.1 General

Many existing buildings in Turkey do not fulfil the requirements of the seismic codes and standards. The main problem in structural RC construction is insufficient production quality such as, inadequate reinforcement detailing, use of plain bars, low concrete strength, and insufficient lap length. Secondly, design problems such as inadequate section sizes, lack of strong column-weak beam connections, torsional irregularities, floor discontinuities, and weak/soft stories should be considered. Consequently, such structural members like columns and beams show brittle behavior during earthquakes.

Infill walls increase the stiffness of reinforced concrete building frames at low displacement demands and thereby help to attain better deformation control (Ockleston 1955, Polyakov 1956, Smith 1962, Read 1965). However, they usually sustain significant damage at large lateral displacement demands due to frame-infill interaction (Fenerci et al. 2016). In addition, the structural contribution of the brick infills is usually ignored at the design stage, where only the weight of infill walls is considered. The significant influence of infill walls on the structural systems in terms of strength must be considered in the framing design.

The presence of unreinforced infill walls limits the lateral displacement of the reinforced concrete frames as a result of the strut action. For this reason, the shear forces at the column ends adjacent to the infill wall increase. At high displacement demands, in plane motion at infill walls cause cracks that penetrate to the structural elements, especially to the columns or beam column joints due to the formation of diagonal compression struts. Damaged buildings during earthquakes demonstrate that crack propagation from the infill walls to the columns may in fact cause life critical situations (Saatcioglu et al. 2001).

Rehabilitation of seismically deficient buildings comes into prominence since possible future earthquakes threaten to cause the loss of lives and endanger public safety. First, the seismic vulnerability of the existing building should be evaluated. Based on the assessment results, rational retrofitting methods should be selected. Generally, adding infill walls to the structure increases the seismic resistance. Experimental studies on strengthened frames with RC infill walls indicate favorable effects on stiffness, strength, energy dissipation, and lateral drift (Altin et al. 1992). Moreover, RC infill walls can significantly enhance the base shear capacity of the building (Canbay et al. 2003) and reduce the lateral displacement demands. However, this technique results in evacuation of the building with increasing construction costs. New types of strengthening techniques have been developed due to these practical and economic reasons. Different strengthening techniques have applied for the retrofit of non-structural infill walls. The Turkish Earthquake code 2007 also recommends methods for the strengthening of infill walls which are special plaster with mesh reinforcement, fiber reinforced polymers and prefabricated concrete panels.

Among these methods, prefabricated panel application on infill walls is practical to apply and has structural benefits. Cyclic earthquake forces on structures cause shear stresses in these panels. Principal tensile stresses cause brittle crack formation due to the low tensile strength of ordinary concrete.  Eventually, the selected panel material should not only have high compressive strength but also ductile behavior.

Experimental studies on the dynamic behavior of RC structures under earthquake loading are mainly conducted by using three test methods namely quasi-static testing, shake table test and pseudo dynamic testing. During quasi-static testing, lateral earthquake loads are applied slowly to the specimens without any inertial effects which may be considered as indirect earthquake loading. The direct way of earthquake loading simulation is by shake table tests. The time and frequency content of the ground motion can be applied to the structure real-time. Despite their advantageous aspects, shake table tests are expensive to conduct and test results are complex to post-process. Moreover, the size and payload capacity of the shake table limits the size and mass of the specimen.

The pseudo dynamic testing method is the combination of experimental and computational processes. The mass and damping of structure are taken as the input of equation of motion. The pseudo dynamic method is executed with a step by step time integration method. Story Displacements obtained from the mathematical model are applied to structure and the resisting forces are measured. New displacements are computed by the numerical model and applied to the structure in the next time step. The pseudo dynamic testing method incorporates the time history of the ground motion and the quasi static testing method. The time interval can be determined by the user; therefore damages can be observed during testing. Besides, large specimens can feasibly be tested by the PSD testing method.

## 1.3 Literature review

The literature review of experimental studies on concrete frames with infill walls, analytical modelling of frames, experimental researches related retrofitting methods and the pseudo-dynamic testing method are summarized in this section. Background material on Engineering Cementitious Composite Materials is presented in Chapter 2.

### 1.3.1 Experimental researches

There are several studies in the literature on studying the structural behavior of infill walls during seismic actions. Some significant studies are briefly discussed in this section.

**Fiorato, Sozen and Gamble (1970)** conducted an experimental program including 27 structural models of reinforced concrete frames with infill walls. All specimens were tested under lateral loading under constant vertical force. Test frames were 8 one-story one-bay, 13 five-story one-bay and 6 two-story three-bay frames. The control variables in the experimental program have been listed below:

- Height or number of stories
- Width or number of bays
- Amount, quality, and arrangement of the frame reinforcement
- Magnitude of vertical load applied to the columns

- Size, shape, and location of wall openings

The experimental study reached the following results about concrete frames subjected to lateral loads:

- Presence of the infill wall made RC frames stronger against lateral loads. The ductility range of the frame was reduced with the addition of the infill wall. Load deformation properties of the wall – frame combination were different from the bare frame at any loading stage.
- The response of the wall – frame system against lateral loads was similar to that of a beam element. However, the load deflection characteristics could be calculated with the knee – braced – frame concept, after occurrence of shear cracks in the infill wall. Openings in the infill wall did not reduce the capacity of the structure. Frictional forces between the wall segments lessened the influence of the openings.
- Transverse reinforcement in the columns of the frame increased the ductility and in some cases the strength of the system.

**Zarnic and Tomazevic (1984)** tested four type of specimens which were: RC frame without infill, RC frame with unreinforced masonry filler wall, RC frame with horizontally reinforced masonry filler-wall, and RC frame with horizontally reinforced masonry filler-wall connected to frame. These tests specimens were produced with ½ scale. Constant vertical load and cyclic lateral loads were applied on each specimen simultaneously. The following conclusions were drawn from this study:

- The lateral resistance of the RC frame with the horizontally reinforced masonry filler-wall connected to the frame was 15% more than the RC frame with horizontally reinforced masonry filler-wall. However, their structural behavior was similar. The strength and deformability of the infilled frame system was not influenced by the type of infill.
- The infill increased the initial lateral stiffness of the frame by twenty times.
- The infilled frame had a lower story drift angle with respect to the frame with no infill. Severe strength degradation of infilled frame was observed when the column reinforcement started to yield.

**Govindan, Lakshmipaty and Santhakumar (1986)** assessed the failure mode of brick infilled frames and discussed the strength, ductility, and energy absorption characteristics of the infilled frame. Two identical quarter scaled seven story test frame were tested with and without infilled walls. Cyclic lateral load was applied on test frames. The aim of the study was to investigate the behavior of the brick masonry infilled frames under cyclic loads as wind or earthquake forces, to quantify the ductility, stiffness, and strength degradation of multi-story infilled frame. The following conclusions were drawn based on in the study.

- The load carrying capacity of the infilled frame was twice that of the reinforced concrete bare frame frame.
- The infilled frame was stiffer than the bare frame. However, the reinforced concrete frame showed a more ductile behavior than the infilled frame.
- Energy dissipation capacity increased with the application of the infill wall.
- Damage to the infill wall caused wall crushing and spalling that could endanger occupants.

**Mehrabi, Shing, Schuller and Noland (1994)** focused on the influence of masonry infill walls on the seismic performance of RC frames. Twelve ½ scale, single – story, single – bay, frames were tested. The strength of the infill wall with respect to that of the bounding frame, panel aspect ratio, distribution of vertical loads and lateral – load history topics were studied in this experimental research. Two different types of frames were designed. The first model was not compatible with the current seismic design standards. The second frame design was compliant with the regulations. Key conclusions from the experimental study are given below.

- The existence of infill walls significantly enhanced the performance of RC frames in terms of load resistance and energy dissipation capability. The strong frame and strong panel combination gave better results than the weak frame and weak panels.
- Brittle shear failures were observed on the columns of the weak frame and strong panel specimens beyond 1% drift levels. The energy – dissipation capability of the weak frame and strong panel was better than the weak frame and weak panel

combination. Nevertheless, the damage level of the weak frame and strong panel endangered the overall structure.

- The lateral load resistance of frames with infill walls regardless of the infill-frame types was more than the bare frame when the drift levels taken into consideration.

**Negro and Verzeletti (1996)** conducted a series of pseudo – dynamic tests on a full – scale four story reinforced concrete building designed according to Eurocodes 2 and 8 (Figure 1.1). The building was 10 m long, 10 m wide and 12.5 m high. The first test was applied to the bare frame. The second test was carried out on an identical frame with the infill walls on two external frames in all four stories. This provided uniform infill distribution. The third test was performed on same structure without infills at the first story to create a soft story effect. The results from this study are:

- The existence of the uniform infill walls along the building height decreased the energy dissipation of the frame. However, infill wall failures and irregularities at first two stories caused larger damage to the frame. It was recommended that non-structural infill walls should be considered in the design stage.
- Simplified SDOF techniques were used to evaluate the structural behavior of the test specimens based on energy considerations. The irregular distribution of infill walls was taken into account by comparing the differences in the SDOF energy demands with respect to the bare frame.

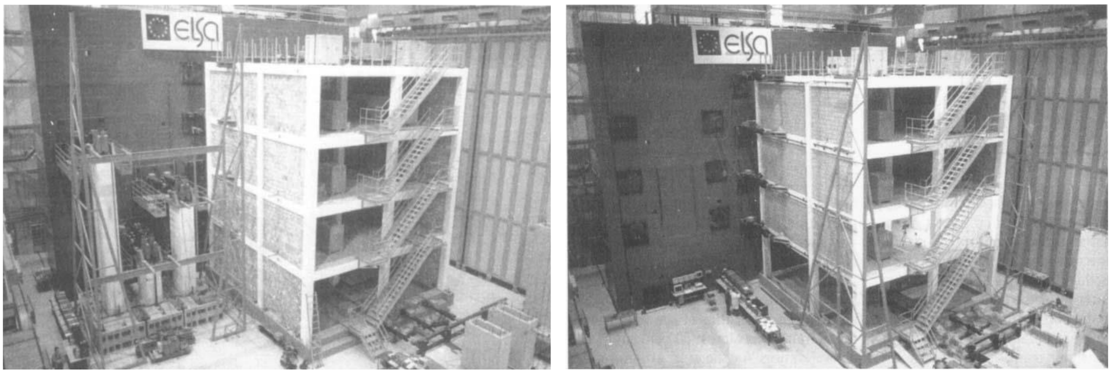

Figure 1.1 Uniformly infilled frame and soft-story infilled frame (Negro and Verzeletti, 1996)

**Marjani and Ersoy (2002)** performed reversed cyclic tests on six, two story, one bay brick infilled frames. Furthermore, six infill panels were tested to determine the infill characteristics. The effects of concrete quality and presence of plaster on the brick infill were investigated. The stiffness, strength, and behavior of the frames were studied with the following major results:

- The presence of the infill wall increases both strength and stiffness significantly. The strength increase as compared to the bare frame was about 240% for specimens with unplastered infills and 300% for the plastered ones. Moreover, plastering both faces of the walls enhanced the infill wall strength significantly.
- Plastering reduced the diagonal cracking and improved ductility. The deformation level of the non-plastered specimen was limited with respect to plastered one with high load carrying capacity.

**Kakaletsis and Karayannis (2008)** conducted an experimental program including seven tests on single-story, one-bay, ⅓ scale reinforced concrete frame specimens with infills of weak and strong brick units. These specimens were tested under cyclic horizontal loading up to a drift level 40%. The first specimen was a bare frame and the others were: fully infilled frame, infilled frame with concentric window and infilled fame with concentric door. Infilled frames were reproduced with strong and weak brick units. The important conclusions of the study were:

- The presence of the infill wall significantly improved the performance of RC frames, even with openings in the wall. If the infill wall cracking resistance was less than the shear resistance of columns, shear failures of columns were avoided and beam plastic hinge formation was prevented. Moreover, door and window openings did not cause a brittle frame failure.
- The load resistance, stiffness, ductility, and energy dissipation capacity of the strong infilled specimens were better than the weak infilled specimens. Moreover, a better distribution of the cracking on the strong walls caused a more effective mechanism for energy dissipation.
- The energy dissipation of infilled frames with openings was higher than the bare frame during low lateral displacements. However, the energy dissipation of infilled

frames with openings was reduced because infills could not absorb energy at high lateral demands.

**Misir, Özçelik, Girgin and Yücel (2016)** investigated the in-plane and out-of-plane actions of the infill wall by introducing progressively increased cyclic in-plane loads on the frame and monotonic out-of-plane loads on the infill wall (Figure 1.2). Frame with pumice blocks (PWF), frame with hollow-fired clay heat insulation bricks (IWF), frame with autoclaved aerated concrete blocks (AWF), frame with double-leaf infill walls without z ties (SW) and frame with double-leaf infill wall with z ties (SWZF) were tested in this research. The following results were obtained:

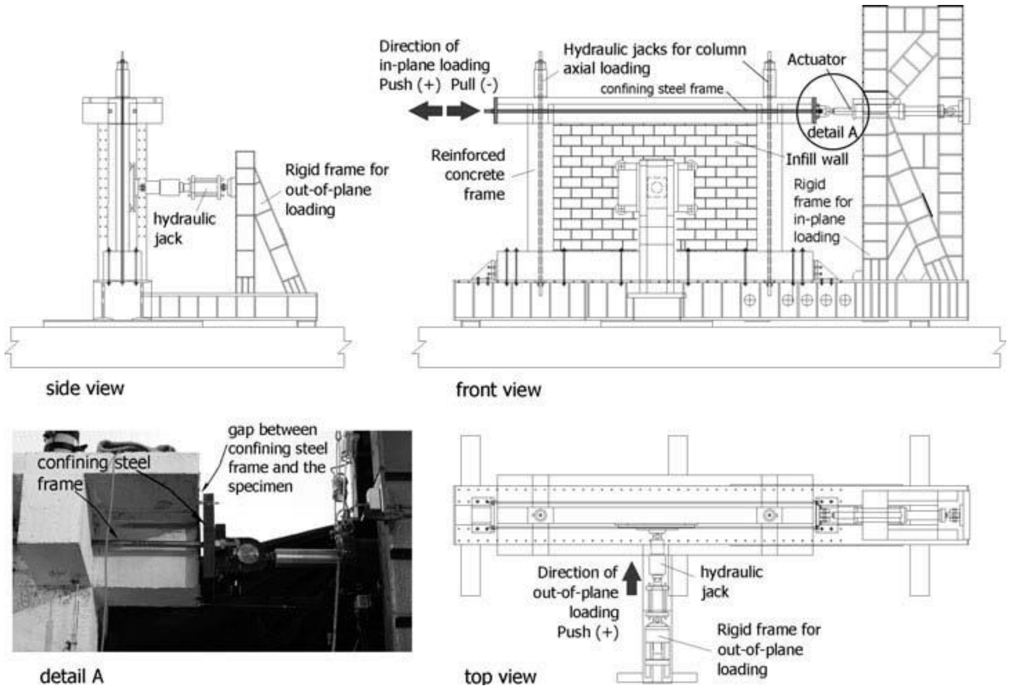


Figure 1.2 Three views of test set-up (Misir et al. 2016)

- The infill walls increased the strength, stiffness, and the energy dissipation capacity. Z ties prevented out-of-plane motion of the wall up to 1% drift ratio, as a result double leaf wall contributed to the in-plane strength.

- Two different failure modes occurred during the tests. Corner crushing was observed in PWF and IWF tests. Diagonal tension and shear sliding were observed in AWF, SWF, and SWZF specimens.
- Out-of-plane tests demonstrated that the failure mode of horizontal hollow clay bricks (SWZ), and autoclaved aerated concrete blocks (AW) was different from classical arching action under biaxial loading. Damages in the infill wall caused diagonal failure of the wall.

### 1.3.2 Numerical studies

Several numerical studies were conducted to obtain the infill wall contribution to the RC structure and to get an accurate infill wall model. The modelling of the infill wall was a challenging task due to its complicated nature. There were various types of infill wall models recommended by researchers in the literature. Macro modelling approaches with the diagonal strut model are the focus of this thesis.

**Rivero and Walker (1982)** recommended a nonlinear dynamic model to capture the behavior of frames infilled by masonry walls. Interaction between the frame and wall, cracking and failure of the wall, the bracing effect that the wall had on the frame, the discontinuities between the frame and wall, and the inelastic behavior of the frame were the assigned key nonlinearities of the model. The model was composed of beam – column elements, wall elements, joint elements, and gap elements.

The researchers simulated a three story, one bay frame with masonry infill walls. Columns and beams were line elements which could carry moment, shear and axial load. Moreover, zero length nonlinear hinge elements were defined at the end of these elements to obtain inelastic behavior. The element chosen to represent the wall was the constant stress triangle. Gap and joint elements were modelled between the wall and frame. Gap elements represented the space that exists between the wall and frame. After the frame and wall came into contact, gap elements provided force continuity. Joint elements served initially to define force continuity between the wall and frame elements. The analytical study reached the following results.

- Analytical results with different modes of behavior were able to match the experimental studies.
- The fundamental elastic frequency of bare frame did not sufficiently represent the frequency or the behavior of the infilled frame.
- The gap size, the strength of infill wall, and time of the maximum response of the bare frame were found to be the important variables in the model.

**Madan, Reinhorn, Mander and Valles (1997)** proposed a hysteretic material model (Figure 1.3) for simulating the masonry infill wall. Stiffness, strength degradation, and pinching effect were the main control parameters. Hysteretic formulation of the infill wall model was time rate independent thus it could be used for static nonlinear analysis and time history analysis. After the hysteretic model was obtained, two diagonal masonry struts were adopted to macroscopically model the infills, depending on geometric and material properties. A one-third scaled, three story lightly reinforced concrete frame was modelled for the time history analysis to evaluate the influence of masonry infill panels. The concluding remarks are listed below:

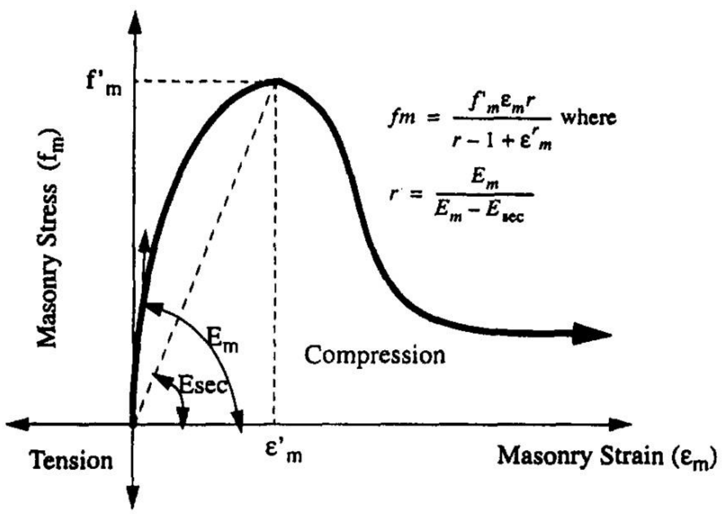


Figure 1.3 Constitutive model for masonry (Madan et al. 1997)

- Using diagonal struts in the macro model was found to be a convenient tool to obtain the inelastic response of the overall structure. The computed force deformation response of the structure was found to provide accurate information about structural damage and its distribution.
- The macro modelling approach did not reflect the local effects as frame-infill interaction in spite of depicting accurate global behavior of the infill wall on the structural system. More detailed micro modelling approaches such as the finite element modelling need to be used to obtain local conditions.

**Hashemi (2007)** performed shake table and pseudo dynamic tests on ¾ scaled specimens (Figure 1.4) which represented the interior frame of a five story, three bay by two bay prototype building. Three ground motions were applied to the test specimens. These three stages considered were (1) infilled structure with columns post-tensioned, (2) after removal of the collapsed URM infill wall, and (3) after removal of the columns post –tensioning to bring the test structure to the verge of collapse. The base shear, maximum drift, residual displacements, natural frequency, stiffness, and damping ratio parameters were evaluated for all three stages of the experiment. Moreover, analytical models were constituted to represent infill walls in RC structures. The compression only strut model, strut and tie model, and finite element models were used during simulation.

- Unreinforced masonry infill walls should be taken into account during the analysis and design stages due to their effects on strength and ductility of RC frames. These walls make the structure significantly stiffer, reduce the natural period of the structure and increase the damping coefficient. Locally, they could create unpredictable force distributions on structural elements.
- Simple compression-only strut models or more complex SAT models represent the structural behavior accurately before the mortar cracking or failure of unreinforced masonry infill walls. Beyond this limit, models should be adjusted with experimental results or finite element studies of infill walls.

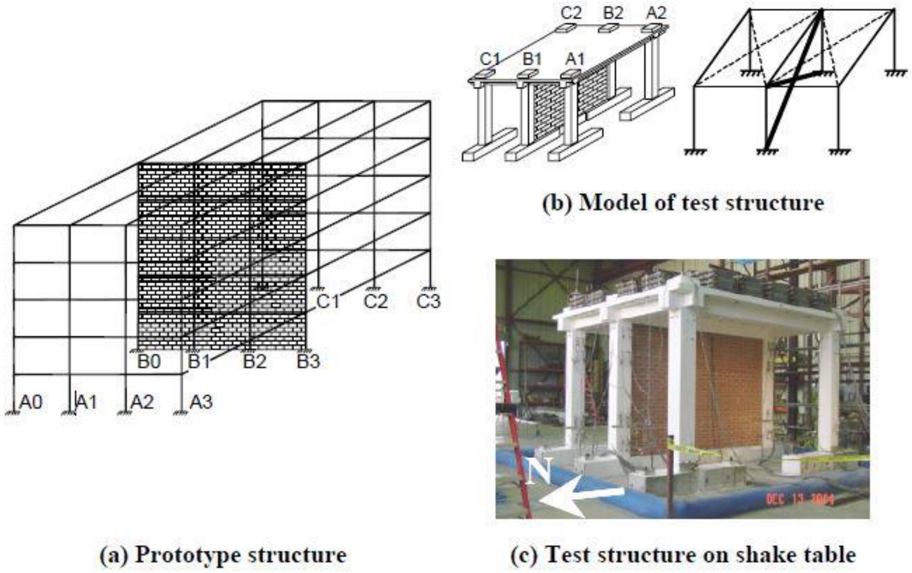


Figure 1.4 Relationship between shake-table and pseudo-dynamic experiments. (Hashemi, 2007)

**Kadysiewski and Mosalam (2009)** proposed an analytical fiber-section interaction model for unreinforced masonry infill walls to represent in-plane and out-of-plane behavior of the infill wall. This study was a part of research program of investigation into RC frames with unreinforced masonry infill (Hashemi, 2007). A new model composed of a single diagonal with two beam-column elements and a node at mid-span was assigned with a mass in the out-of-plane direction (Figure 1.5). This model was adapted to a five story RC moment frame building. The model was exposed to a time history analysis using 20 sets of ground motion.

- Beam column elements with cross sections composed of nonlinear fibers were provided to capture the strength and elastic stiffness properties of the infill wall.
- The panel model preserved strength and stiffness after passing the collapse limit state. This situation caused errors in the calculated global responses of the building model.

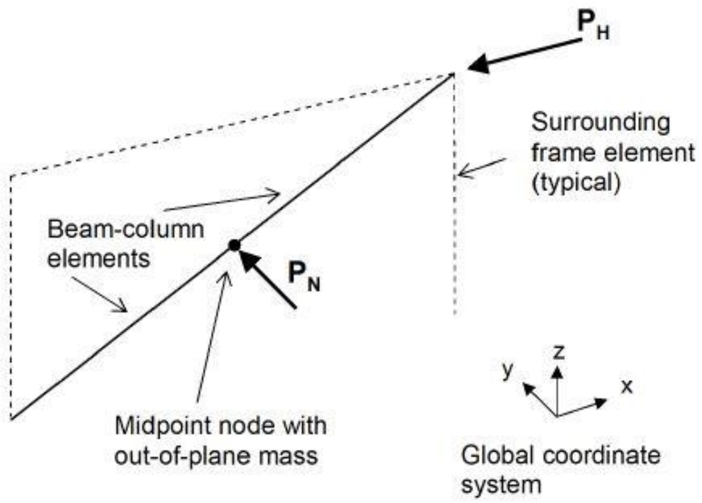


Figure 1.5 Proposed infill model using beam-column elements with fiber discretization. (Kadysiewski and Mosalam, 2009)

**Kurt, Binici, Kurç, Canbay, Akpınar and Özcebe (2011)** conducted PsD tests on a seismically deficient, ½ scale, two story, three bay deficient type of RC frame (Figure 1.6) and evaluated its seismic performance. Moreover, a nonlinear time history analysis was conducted. Masonry infill walls were modelled with strut elements. Forced based fiber elements were selected for the beam and columns. An element removal mechanism was used to model the collapse of infill walls.

- Three successively increasing ground motions applied to the frames resulted in minimum, significant and severe damage states on the test specimen. The infill wall enhanced the lateral strength by about 65%. Soft and weak story behaviors were observed after the failure of the infill wall.
- Nonlinear time history analysis gave acceptable results compared with the experimental results. Analysis results converged better to PsD test results when element removal was used.
- The analyses were better at estimating the global demand parameters such as drift ratios or story shear forces than local responses of the experiment such as curvatures, strains and cyclic loops of elements.

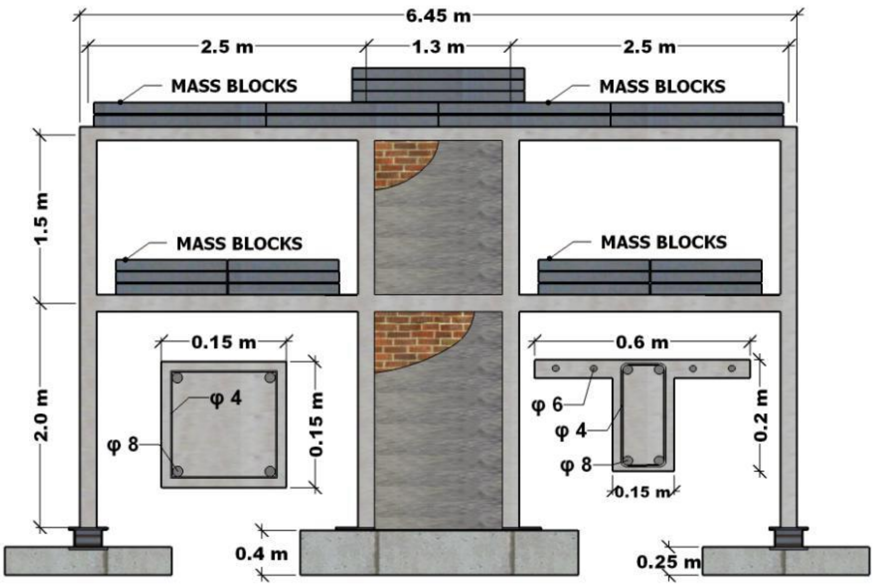


Figure 1.6 Illustration of reference frame (Kurt et al. 2011)

**Sucuoğlu and Siddiqui (2014)** carried out experiments on two code compliant RC frames by the PsD testing method. These specimens were ½ scale, three story, three bay frames. The first specimen was a bare frame and the second was infilled with AAC blocks in the middle bay. The researchers investigated the effect of AAC infills on the seismic performance of reinforced concrete frames and developed an AAC strut model. Strut elements were placed on the mid bay of each story. The material model of the strut element was calibrated with compression tests of Autoclave Aerated Concrete. The concluding remarks are listed below.

- During PsD testing, diagonal tensile cracking on infill wall occurred at 0.5% drift ratio. Furthermore, corner crushing of AAC panels observed at 0.8% drift ratio. After a drift ratio of 2%, the AAC panels lost their integrity.
- AAC panels did not significantly decrease the deformability of the RC frame.
- AAC panels transferred much lower shear forces to the edge columns than clay brick infills.

### 1.3.3 Studies on retrofitting methods

Many researchers carried out studies on different types of seismic retrofitting methods. Especially, the seismic strengthening of RC frames using different types of materials applied to brick infill walls has become the center of attention considering the studies conducted at the Middle East Technical University Structural Mechanics Laboratory over the past decade. These studies are as follows:

Canbay et al. (2003) conducted reversed cyclic load tests on 1/3 scaled, three bay, and two story, lightly reinforced concrete frame to observe the behavior of frames in which only some of the bays are infilled and to understand the internal force distribution in reinforced concrete (RC) frames with added RC walls. Anil and Altin (2007) investigated the behavior of ductile reinforced concrete (RC) frames (One-bay, one-story, 1/3 scale nine test specimens) strengthened by introducing partial infills under cyclic lateral loading. Altin et al. (2008) tested ten specimens under cyclic lateral loading to investigate experimentally the behavior of strengthened masonry infilled reinforced concrete (RC) frames using diagonal CFRP strips. Sevil et al. (2010) conducted reversed cyclic load tests on 1/3 scaled, one bay, and two story RC frame to observe the seismic performance of steel fiber reinforced mortar which was applied to a plastered infill wall. Kurt et al. 2012 used the PsD method for testing four, ½ scaled, three bay, and two-story, lightly reinforced concrete frames which were served as reference frames (Kurt et al. 2011), a fiber reinforced polymer (FRP) retrofitted frame, a precast concrete panel (PCP) retrofitted specimen and a reinforced concrete infill wall application. Özçelik et al. (2012) tested two, ½ scaled, two-story, three bay reinforced concrete frames with and without chevron braces in the Structural Mechanics laboratory. Aykaç et. al. (2017) tested 13 brick wall specimens, one being a reference and the remaining 12 strengthened, under reversed cyclic loading. The aim of this study was to strengthen existing infill walls using perforated steel plates, as well as to improve the seismic performance.

ECC has been applied in the civil engineering field progressively due to its unique properties. The main topic of this thesis is retrofitting RC structures with ECC. For this reason experimental studies related ECC application on infill walls will be discussed in this part.

**Bae, Park, Choi and Choi (2010)** performed in-plane lateral loading tests on retrofitted unreinforced masonry walls. Sprayed ECCs were used as the retrofit material. Three types of specimen were used in the tests. The first specimen was the reference with unreinforced masonry wall; the second specimen was the retrofitted specimen with sprayable ECC and anchor to prevent overturning, and the last specimen was retrofitted with sprayable ECC and had wire-mesh. Lateral cyclic load was applied to the specimens. The following results were obtained in this research program.

- All specimens failed due to rocking and toe crushing in flexural mode.
- The strength and ductility of the retrofitted masonry walls increased. Moreover, wire-mesh prevented abrupt deterioration of strength beside the enhancement of strength and ductility.
- The ECC layer on the infill wall was not sufficient for high energy dissipation due to overturning effect of wall. Wire-mesh transferred stress more effectively in the ECC layer and this improved energy dissipation capacity.

**Maalej, Lin, Ngunyen and Quek (2010)** tested 18 masonry wall panels under both quasi-static and dynamic loading to investigate the out-of-plane motion of the retrofitted masonry walls. These wall panels were retrofitted with an ultra-ductile hybrid-fiber ECC in which PVA and steel fibers were used. Strengthened layers were applied to one face or both faces of the specimens. Moreover, 8 mm-diameter steel mesh was used in the ECC layer. The specimens can be listed as: control specimen, single face retrofitted specimen, double face retrofitted specimen, single face retrofitted specimen with steel mesh, and double face retrofitted specimen with steel mesh. Three types of loading scheme namely patch load, uniformly-distributed load and low-velocity projectile impact were used for the specimens.

- The quasi-static loading tests demonstrated that the ECC-strengthening systems improve the out- of-plane resistance of masonry walls significantly.
- The ECC layers could resist low velocity impact loads. Fragmentations due to impact were also reduced significantly.

**Koutromanos, Kyriakides, Stavridis, Billington and Shing (2012**) conducted shake table tests on a 2/3-scale, 3-story, 2-bay, masonry infilled non ductile RC frame (Figure 1.7). One bottom story wall was retrofitted with sprayable ECC and welded wire mesh. Moreover, the ECC layer was attached to the top beam and bottom foundation by means of shear dowels. Experimental observations and results of nonlinear finite element analyses indicated the influence of this retrofit on the performance of the structure. After shake table tests, the damaged second story wall was repaired by injecting epoxy into cracked mortar joints and strengthened with a glass-fiber reinforced polymer overlay and the shake table test was repeated.

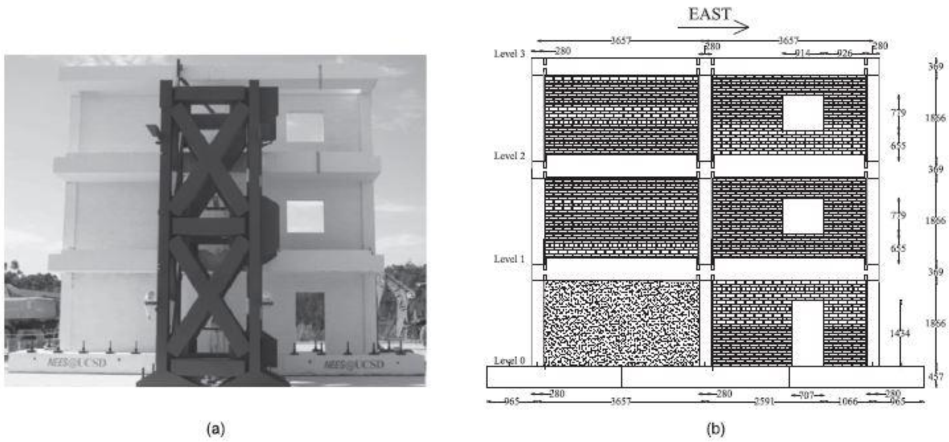


Figure 1.7 Three-story masonry-infilled RC frame and reinforcement details (dimensions in millimeters): (a) elevation view of specimen; (b) dimensions of specimen (Koutromanos et al. 2012).

- This research pointed out the improvement of lateral strength and base shear capacity of the frame with the ECC layer. Furthermore, ECC layer interfered with the crack propagation to structural elements, so this technique avoided diagonal shear failures of the RC columns.
- After failure of the shear dowels, the retrofitted wall behaved purely as a strut mechanism. The base shear capacity of the structure was reached when the exterior beam-to-column joint adjacent to the infill wall developed a horizontal shear crack.

**Kyriakides and Billington (2013)** tested one story, one bay, 1/5 scale, non-ductile reinforced concrete frames (Figure 1.8) with an in-plane, quasi-static, cyclic lateral loading scheme. One unretrofitted wall and three different retrofitting schemes were evaluated. Sprayable ECC with welded wire fabric steel mesh was implemented for retrofitting purposes on the infill wall. Moreover, shear dowels were assembled between the ECC layer and RC members at the top and bottom of the wall in the second and third retrofitted frames. Eight shear dowels rather than ten were used both at the top and bottom of the last retrofitted frame. Furthermore, the dowels used at the base were unbonded from the ECC to allow solely shear force transfer.

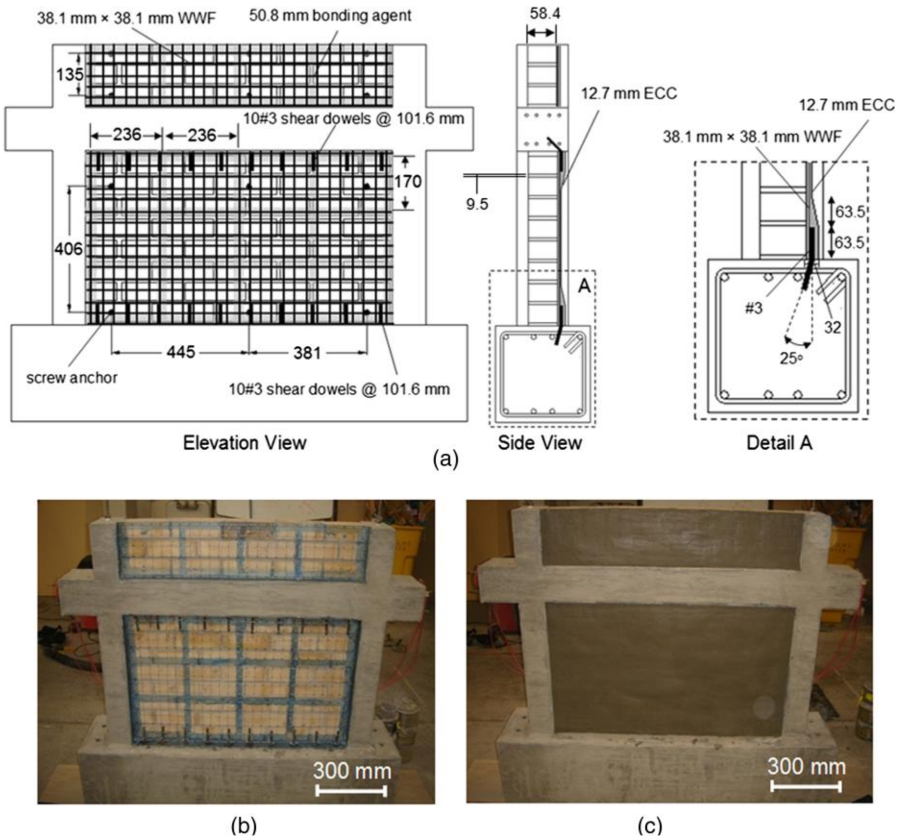


Figure 1.8 Test specimen strengthened with wire mesh and sprayble ECC (Kyriakides and Billington 2013)

- This retrofitting method prevented the bed joint sliding and diagonal cracking of the infill wall. More ductile behavior and higher drift level were obtained for the retrofitted frame with no shear dowels, despite of shear failures occurring in the columns.
- Shear dowels enhanced the lateral strength of the frame further. Unbonded shear dowels in the last specimen ensured no ECC-masonry delamination and also multiple cracking on the ECC layer promoted ductile behavior.

**Dehghani, Nateghi-Alahi and Fischer (2015)** investigated the behavior of masonry infilled reinforced concrete (RC) frames strengthened with fiber reinforced engineered cementitious composites. The aim of this study was to increase the lateral strength of infilled RC frames and maintain the integrity of masonry infills during loading. Three 1/2 scaled one bay, one story deficient type RC specimens were tested under quasi-static lateral loading (Figure 1.9). The bare frame (BF), the masonry infilled frame and the strengthened infilled frame with 15 mm ECC layers troweled on both sides of the infill wall were evaluated in this study focusing on in-plane behavior.

- Enhanced lateral strength and energy absorption capacity of the retrofitted frame demonstrated the effectiveness of the ECC overlay system.
- No premature debonding failure was observed even no mechanical anchorage was provided to the ECC layer. Multiple cracking mechanisms occurred on the strengthened infill wall.

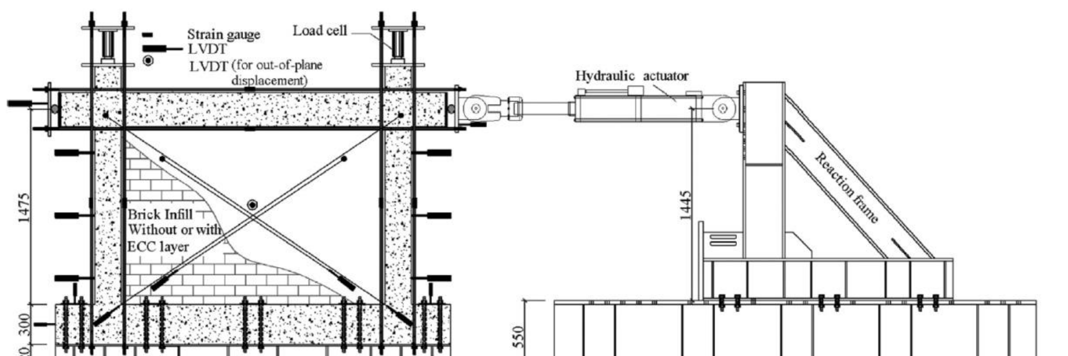


Figure 1.9 Test setup, loading system, and instrumentation (Dehghani et al., 2015)

### 1.3.4 Background on pseudo-dynamic tests

Understanding the seismic performance of buildings is a crucial issue. For this purpose, various experimental techniques such as the pseudo-dynamic, shaking table, forced vibration, and quasi static testing methods have been performed within the scope of past experimental studies. The pseudo-dynamic testing technique was used in the present experimental research program. When reliability and simplicity are considered, pseudo-dynamic testing is found to be an acceptable procedure to understand structural behavior of the test specimens. The pseudo-dynamic testing technique is a computer controlled procedure by simultaneous simulation of ground motion. The pseudo-dynamic testing method increased its importance as an alternative to the shaking table test in the course of thirty years (Takanashi et al., 1975). The following researchers have especially investigated sensitivity of measurement and control errors in pseudo-dynamic testing.

**Mahin and Shing (1985)** examined the capabilities and limitations of the pseudo-dynamic testing method by describing numerical and experimental techniques. They demonstrated that the step-by-step integration procedure caused accumulation of experimental errors. High performance test equipment and appropriate instrumentation techniques could reduce experimental errors. The nonlinear behavior of structures subjected to seismic excitations could be evaluated with the pseudo-dynamic testing method due to well-controlled experimental conditions.

**Aktan (1986)** introduced scaled ground motion on a 1/5-scaled seven-story reinforced concrete frame-wall structure by using the pseudo-dynamic testing method. He recommended a new method which enhanced the accuracy of the pseudo-dynamic testing method for large or full scaled structure experiments. The advantages of this method were user-defined accuracy by using inertia and stiffness properties and limitations related  force constraints.

**Mahin, Shing, Thewalt and Hanson (1989)** explained the basis of the Pseudo-dynamic testing method and its examined capabilities and limitations by evaluating recent research results. Structural idealization coming from minimizing the loading apparatus or discretization of the structure, the damping effect and rate effect arising from time scaling were considered as limitations of the pseudo-dynamic testing method. Experimental errors stemmed from displacement control errors and force measurement errors. Special controllers and control procedures need to be developed to reduce errors and obtain more accurate solutions of the equations of motion. Also, unconditionally stable implicit integration form could be used to enhance reliability, accuracy, and applicability of the pseudo-dynamic test method.

**Peek and Yi (1990)** investigated the error analysis to reduce measurement and control errors occurring during pseudo-dynamic testing. The error analysis was recommended for implicit time integration schemes in the implementation of the pseudo-dynamic method. This method was based on the consistency of displacement, velocity, acceleration and resisting force values which satisfied the time-discretized equations of motion.

**Shing, Nakashima and Bursi (1996)** gave an overview of pseudo-dynamic testing from the user's perspective. This study included testing methodology, research applications and constraints of the method as subtopics. The researchers evaluated two pseudo-dynamic experiments which were a single degree of freedom structure with explicit scheme, a two degree of freedom structure with implicit scheme, a substructure test with implicit scheme and a substructure test with OS scheme (Nakashima et al., 1990).

**Chang (2002)** recommended an unconditionally stable explicit pseudo-dynamic algorithm. This integration method was accurate in second order equations and had better error propagation properties. When the Newmark explicit method and the central difference method were considered, proposed explicit method was very suitable for the pseudo-dynamic test with the presence of high-frequency modes.

### 1.4 Objective and scope

Experiments and analytical studies come into prominence to modify and improve the modelling parameters of existing codes. In order to improve the seismic assessment and proper rehabilitation of existing buildings, modelling parameters should be verified with experimental and analytical results. The Scientific and Technological

Research Council of Turkey (TÜBİTAK) funded a research project at the Middle East Technical University (METU)'s Structural and Earthquake Laboratory for the verification and validation of the existing assessment and performance-based design methodologies in TEC 2007 through analyzing and testing various concrete frames. Within this scope, an experimental research program related to this topic was conducted in the Middle East Technical University. Thirteen specimens which were 1/2 – scaled, 3 – story, and 3 – bay reinforced concrete frames were produced in this context. Continuous pseudo-dynamic testing was employed for all specimens using synthetic ground motions compatible with the site-specific earthquake spectra developed for the city center of Düzce. Within the scope of the project name called "Developing Performance-Based Evaluation Procedures and Strengthening Methods for the Turkish Seismic Code through Experimental and Analytical Research" and officially documented as "TÜBİTAK 1007, Project #108G034", thirteen frames were tested with the following properties:

- Specimen 1. Bare Frame (Code Conforming)
- Specimen 2. Brick Infilled Frame (Code Conforming)
- Specimen 3. Retrofitted Reinforced Brick Infilled Frame (Code Conforming)
- Specimen 4. Bare Frame (Code Conforming)
- Specimen 5. Bare Frame (Code Non-Conforming)
- Specimen 6. Brick Infilled Frame (Code Non-Conforming)
- Specimen 7. Ecc Infilled Frame (Code Non-Conforming)
- Specimen 8. Air-Entrained Concrete Infilled Frame (Code Non-Conforming)
- Specimen 9. Bare Frame (Code Non-Conforming and Splice Bars at Columns)
- Specimen 10. Bare Frame (Code Conforming)
- Specimen 11. Air-Entrained Concrete Infilled Frame (Code Conforming)
- Specimen 12. Reinforced Concrete Infilled Frame (Code Conforming)
- Specimen 13. Reinforced Concrete Infilled Frame (Code Non-Conforming)

The main theme of this thesis was the testing and analysis of Specimens 5, 6, and 7. All selected frames were deficient (i.e. substandard) types of RC frames. These deficiencies were inadequate steel reinforcement, low material strength and plain bar usage. The first specimen was the bare frame. The second specimen was the infilled framed with infill wall at the middle bay. The last specimen was the strengthened frame, retrofitted with Engineering Cementitious Panels. The experimental setup, details of production of the ECC panels and applications of this strengthening technique are explained in Chapter 3 and Chapter 4.

The lateral strength, deformibility and the rigidity of the infilled walls are crucial for the seismic response of RC Frames with low earthquake resistance. Seismic strengthening with prefabricated concrete panels on existing hollow clay tile infill walls is one of the recommended strengthening techniques given in the TEC (2007). Ease of implementation and endurance against out of plane failure of infill walls are the major reasons for the application of concrete panels. The main problem of the concrete panels is their low tensile strength and deformability. In order to enhance these properties, strengthening panels were produced by using Engineered Cementitious Composites (ECC) concrete. The main purpose of the thesis was evaluating the performance of the proposed strengthening technique by comparing the experimental test results with nonlinear time history analyses of frames. In addition, infill wall effects on the RC frame were studied. The following objectives were set forth in this thesis:

- Evaluation of pseudo-dynamic test results of three deficient reinforced-concrete frame specimens
- Analysis of each test specimen.
- Performance evaluation of each specimen according to TEC (2007) and ASCE/SEI 41-06.

# CHAPTER 2

## ENGINEERED CEMENTITIOUS COMPOSITES

### 2.1 Literature review

The use of high compressive strength concrete has increased in structural applications in recent years. However, its brittle behavior, low tensile strength and ductility demand for structural elements has prompted researchers to develop new types of materials. Researchers from the University of Michigan sought such a material and developed a mortar based material and with very high tensile strain capacity named as an engineered cementitious composite.

Engineered Cementitious Composite (ECC) is a mortar-based composite reinforced with fibers. ECC has very high tensile strain capacity varying between 3% and 7%. Ordinary plain cement paste has strain capacity of approximately 0.01%. Therefore, ECC can be identified as a ductile material.

The ingredients of the ECC are water, cement, fine aggregates, fiber and some common chemical additives. Low water /binder ratio (0.5 or lower) and 2% or less by volume of fiber are the main properties of the ECC required to obtain ductile behavior and suitable structural behavior (Li and Kanda, 1998). The mix proportion along with a uniform fiber distribution are the key factors of ECC. Fiber distribution at preparation stage of the ECC influences mechanical properties, such as the ductility and tensile capacity (Zhou et al., 2012).

ECC was developed with the aid of fracture mechanics and micromechanics. The interaction between the fibers and cement matrix causes many micro-cracks with limited crack width. When ECC cracks under tension, the bridging fibers continue carrying the load across the crack which allows formation of new cracks. This multiple cracking process continues until the maximum bridging stress is reached. This damage process occurs at increasing load resulting in a pseudo strain-hardening behavior for the composite (Li, 1993).

The strain-hardening behavior of ECC also leads to a high flexural strength-to-tensile (first cracking) strength ratio. This property enhances the energy absorption capacity of the material (Maalej and Li, 1994).

ECC can be used with steel reinforcement for many structural applications like flexural elements, column elements, shear beam elements, beam-column connections, wall elements, and frames (Li. 2008). Its high tensile strain capacity makes ECC also an attractive repair and retrofit material (Li et al. 2000). Additionally, ECC has high damage tolerance which enhances the residual strength capacity of the material. PolyVinyl Alcohol (PVA) fibers ensure crack width control and multiple cracking of the material which raise energy consumption capacity of the ECC when the material is loaded (Li. 2003).

ECC is a material with some drawbacks, despite the above mentioned positive material properties. Maintaining the production quality of this material is difficult due to presence of fibers. Inhomogeneous fiber distribution causes degradation of mechanical properties of ECC (Şahmaran et al. 2013). Furthermore, the tensile strength and strain capacity of ECC deteriorate under raised temperatures around 200°C (Kewalramani et al. 2017).

## 2.2 Mix proportion of ECC

ECC is a micromechanically designed material. All cementitious compositions developed with fibers for large ductility may be considered as ECC. Therefore, there is no unique receipt for ECC and no detailed mix proportions can be found in the literature. In this study, a mix proportion was selected to produce ECC panels to retrofit unreinforced masonry walls. Sixteen different mix proportions were tested to investigate the mechanical and shrinkage properties of ECC mortar with varying amounts of cement, fly ash, ground granulated blast furnace slag, silica sand and water by Keskin (2012). Although ECC mixtures with ground granulated blast furnace slag exhibited higher compressive strength than ECC mixtures with fly ash, all samples show similar flexural properties. Moreover, maximum mid span deflection was measured for the ECC mixture with fly ash with low mineral admixture cement ratio by the four-point bending test. This ECC mixture detailed below was selected due to its strain capacity in tension. Detailed information can be obtained from Keskin 2012.

The composition of the ECC mortar is given in Table 2.1. Ordinary Portland cement (CEM I 42.5 R corresponds to ASTM Type I) was used with extremely low water to binder material (cement and fly ash) ratio (0.27) to get high compressive strength. Class F according to ASTM C 618 type fly ash was used in the ECC mix. The chemical composition of the cement and fly ash is given in Table 2.2. The main contribution of this part of the study was to enhance the tensile capacity of the ECC panels. For this purpose, PVA fibers were added to mortar. The fiber properties declared by the manufacturer are presented in Table 2.3. The nominal strength is the tensile strength of the fiber. However, the apparent strength is the tensile strength of fiber with one of its ends embedded in cementitious material (Kanda and Li, 1998). Large aggregate size leads to failure of the multiple cracking mechanism of the ECC. Therefore, the maximum and average aggregate size should be between 200 μm and 110 μm in a typical ECC mixture, respectively. However, maximum and average aggregate sizes in this study were selected as 400 μm and 200 μm, respectively, because of local material availability in Turkey. Polycarboxylate ether type high range water reducing superplasticizer (BASF – Glenium 51) was used for workability of ECC.

Table 2.1 Mix design of ECC

| **Material** | **Weight for 1 $m^3$ (kg)** |
| --- | --- |
| **Cement (CEM I 42.5 R)** | 563.0 |
| **Fly Ash** | 676.0 |
| **Water** | 329.0 |
| **Sand** | 450.0 |
| **PVA Fiber** | 26.0 |
| **Superplasticizer (BASF – Glenium 51)** | 18.5 |

Table 2.2 Chemical composition of cement and fly ash

| Chemical Composition | Portland Cement | Fly Ash |
|---|---|---|
| **CaO (%)** | 61.43 | 1.64 |
| **$SiO_2$ (%)** | 20.77 | 56.22 |
| **$Al_2O_3$ (%)** | 5.55 | 25.34 |
| **$Fe_2O_3$ (%)** | 3.35 | 7.65 |
| **MgO (%)** | 2.49 | 1.8 |
| **$SO_3$ (%)** | 2.49 | 0.32 |
| **$K_2O$ (%)** | 0.77 | 1.88 |
| **$Na_2O$ (%)** | 0.19 | 1.13 |
| **Loss of Ignition (%)** | 2.2 | 2.1 |
| **$SiO_2$+ $Al_2O_3$+ $Fe_2O_3$** | 29.37 | 89.21 |

Table 2.3 Properties of PVA fibers as provided by the manufacturer

| Property | Value |
|---|---|
| **Nominal strength, MPa** | 1620 |
| **Apparent strength, MPa** | 1092 |
| **Diameter, μm** | 39 |
| **Length, mm** | 8 |
| **Young‘s modulus, GPa** | 42.8 |
| **Elongation, %** | 6 |
| **Density, kg/m$^3$** | 1300 |
| **Melting temperature, °C** | 230 |

### 2.3 Mechanical Properties of ECC

The mechanical properties of ECC were determined from standard regular tests such as uniaxial compressive strength, elastic modulus, and bending tests. Three 100×200 mm cylinder specimens were tested to determine the compressive strength of ECC. The average compressive strength of ECC was calculated as 47.4 MPa (47.15 MPa, 51.51 MPa, and 42.96 MPa). Two 100×200 mm cylinder specimens were tested to calculate the elastic modulus of ECC as shown in Figure 2.1. For this purpose specimens were cycled a few times up to 40% of the compressive strength. The elastic modulus of ECC was calculated as 14800 MPa. Three standard square prismatic specimens with 315×75×75 mm dimensions were used for bending tests, Figure 2.2. Additionally, three 510×75×25 mm rectangular prismatic specimens were produced in order to better simulate the thin ECC panel behavior, Figure 2.3. Simply supported beams were tested under four-point loading. The two symmetric loads were applied at 1/3 of beam clear length. Figure 2.4 shows the flexural stress vs. mid vertical displacement of the test beams and elastic modulus test results. Stresses were calculated by the simple elastic stress formula $\sigma = My/I$ where $\sigma$ is the stress, $M$ is the moment, $y$ is the distance from neutral axis and taken as half the thickness, and $I$ is the moment of inertia of the cross-section. The distance between the supports was 280 mm and 340 mm for the standard and thin tests, respectively. As expected the standard square specimen shows much less bending displacement due to its mechanical properties. Plate specimen showed much ductile behavior. The average flexural strengths of standard and thin specimens were calculated as 10.60 MPa and 9.66 MPa, respectively.

Figure 2.1 Uniaxial compressive test with elastic modulus apparatus

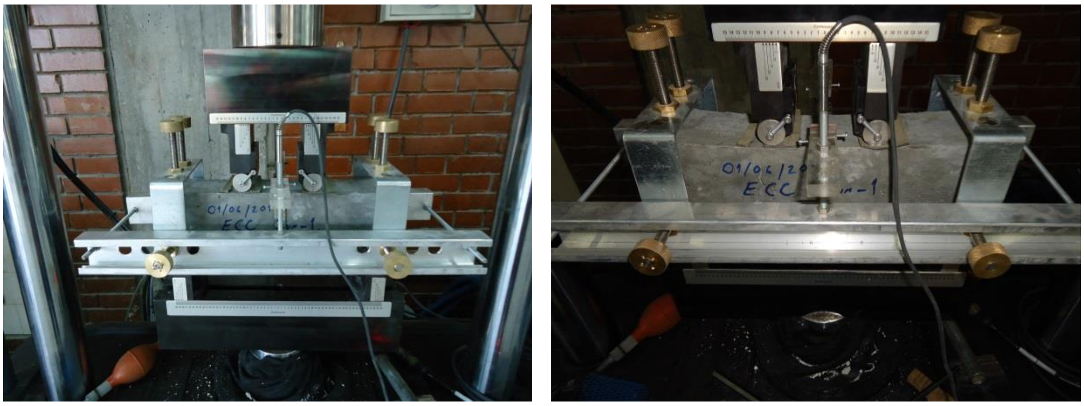

Figure 2.2 Bending test of 315×75×75 mm specimens

Figure 2.3 Bending test of 510×75×25 mm specimens

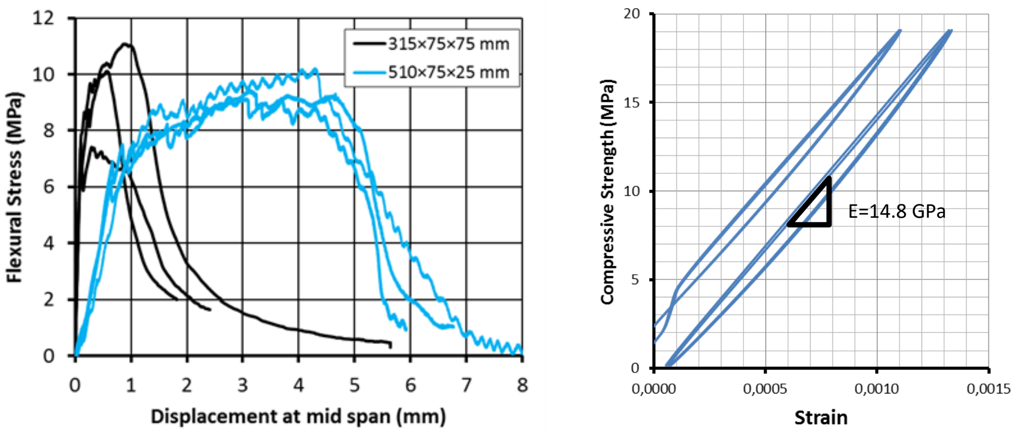


Figure 2.4 Bending and elastic modulus test results

## 2.4 Production of ECC Panels

For the production of ECC mortar, first, silica sand, fly ash and cement were mixed slowly and water was added to this mix. Afterwards, the super plasticizer was placed for better mortar workability and flowability. Later, the mixing speed was accelerated to achieve intended consistency. Finally, PVA fibers were put in the mortar and blended further for a few moments. Afterwards, ECC mortar was cast into the plywood molds (Figure 2.5).

Figure 2.5 Production of ECC panels

# CHAPTER 3

## EXPERIMENTAL PROGRAM

In this chapter, the pseudo-dynamic testing method, the preparation of the test frames, material properties, instrumentation details, test setup and loading system are explained in detail. Furthermore, specimens with differences and similarities of frames are provided.

### 3.1 Pseudo dynamic testing method

In this method, the physical testing and computational part of the experiment are conducted simultaneously. The mass, damping and response of the structure are mathematically modelled. The well-established step by step time integration method is used to perform pseudo-dynamic testing. Specified ground motion imposes deformations on each story at each time step and resisting forces are measured. New displacements are computed through the instrument of discrete parameter model of mass and damping. Mass, damping and the ground motion features of the specimen are postulated. In the meantime resisting forces are acquired directly from the experimental set-up by means of load cells as a quasi-static experiment. Calibration of the load cells are conducted prior the experiment. The numerical integration of the second order differential equation of motion is carried out to obtain the displacement history for further steps with restoring forces as input values of equation (Figure 3.1).

Experimental results were obtained from the PsD method by using the procedure proposed by Molina et al. (1999). The equation of motion (Eq. 2.1) was solved at discrete time intervals. The restoring force was experimentally measured while deformations were applied.

$$Ma(n) + r(n) = f(n) \tag{2.1}$$

$M$ : 3×3 diagonal mass matrix

$a(n)$ : 3×1 acceleration matrix

$f(n)$ : 3×1 external force matrix

$r(n)$ : restoring force

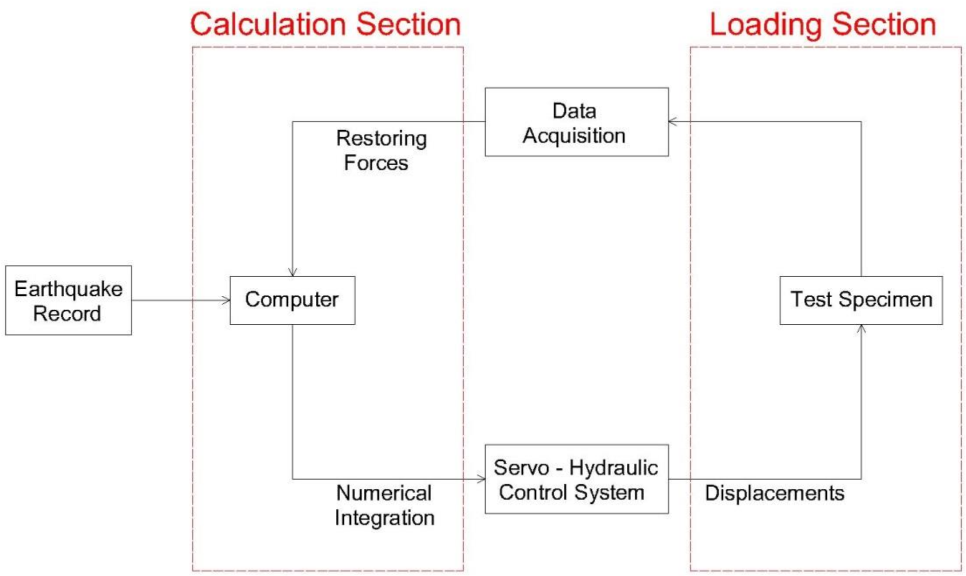


Figure 3.1 Pseudo-dynamic testing loop

## 3.2 Preparation of the test frame

### 3.2.1 Foundation

Foundations to attach the test specimens were designed to remain elastic during the course of this study. The same foundations were used for all specimens. Three different foundations were produced as shown in Figure 3.2 to minimize the concrete amount and to enable easy handling. All foundations were fixed to the strong floor firmly by post – tensioning, which prevented uplifting and sliding during tests. The middle foundation had dimensions of 470 × 1500 × 3750 mm. The left and right footing were constructed with dimensions of 250 × 1500 × 1500 mm and the other one had dimensions of 250 × 1750 × 1500 mm, respectively. The difference between the heights of foundations was due to the special force transducers placed at the bottom of exterior columns as shown in Figure 3.2.

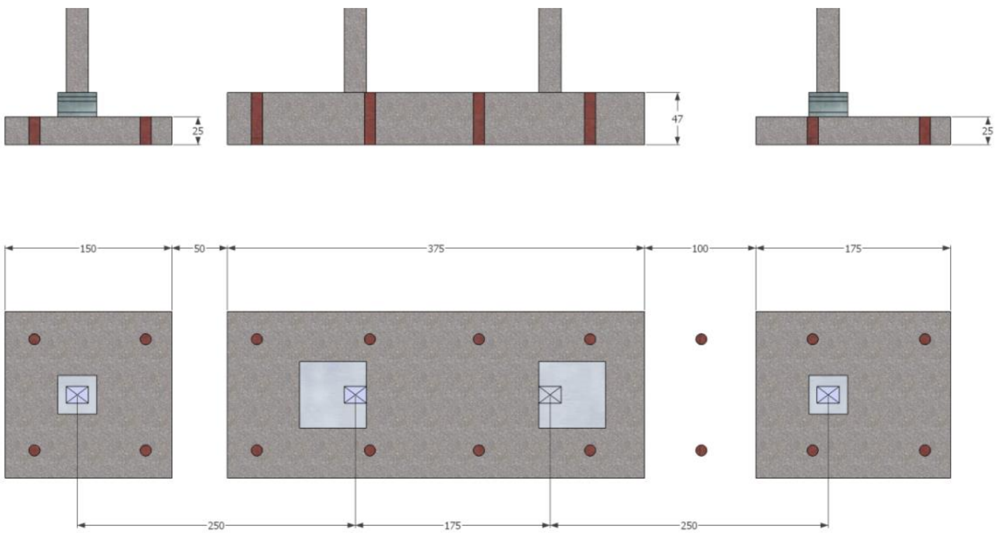


Figure 3.2 Dimensions of the foundations

As shown in Figure 3.3, timber was used as the foundation formwork. After installation of the foundation reinforcement, steel plates with high strength bolts were welded precisely to the reinforcement of exterior foundations to enable installation of special force transducers as shown. Additionally, two steel plates were welded to the middle foundation to enable welding of longitudinal reinforcement of interior columns. Holes were formed in the foundations with plastic pipes.

Ready mixed concrete was used in casting of the foundations. Concrete was compacted properly by means of vibrations. Cylinder specimens were taken from each truck. The grade of concrete was chosen as C35. Foundation concrete reached a 38 MPa compressive strength at 28 days. The 70 cm thick strong floor of the Structural Mechanics Laboratory had uniformly and orthogonally distributed holes which are 1 m apart. Foundations were fixed to the strong floor by post tensioning 50 mm diameter high strength anchor bars.

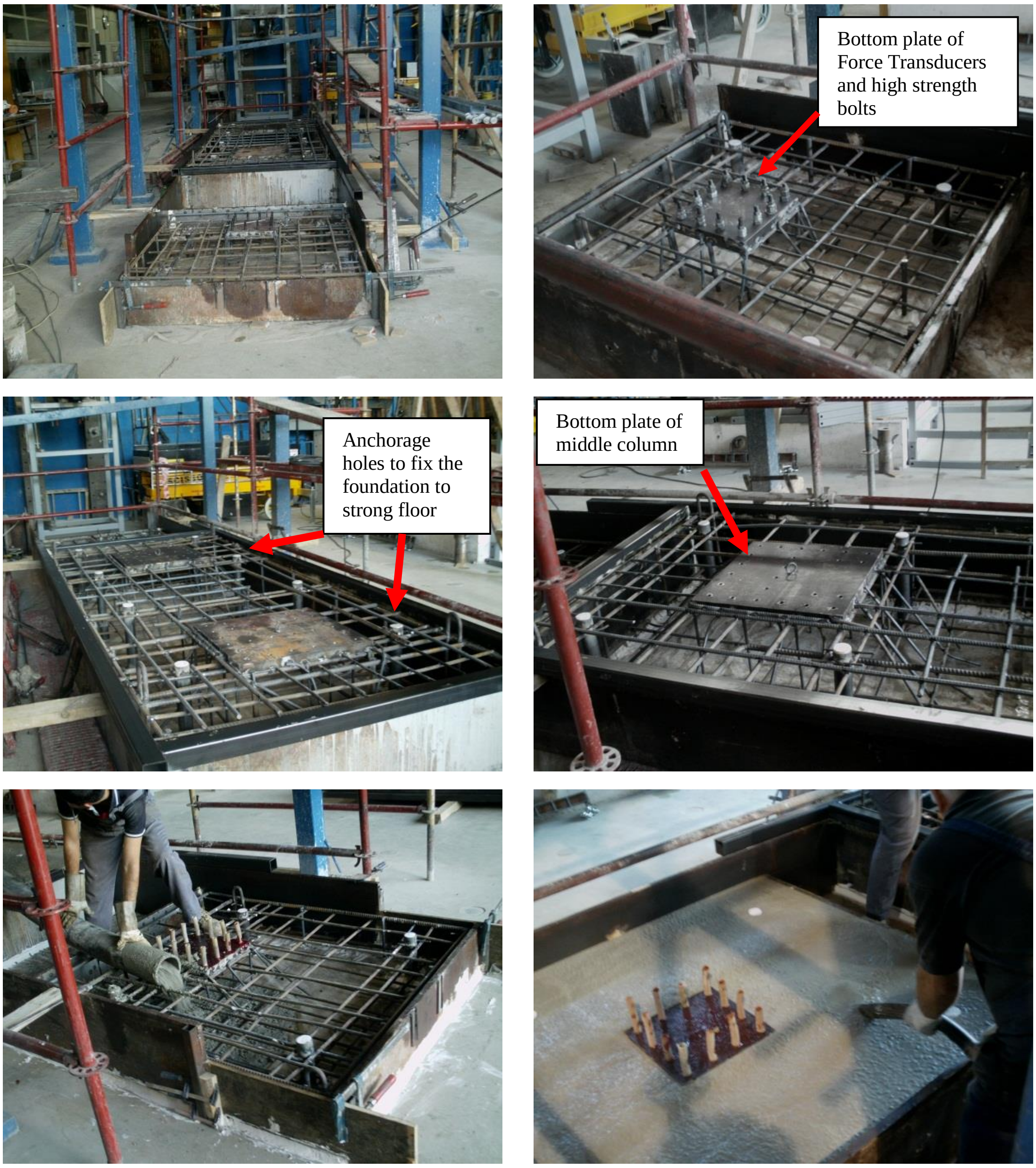


Figure 3.3 Construction of the foundations

### 3.2.2 Formwork

All specimens were cast in-place by using steel formworks. All specimens had the same dimensions. For this reason the same formwork was used for all specimens (Figure 3.4). Galvanized steel plates were selected as the material for the formworks to provide precise dimensions. Furthermore, this formwork enabled a smooth concrete surface. The plate thickness was selected as 3.5 mm to give required stiffness during concreting and it prevented any undesired sag of the formwork. Steel plates were cut, drilled and bent to the desired shapes accurately with special machines. Formworks were assembled together by bolts. The assembled formworks are shown in Figure 3.4.

Figure 3.4 Assembled formworks

### 3.3 Materials

#### 3.3.1 Concrete

Concrete for the test frames was prepared at the Structural Mechanics Laboratory of the Middle East Technical University. Concrete trial mixes were prepared for the desired target compressive strength. Materials used in the mix design are presented by weight for a unit cubic meter (Table 3.1). Portland Composite Cement (CEM II/B-M (P-L) 32.5 R) was used for the concrete mix. This cement was also used for plaster and masonry mortar (for the infilled frame and strengthened frame). Crushed stone was used as aggregate. Concrete was properly cured to get the target strength. Same curing conditions were provided both for frame and cylinder concrete. The dimensions of cylinder specimens were 150 × 300 mm (Figure 3.5). Concrete target strength was selected lower than the provision given in Turkish Earthquake code to provide deficient frames. Cylinder test results are summarized in Table 3.2.

Table 3.1 Mix design of frame concrete (weight for 1 $m^3$ of concrete)

| | **Unit** | **Amount** |
|---|---|---|
| **Cement** | kg | 350 |
| **Aggregate (Sand 0-3 mm)** | kg | 700 |
| **Aggregate (Crushed Stone 7-15 mm)** | kg | 1075 |
| **Water** | kg | 250 |
| **Total** | kg | 2375 |

Table 3.2 Uniaxial compressive strength of the concrete cylinders

| **Uniaxial Compressive Strength (MPa)** | **1st Story** | **2nd Story** | **3rd Story** |
|---|---|---|---|
| **Bare frame** | 14,0 | 11,7 | 10,1 |
| **Infilled frame** | 12,7 | 13,9 | 14,0 |
| **Strengthened frame with ECC** | 15,0 | 15,8 | 13,8 |

Figure 3.5 Concrete cylinder specimens

### 3.3.2 Reinforcement

Plain bars were used as the reinforcement in all columns and beams. Longitudinal bars were used from the same batch of reinforcement for each specimen. Therefore, reinforcement tensile strength differences between each specimen were minimized. Three coupons were tested for each different bars under a tensile testing machine. The test results are presented in Table 3.3. Bar diameters of 8 mm for columns, 10 mm for beams for longitudinal bars and 4 mm at both columns and beams as transverse reinforcement were selected.

Table 3.3 Mechanical Properties of Reinforcement

| **Bar Diameter (mm)** | **$f_y$ (MPa)** | **$f_u$(MPa)** | **Surface condition** |
|---|---|---|---|
| **8 mm** | 320 | 460 | Plain |
| **10 mm** | 355 | 555 | Plain |
| **4 mm** | 240 | 340 | Plain |

### 3.3.3 Brick

Scaled dimensions were required for the brick units due to the use of the ½ scaled frame sizes. 190 mm × 85 mm × 95 mm was selected as brick dimensions. Split horizontal perforated clay masonry units were used for infill walls (Figure 3.6). The compressive strength (perpendicular to brick holes) was determined as 2.0 MPa.

Figure 3.6 Brick and infill wall

### 3.3.4 Mortar

Mortar and plaster were prepared in the laboratory. The mix design of this mortar is given in Table 3.4. The masonry mortar thickness was approximately 8 mm. The plaster mortar thickness was 10 mm and the total infill wall thickness was about 105 mm. The column dimension in this direction was 150 mm which allowed a free space of 45 mm for ECC panel application. Cylinder samples of 100×200 mm were taken for uniaxial compression tests. The average values of test results are represented in Table 3.5

Table 3.4 Mix design of mortar and plaster

| | Unit | Amount |
|---|---|---|
| **Cement** | kg | 15 |
| **Aggregate (Sand 0-3 mm)** | kg | 64,8 |
| **Water** | kg | 14,7 |
| **Lime** | kg | 5,5 |
| **Total** | kg | 100 |

Table 3.5 Uniaxial compressive strength of the cylinders of mortar

| Uniaxial Compressive Strength (MPa) | 1st Story | 2nd Story | 3rd Story |
|---|---|---|---|
| **Reference Frame** | 8,9 | 8,4 | 8,2 |
| **Strengthened frame with ECC** | 8,6 | 9,2 | 7,2 |

### 3.3.5 Engineered cementitious composites

Details of ECC material properties, material tests and panel production are explained in Chapter 3. The experimental setup, details of production of ECC panels and applications of this strengthening technique are explained in the forthcoming sections. The installation of the panels for strengthening purposes is explained in section 3.5.4.

## 3.4 Instrumentation

Displacement and load measurements were the primary objectives of the instrumentation. Several LVDTs (Linear Variable Displacement Transducer) and Heidenhains were used for displacement measurements. Load cells and 2 special transducers (Canbay et al., 2004) were utilized to obtain load measurements during the experiments. General views of the instrumentation are shown in Figure 3.7 and Figure 3.8.

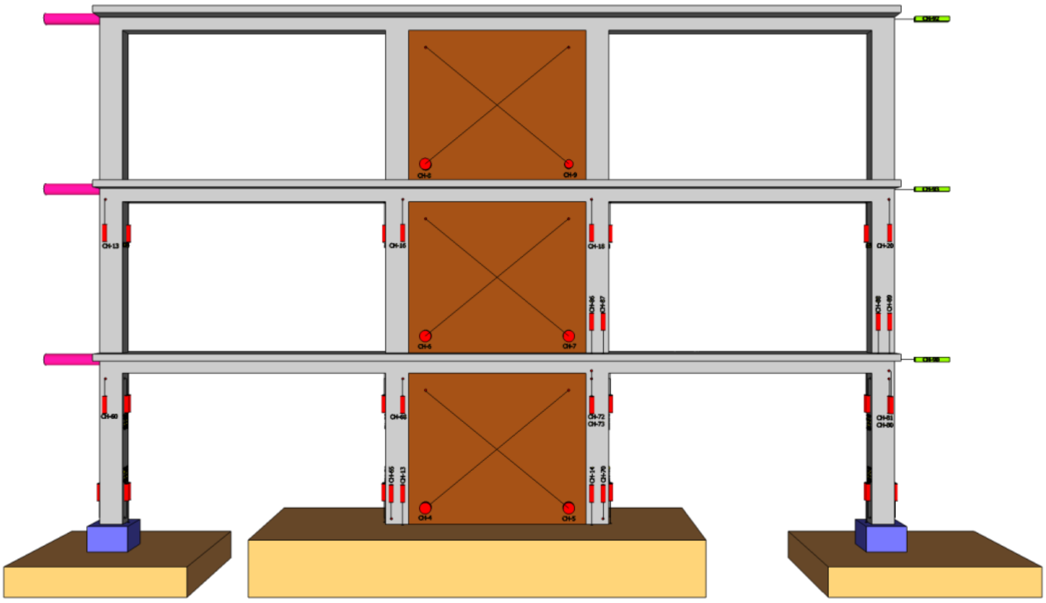

Figure 3.7 General view of instrumentation (Front and back view of test specimen)

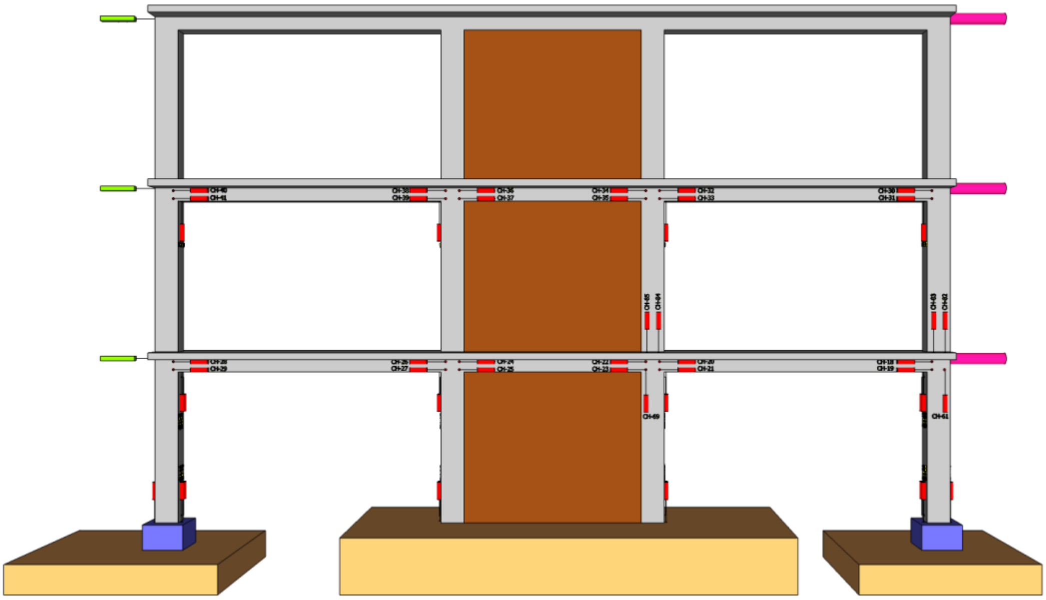

Figure 3.8 General view of instrumentation (Front and back view of test specimen)

For curvature measurement, 30 mm and 50 mm stroke LVDTs, were located on the specimens. Four 50 mm capacity LVDTs were placed on opposite faces of the columns for first story curvatures measurement. Different gage lengths were selected to monitor the curvatures at the base of columns. For instance, two LVDT's were attached relative to the ground with 200 mm gage length on the opposite face of the column base.

Two additional LVDT's were attached on the column base with 150 mm gage length without touching the ground (Figure 3.9-I-II-III-IV). Two 30 mm capacity LVDTs were attached to each end of beams to obtain beam curvatures at the first and second story (Figure 3.9-VII-VIII). Two 50 mm capacity LVDTs were installed on the infill wall diagonally to obtain shear deformation under lateral forces (Figure 3.9-IX). Figure 3.10 shows the assembled LVDS on structural elements.

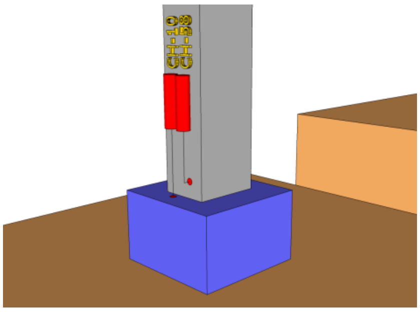

I-Exterior column bottom end (first story)

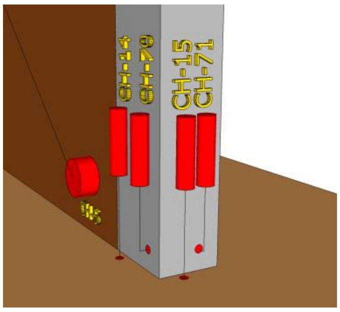


II-Interior column bottom end (first story)

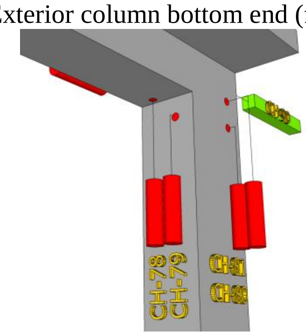


III-Exterior column upper end (first story)

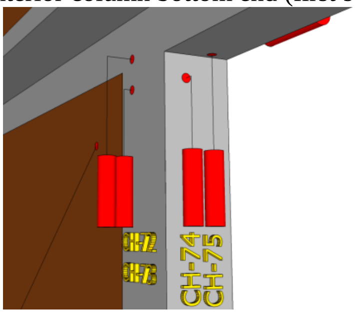


IV-Interior column upper end (first story)

Figure 3.9 Location of LVDTs on structural elements (columns, beams and infill wall) (cont'd)

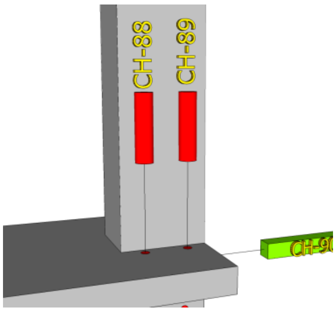

V-Column bottom end (second story)

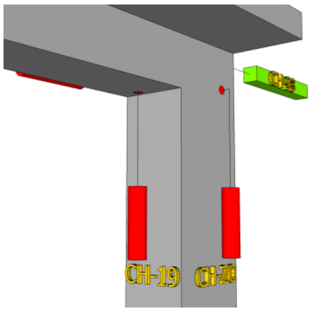

VI- Column upper end (second story)

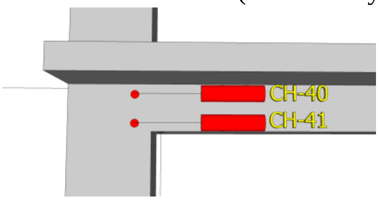

VII-Beam end of exterior joint

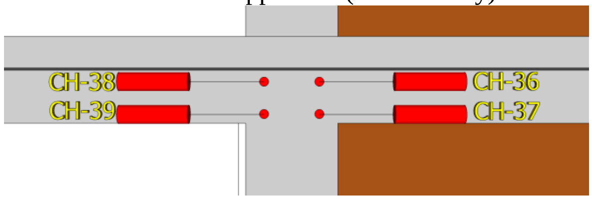

VIII-Beam end of interior joint

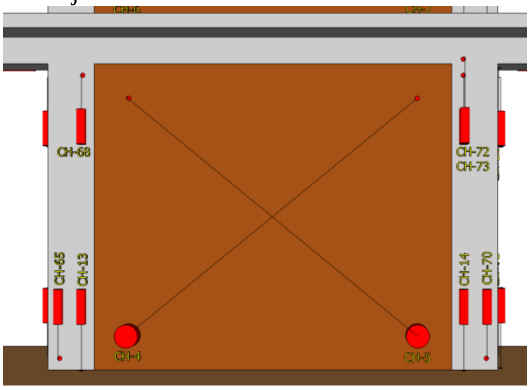

IX-Infill wall

Figure 3.9 Location of LVDTs on structural elements (columns, beams and infill wall) (cont'd)

Two LVDTs were used at each floor to measure horizontal displacements at story levels. 200 mm capacity LVDTs were used at the first and second floor and 300 mm capacities LVTDs at the third floor. Also, a Heidenhain was placed at each floor in addition to LVDT's. Heidenhains measured data to the PSD controller computer system to provide feedback for the next step of the PSD testing procedure. PSD testing procedure requires very high resolution of displacement measurement.

To obtain load measurements, load cells were assembled to actuator heads (Figure 3.11). A 250 kN capacity load cell was used at the first floor. On the other hand, 500 kN capacity load cells were mounted to the second and third floor actuators.

Column bottom end

Column bottom end

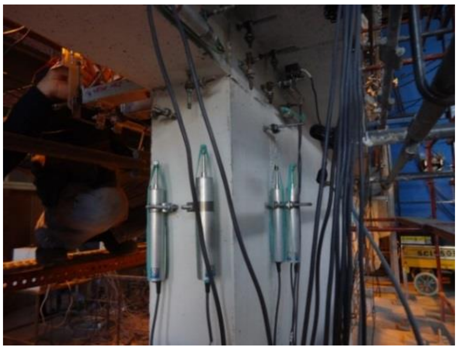

Column upper end

Interior joint

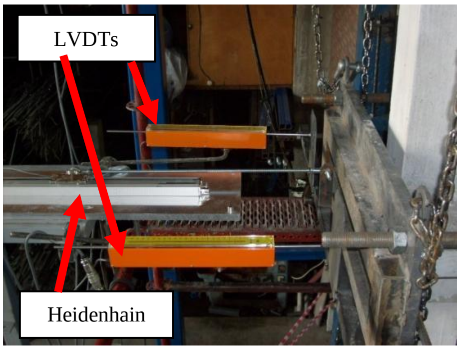


Story level

Figure 3.10 General view of LVDT's after installation

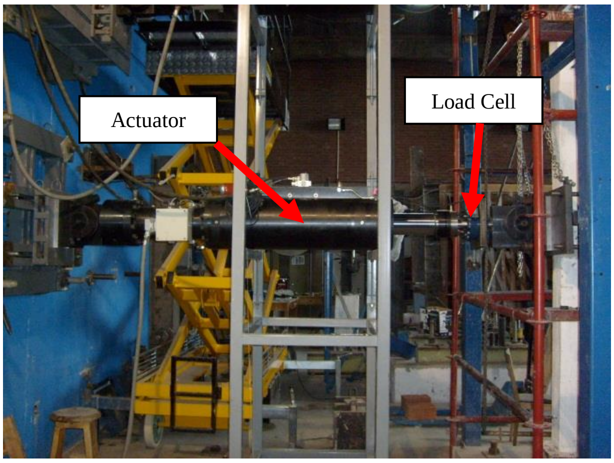


Figure 3.11 Actuator at the first floor

Special transducers were produced by Canbay et al. (2004), which are capable of measuring axial force, shear force and moment in – plane. Two new transducers were manufactured with higher load capacity. Production details are given in Figure 3.12 – 3.14. These transducers were placed under the exterior columns.

To attain moment, shear and axial forces simultaneously six minor load cells were assembled in each transducer. Four of these load cells were placed vertically whereas other two were placed diagonally. Six axial load readings were transformed later on to axial force, shear force and moment via a transformation matrix which was obtained after many calibration tests.

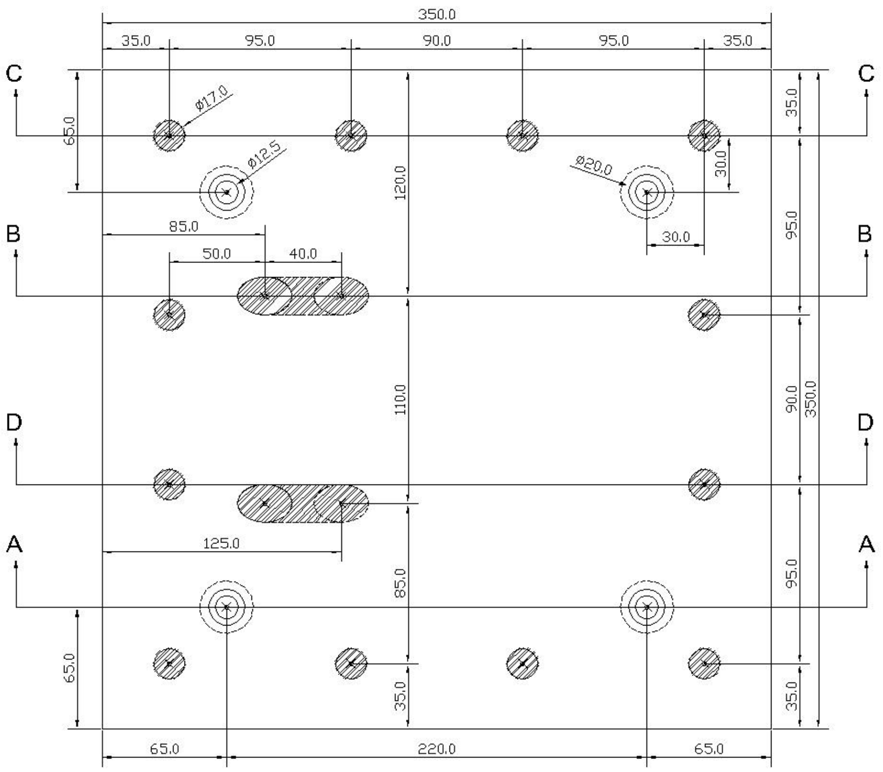


Figure 3.12 Plan of the transducer

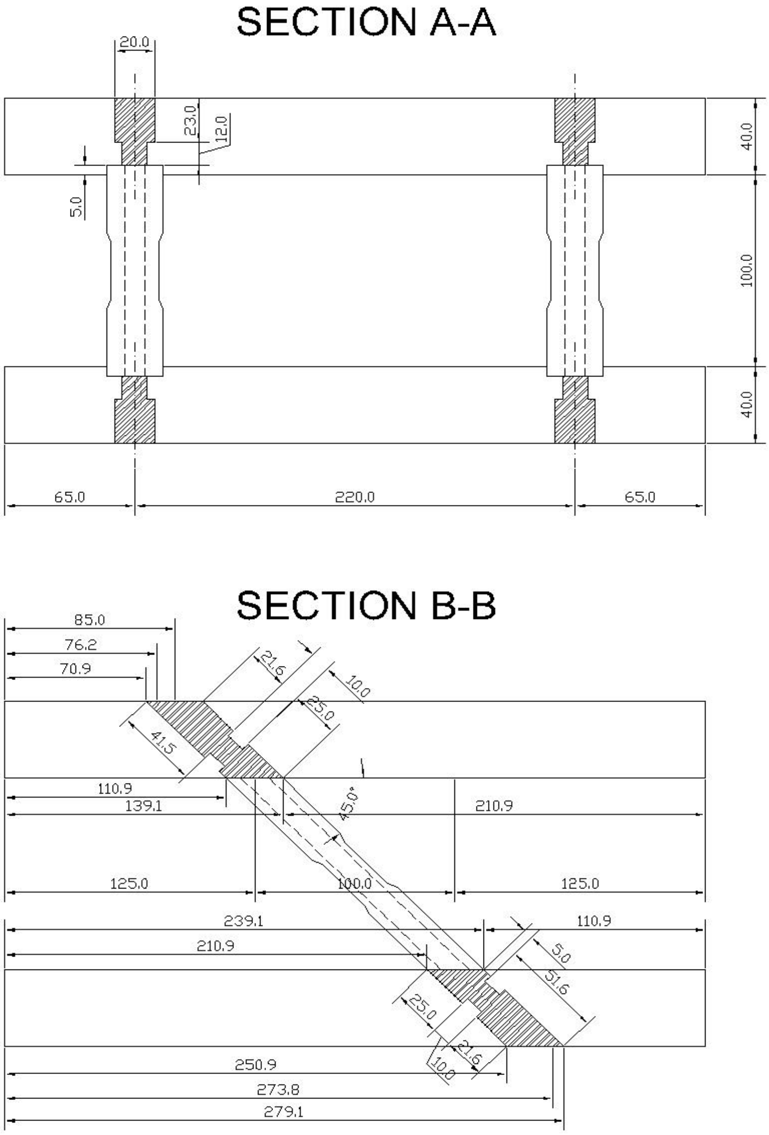


Figure 3.13 Details of the Section A-A and B-B

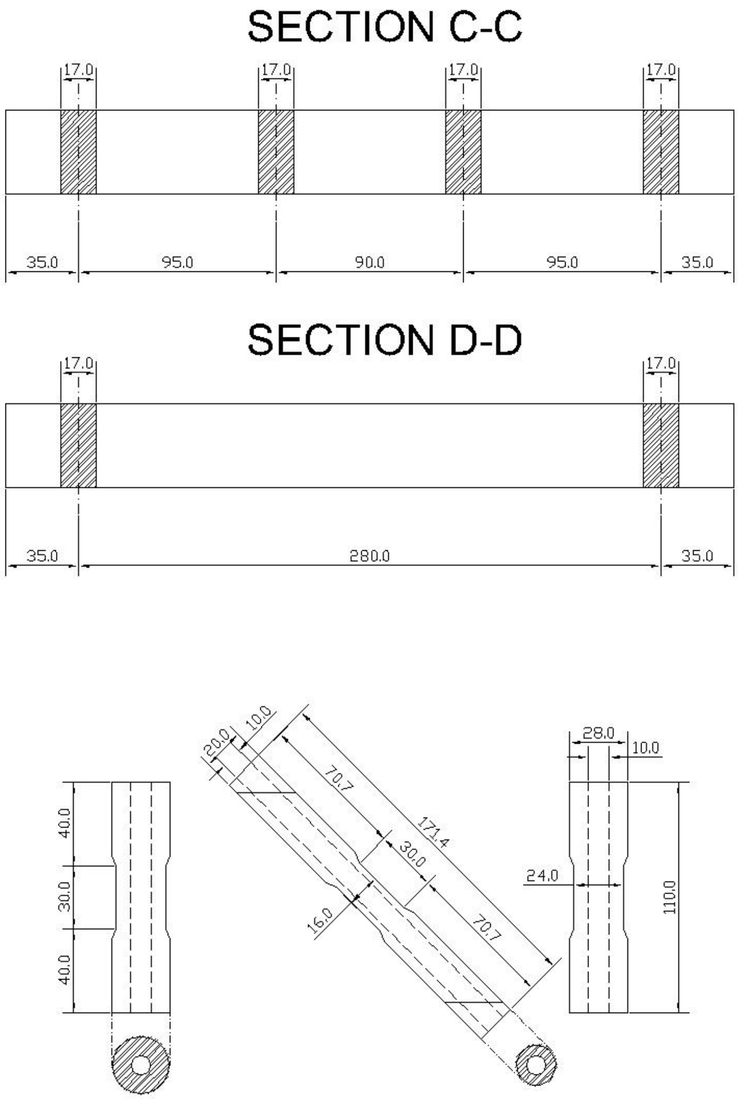


Figure 3.14 Details of the Section C-C and D-D and bar details of the transducer

### 3.5 Test setup and loading system

The testing system was composed of the foundation, reaction wall, computer controlled actuators, loading equipment, instrumentation and data acquisition system (Figure 3.15). Besides, a steel frame was constructed around the specimen for emergency purposes. The steel blocks on the beams were hung with steel cables to the emergency steel frame around the test frame to prevent any accidental fall.

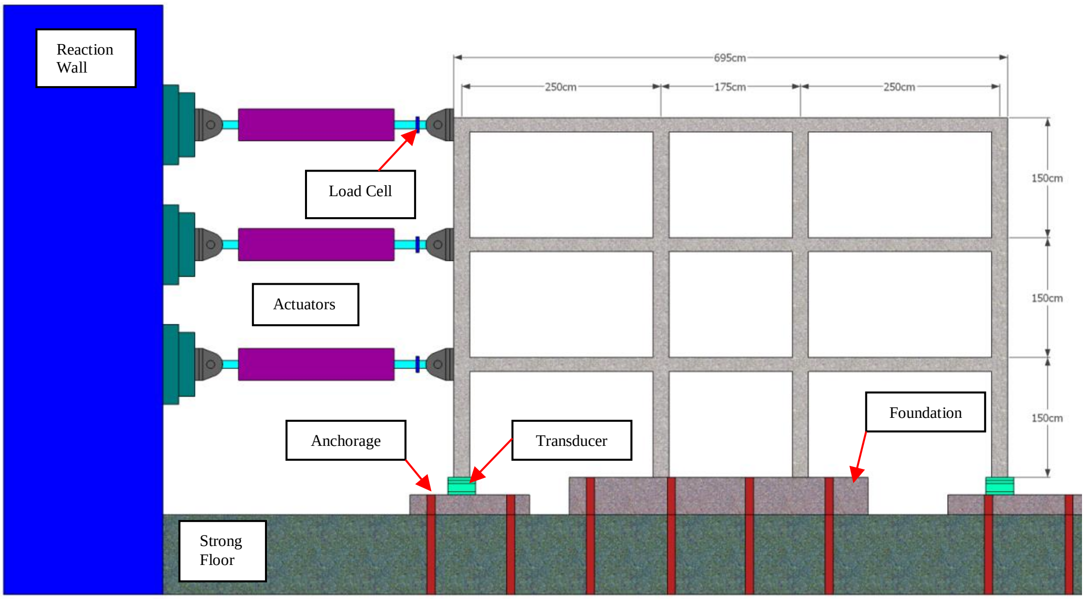


Figure 3.15 Test Setup

Lateral forces were applied by means of the strong reaction wall of the laboratory. The lateral loading system consisted of three actuators. The 250 kN capacity actuator was used at the first floor and 500 kN capacity actuators were mounted at the second and third floor. The actuators were attached to the reaction wall. In order to ease the alignment of actuators, moveable steel adaptors were designed and located between the reaction wall and actuators (Figure 3.16).

Actuators were pin – connected at both ends to the reaction wall and test frames in order to give pure axial load, excluding any moment. Pushing force was applied via the reaction wall and actuators directly to the test frames. Reverse loading was applied again as compression from the opposite side of actuators by pulling high strength bars extending throughout the length of frames. Symmetrically placed four bars were used for pulling the frame as shown in Figure 3.17.

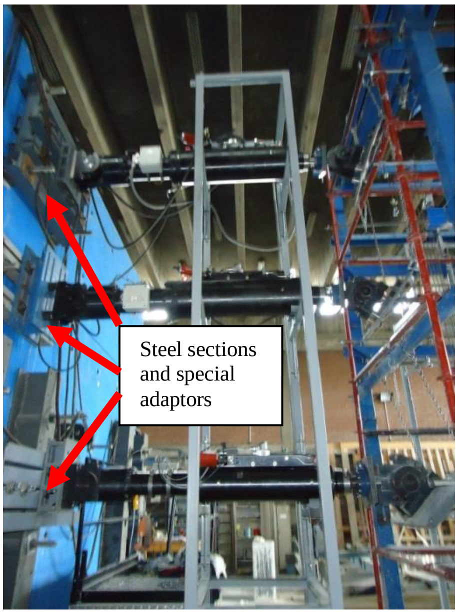


Figure 3.16 Actuators and rigid wall connections

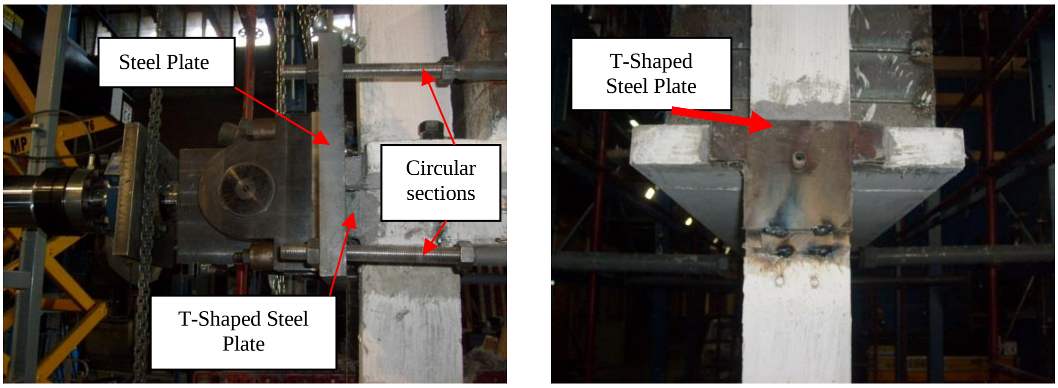


Figure 3.17 Actuator frame connection region

Story loads were employed by using steel blocks. As given in Table 3.6, two different block dimensions were employed to get different load combinations. The distribution of the load for bare and infilled frames is provided in Table 3.7 and Figure 3.8. A general view of the mass blocks is shown in Figure 3.19, Figure 3.22 and Figure 3.23.

Table 3.6 Weight of mass blocks and distribution of the blocks on each floor

| **Dimensions of Plates** | **100×500×500 mm** | **100×200×500 mm** |
|---|---|---|
| **Number of Plates** | **Weight of Blocks (kg)** | **Weight of Blocks (kg)** |
| **3** | 589.5 | 235.8 |
| **4** | 786 | 314.4 |
| **5** | 982.5 | 393 |
| **6** | 1179 | 471.6 |

Table 3.7 Weight distribution of the blocks on each floor (bare frame)

| | **Exterior Bay (ton)** | **Middle Bay (ton)** | **Total mass of Story (ton)** |
|---|---|---|---|
| **1st Floor** | 3.93 | 2.55 | 10.41 |
| **2nd Floor** | 3.93 | 2.55 | 10.41 |
| **3rd Floor** | 2.59 | 1.77 | 6.96 |
| | | **Total Mass** | **27.79** |

Table 3.8 Weight distribution of the blocks on each floor (infilled and strengthened frame)

| | **Exterior Bay (ton)** | **Middle Bay (ton)** | **Total mass of Story (ton)** |
|---|---|---|---|
| **1st Floor** | 4.72 | 0.00 | 9.43 |
| **2nd Floor** | 4.72 | 0.00 | 9.43 |
| **3rd Floor** | 3.26 | 2.36 | 8.88 |
| | | **Total Mass** | **27.75** |

### 3.6 Details of test specimens

The test frame was selected from the middle axis of a 3 story prototype building as shown in Figure 3.18. In order to realistically represent building behavior, a three story frame was chosen as the test frame. Due to the physical limitations of the laboratory, the test frame was scaled down to ½.

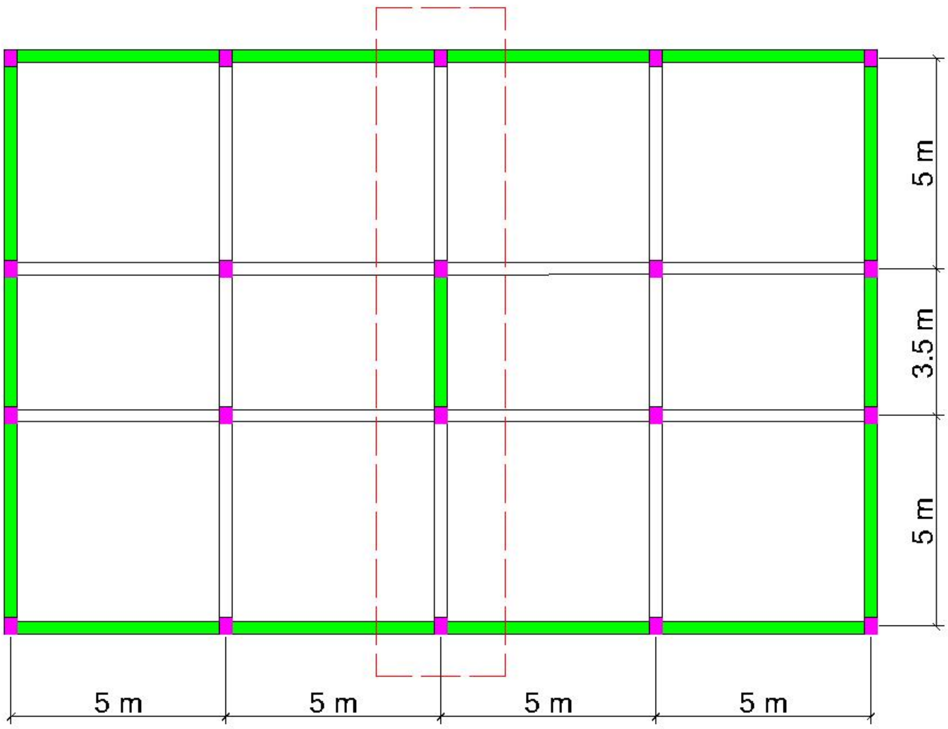


Figure 3.18 Plan view of prototype building

### 3.6.1 Bare frame

The bare frame was designed to represent deficiencies observed in code non-conforming reinforced concrete buildings. A list of the deficiencies and requirements is shown in Table 3.9. A general view of the bare frame is represented in Figure 3.19. Material properties of the bare frame have previously been given in the Section 3.2.

The dimensions of the structural elements and reinforcement details are presented in Section 3.5.1. The deficient frame (according to the Turkish Earthquake Code) was obtained by selecting material properties and reinforcement detailing. Dimensions of the column and beams were 150×200 mm and 175×150 mm, respectively. The beam was designed with a flange of 60 mm thickness and 500 mm width to represent the slab. Moreover, these flanges provided space to place the steel blocks.

Table 3.9 Deficiencies of bare frame and requirements

| **Deficiencies** | **Requirements** |
|---|---|
| Low concrete compressive strength | Minimum concrete compressive strength |
| Low reinforcement yield and ultimate strength | Minimum reinforcement yield and ultimate strength |
| Usage of plain bars | Usage of deformed bars |
| 90-degree hooks of ties | 135-degree hooks of ties |
| inappropriate detailing of longitudinal reinforcement | Code conforming detailing of longitudinal reinforcement |
| Insufficient confinement of both beams and columns | Code conforming confinement of both beams and columns |
| lack of transverse reinforcement at beam-column joints | Use of transverse reinforcement at beam-column joints |
| Strong beam – weak column | Strong column – weak beam |
| Insufficient lateral load carrying capacity | Proper lateral load carrying capacity |
| Soft story | Limited relative story drifts |


Figure 3.19 General View of bare frame

Reinforcement was detailed such that it violated the Turkish Earthquake code provisions. 8ϕ8 plain bars were used as longitudinal reinforcement in columns. There was no confined zone at the column ends and ϕ4 plain bars were used as ties with 100 mm spacing. 3ϕ10 plain bars were placed at the midspan of beams as tension reinforcement. 4ϕ10 plain bars were provided at the support region as tension reinforcement and two of them continued to the midspan of the beam as hanger bars. A 50 mm tie spacing was selected at the confined zone of beams for 350 mm distance. Tie spacing was increased to 80 mm at mid region. ϕ4 plain bars were used also as stirrups for beams (Figure 3.20). Although the Turkish Earthquake Code (TEC 2007) specifies oblique 135° hooks, tie – ends were bent only 90° and furthermore, tie were not continued at the joints (Figure 3.21).

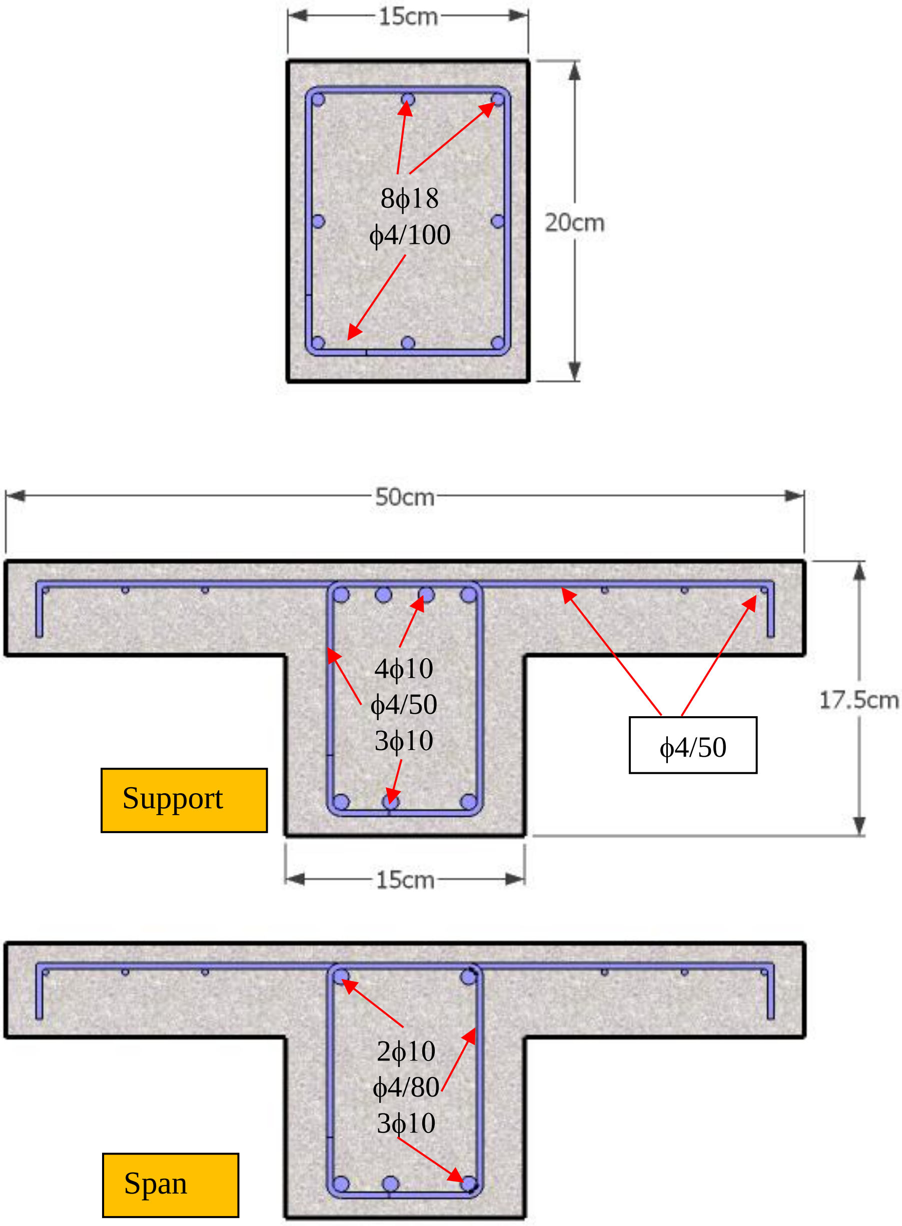


Figure 3.20 Reinforcement details of columns and beams

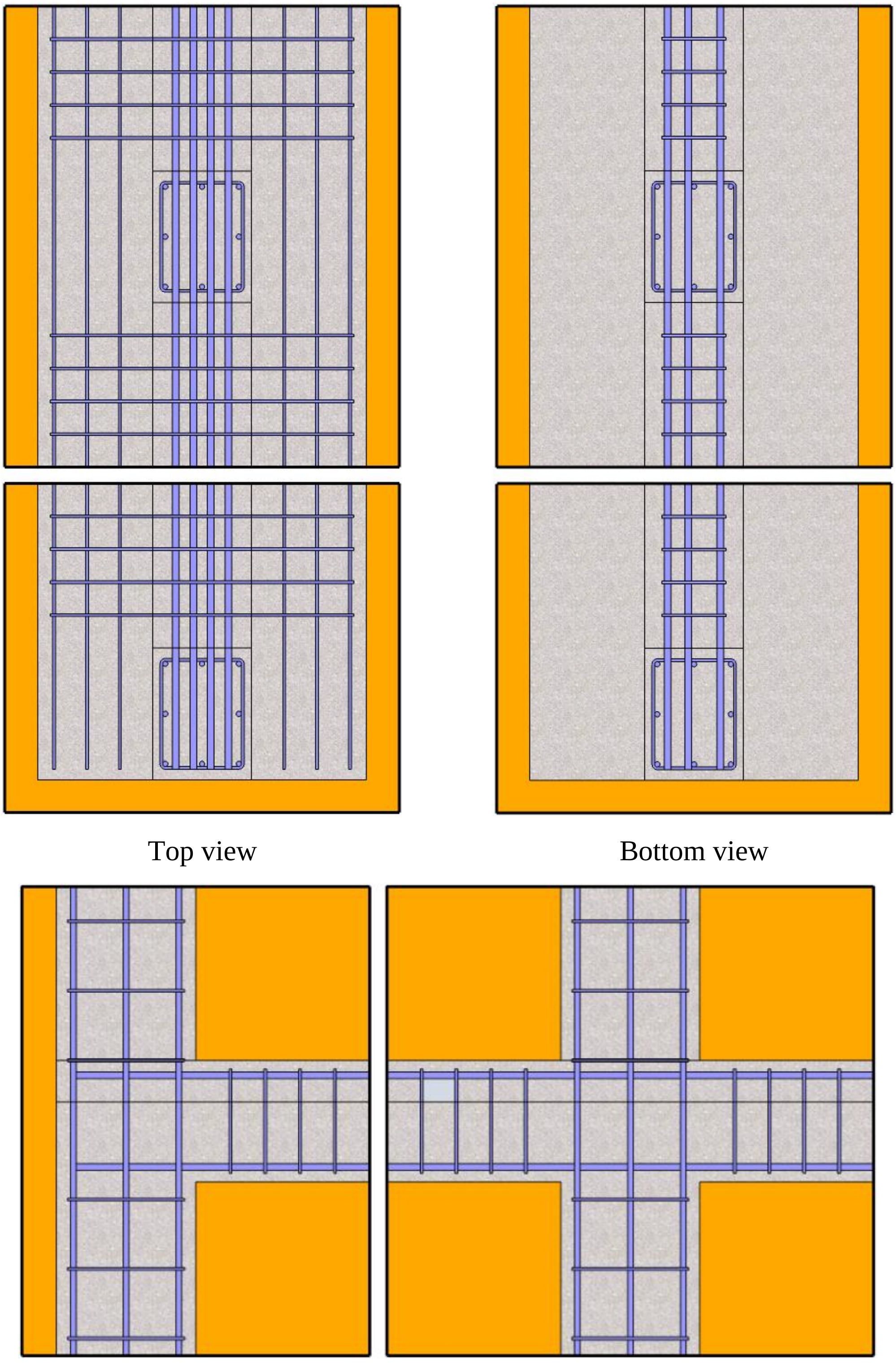


Figure 3.21 Reinforcement details with top, bottom and side views

### 3.6.2 Infilled frame

The same reinforcement detailing was followed for the infilled frame. Moreover, the same concrete strength was targeted to enable the comparison of the test results. Infill walls, although regarded as non –structural components, do have a crucial impact on frame behavior as explained previously. In order to better comprehend this effect, infill walls were constructed at the middle bays of each stories. Figure 3.22 shows this layout clearly. Material properties of the bricks and mortar are presented in Section 3.2.4.

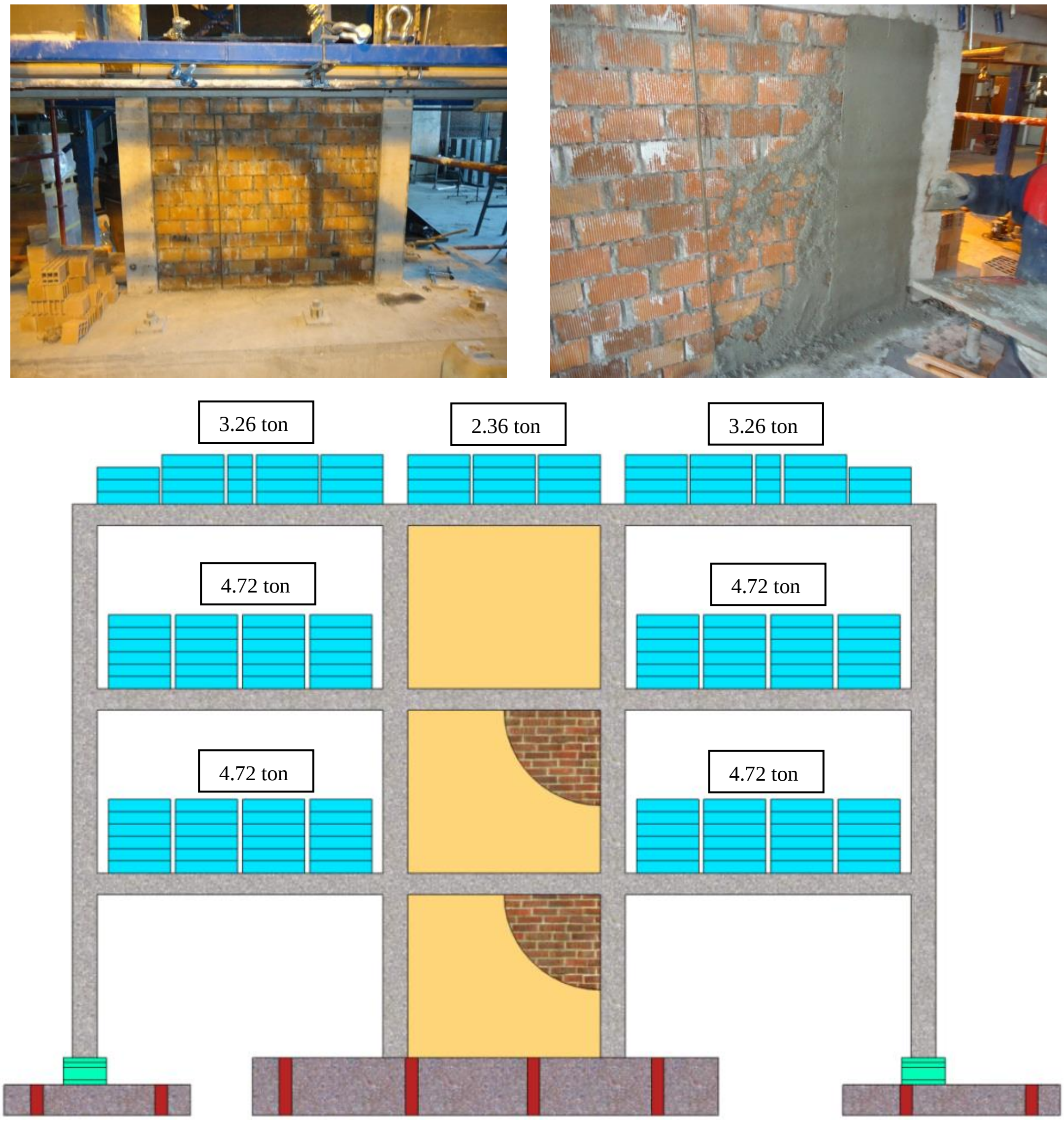


Figure 3.22 General view of infilled frame

### 3.6.3 Strengthened frame

A specimen identical to the infilled frame was constructed with similar sectional details and similar material properties. Infill walls were afterwards strengthened with ECC panels as shown in Figure 3.23. The material properties were already mentioned in Chapter 2. Nine precast ECC panels with 25 mm thickness were bonded on the front sides of the infill walls at each floor with epoxy adhesive mortar (Sikadur 31). The epoxy adhesive mortar had 55 MPa compressive strength, 6 MPa tensile strength, 3.5 MPa adhesion to concrete, and 20 MPa adhesion to steel. The mechanical properties of adhesive mortar were taken from the product data sheet. Panel dimensions varied slightly, but had approximately 510×435 mm rectangular shape.


Figure 3.23 General view of strengthened frame

To enable proper force transfer between the strengthened infill wall and surrounding frame, 10 mm anchorages were used for proper interaction between the structural elements (beam and columns) and ECC panels. 14 mm holes were drilled diagonally into the beam and column cores and anchor bars were attached with epoxy to the frame (Figure 3.24). Drilling procedure for anchorages should be conducted precisely and carefully to avoid unexpected damages on column or beam reinforcement bars. Construction stages are provided in Figure 3.25.

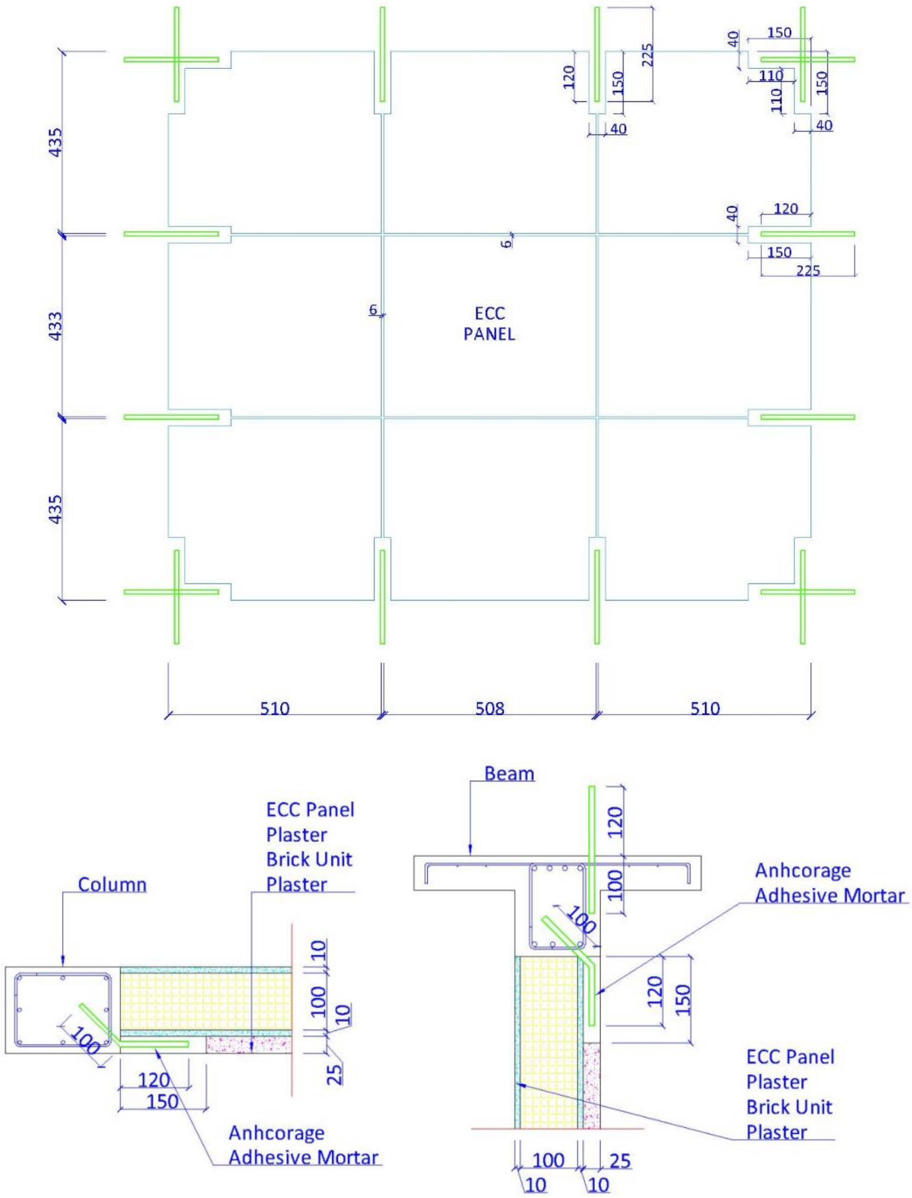


Figure 3.24 ECC panel dimensions and anchorage details

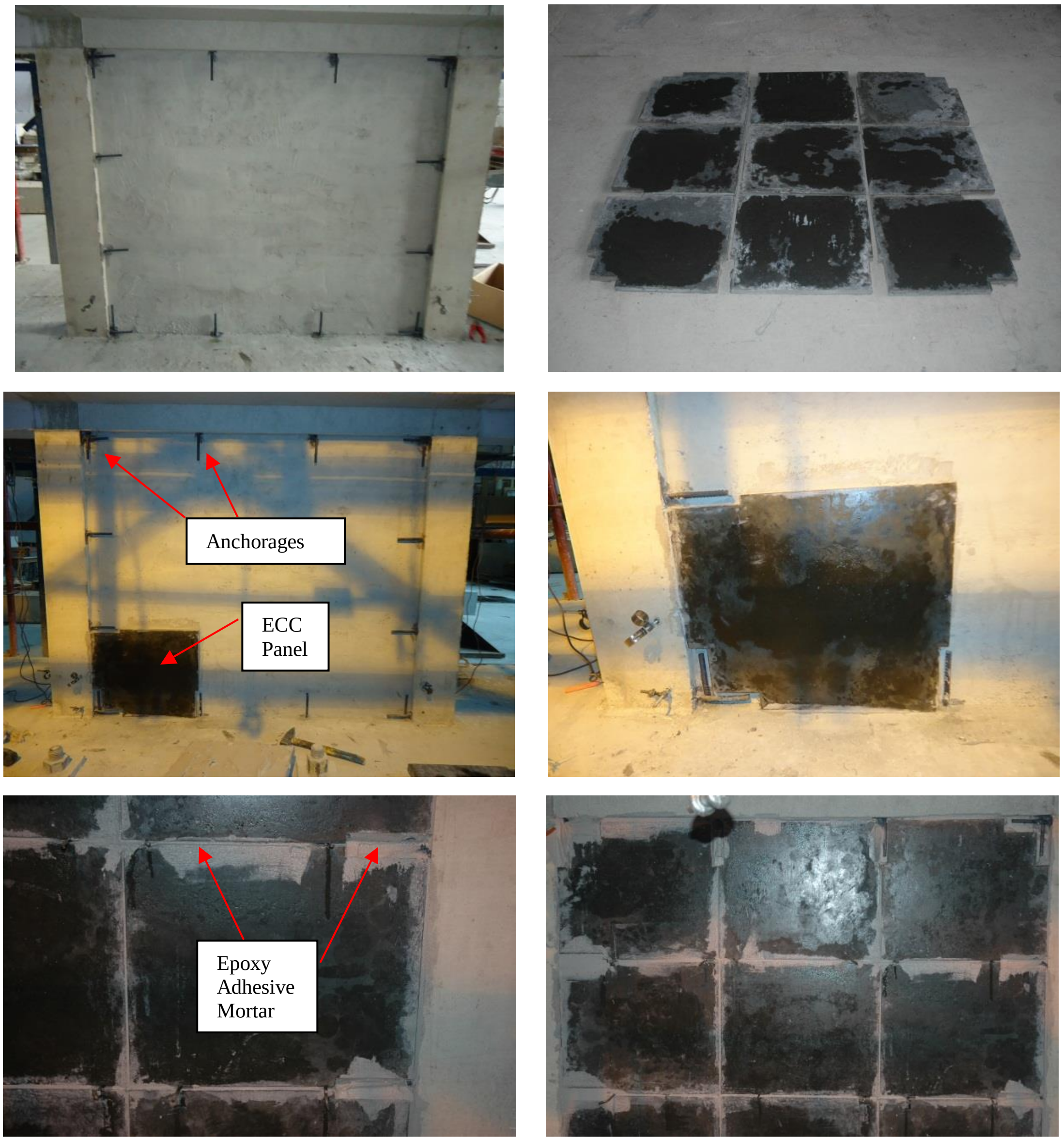


Figure 3.25 Assemblage of ECC Panels on test Frame

# CHAPTER 4

# EXPERIMENTAL RESULTS

## 4.1 Synthetic ground motion

Synthetic earthquake ground motions were generated from the Düzce Earthquake record, which match the design spectrum of the Turkish Earthquake Code. The properties of the generated motions are listed below and shown in Figure 4.1 and Figure 4.2 as ground acceleration and spectral acceleration.

- D1: Exceedance Probability of 50% in 50 years for local site class Z1/Rock
- D2: Exceedance Probability of 10% in 50 years for local site class Z1/Rock
- D3: Exceedance Probability of 10% in 50 years for local site class Z3/Soft Soil

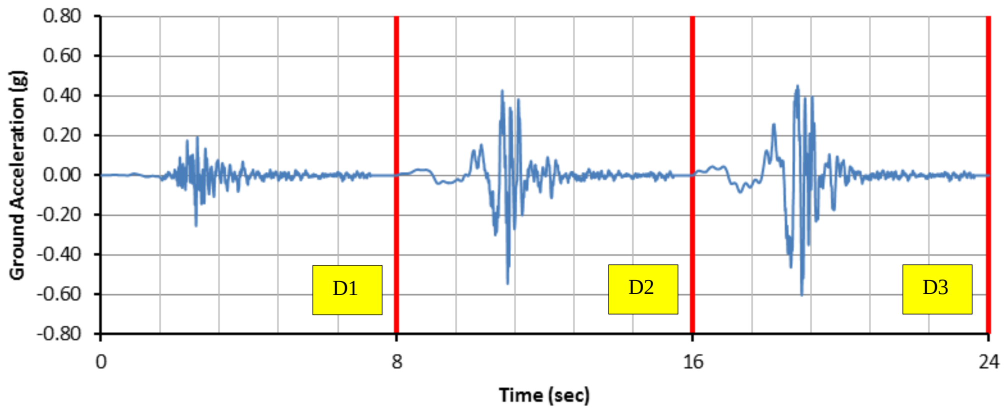


Figure 4.1 Ground acceleration time history

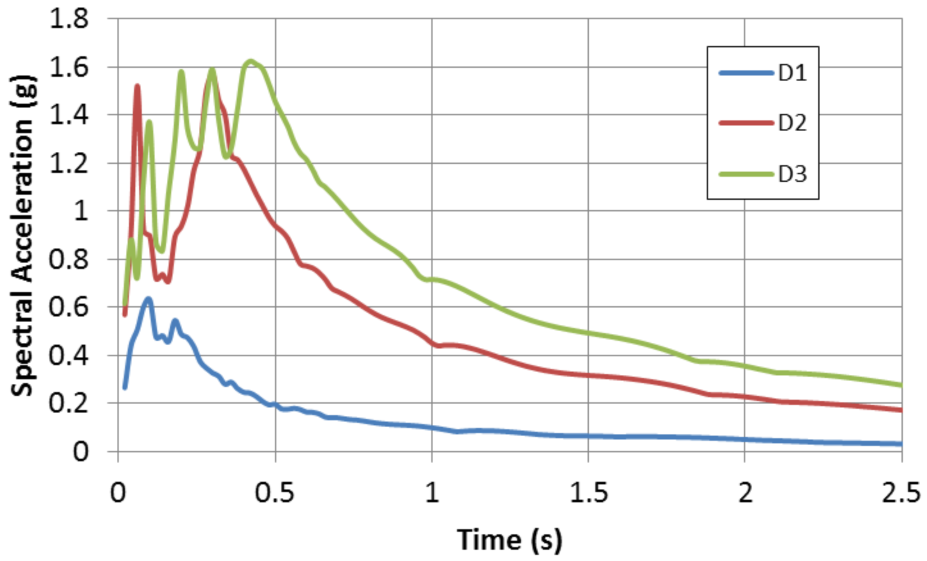


Figure 4.2 Response spectra of ground motions

### 4.2 Test results

All frames (bare frame, infilled frame and strengthened frame) were tested for each ground motion, D1, D2 and D3, successively. The roof displacement time history graphs, observed damages at certain stages marked on time history graphs, inter – story drift ratio time history graphs, and base shear – roof displacement graphs have been provided in this section. These graphs comprise all ground motions, D1, D2 and D3.

#### 4.2.1 Bare frame

No noticable damage was observed on the bare frame during the D1 motion. D1 motion caused 9 mm maximum roof displacement and 0.27% maximum inter-story drift ratio. There was almost no residual displacement at the end of D1 motion (Figure 4.3). During the D2 earthquake, roof displacement increased to 47 mm. There were local flexural cracks in both exterior and interior columns, and also diagonal shear cracks at joint regions (Figure 4.4). It should be noted that columns had no confined zones at the ends and there was no transverse reinforcement in the beam-column joint regions. The maximum inter-story drift ratio was 1.31% during D2 (Figure 4.5).

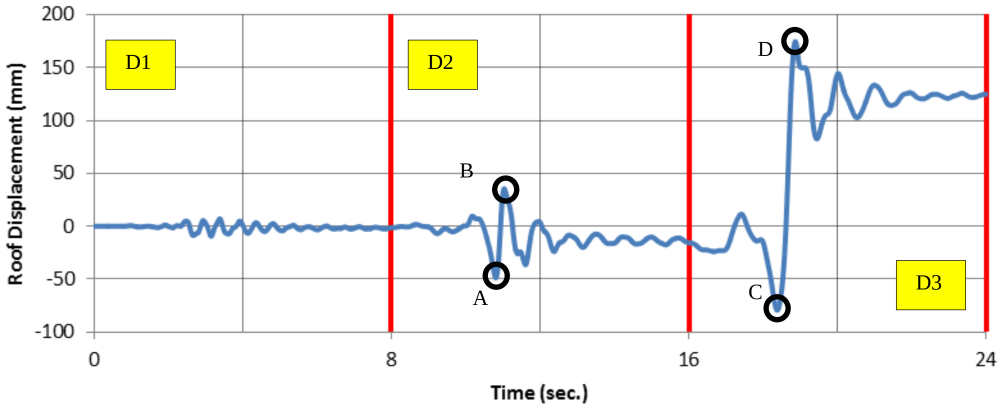


Figure 4.3 Roof Displacement Time History (bare frame)

Column longitudinal reinforcement was bent in L – shape in the beam-column joint region at the top floor. The longitudinal reinforcement of the bare frame was cut at the top floor level for observing this type of deficiency. Cracks formed at the upper part of the column ends during the D3 ground motion. Therefore, the maximum roof displacement and permanent deformations increased.

The base shear–roof displacement curve exhibited nonlinear behavior during this earthquake excitation (Figure 4.6). The D3 earthquake resulted in a roof displacement of 190 mm and a maximum inter-story drift ratio of 4.93%. There were severe flexural cracks at the beam ends, and the base of the exterior and interior columns. The top of the third-floor columns had serious flexural cracks. Joint diagonal cracks spread even into the slab. Large residual displacements (1st story: 42 mm, 2nd story: 94 mm and 3rd story: 140 mm) were measured at the end of the experiment.

The maximum column end rotations of the first and second story are represented in Table 4.1. Peak rotations measured at D3 ground motion pointed out significant flexural plastic damages. Joint deformations and column rotations contributed to the lateral displacement of the bare frame.

-A-

-A-

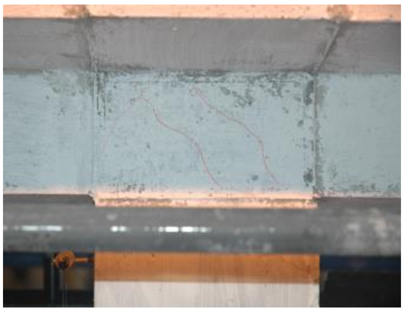

-B-

-B-

D2 Earthquake (bare frame)

-C-

-C-

-D-

-D-

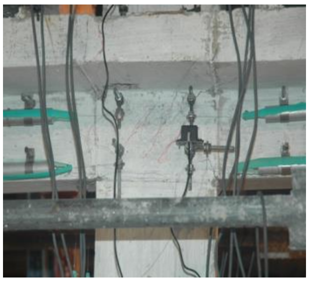

-D-

-D-

D3 Earthquake (bare frame)

Figure 4.4 Observed Damages Related to D2 and D3 Earthquake (bare frame)

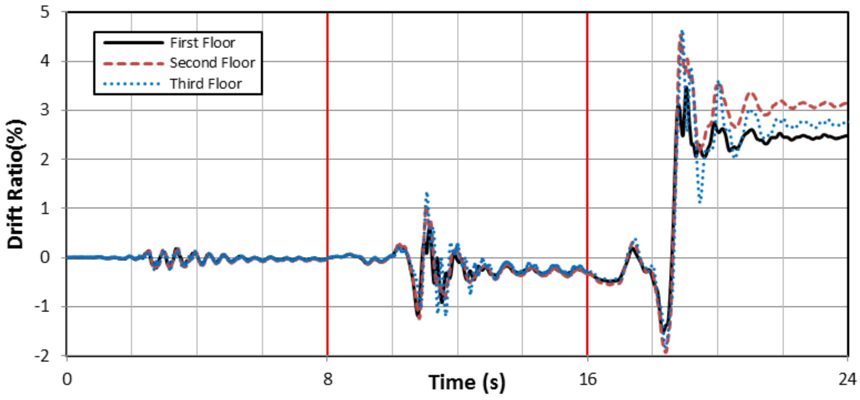


Figure 4.5 Inter Story Drift Ratio Time History (bare frame)

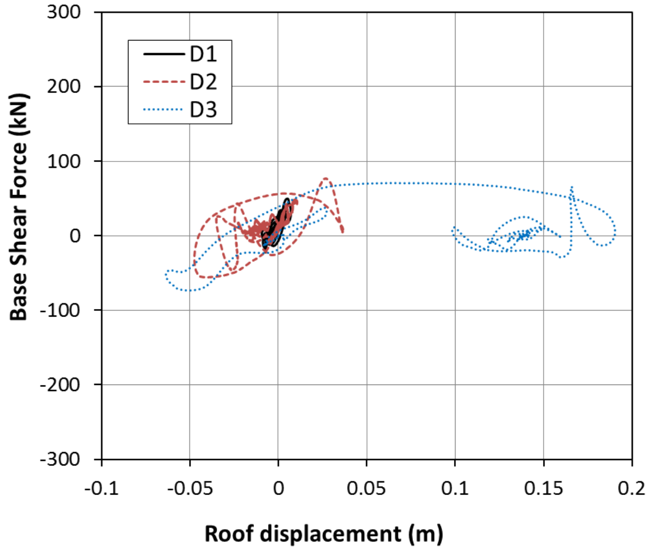


Figure 4.6 Base shear vs. roof displacement curves of bare frame

Table 4.1 Maximum column end rotations of bare frame

| | 1st Story | | 2nd Story | |
|---|---|---|---|---|
| | Bottom | Top | Bottom | Top |
| D1 | 0.00136 | 0.00137 | 0.00079 | 0.00148 |
| D2 | 0.01088 | 0.00738 | 0.00596 | 0.00707 |
| D3 | 0.04272 | 0.02192 | 0.01639 | 0.03422 |

### 4.2.2 Infilled frame

The D1 motion caused 4 mm maximum roof displacement and a maximum drift ratio of 0.1% (Figure 4.7). The masonry infill wall reduced the displacement demands significantly under the same earthquake as compared to the bare frame. Minor boundary cracks formed in the first-floor level between the interior columns and the infill wall. Furthermore, hairline flexural cracks were observed in the first story beams. The D1 earthquake caused almost no residual displacement. The beneficial effect of the infill walls at small deformation demands was confirmed with these observations. During the D2 earthquake, the maximum roof displacement and drift ratio were 21 mm and 0.48%, respectively. These values were less than half of those measured in the bare frame test. The corner of the plaster on the infill wall crushed during this earthquake level (Figure 4.8). Diagonal shear cracks were visible on the infill wall due to the strut and tie mechanism. The compression strut caused diagonal shear cracks at the column ends. The maximum roof displacement and drift ratio were 41 mm and 1.88% during the D3 ground motion. The maximum drift was observed at the first floor. Maximum drift ratios at the second and third floor were 0.72% and 0.66%, respectively (Figure 4.9). Separation and closure between the infill wall and neighbor column was significant during the D3 motion. There were severe shear cracks at the top of the first story columns. After spalling of the cover concrete at this region the longitudinal reinforcements buckled.

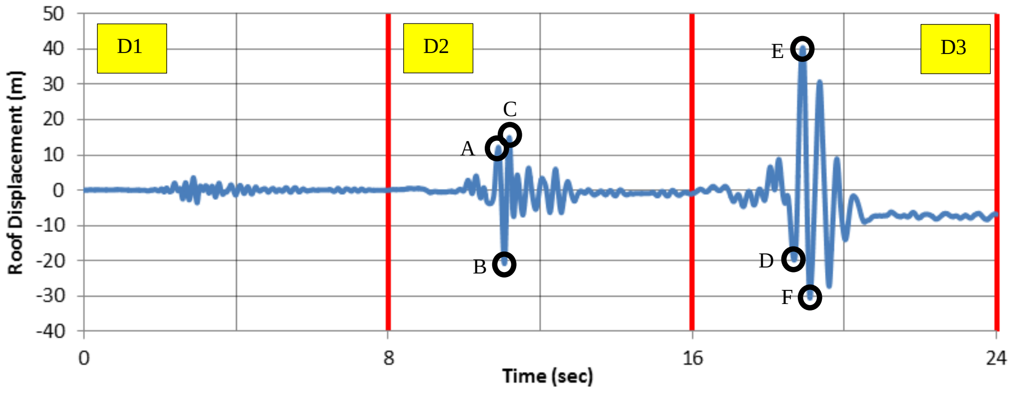


Figure 4.7 Roof displacement time history (infilled frame)

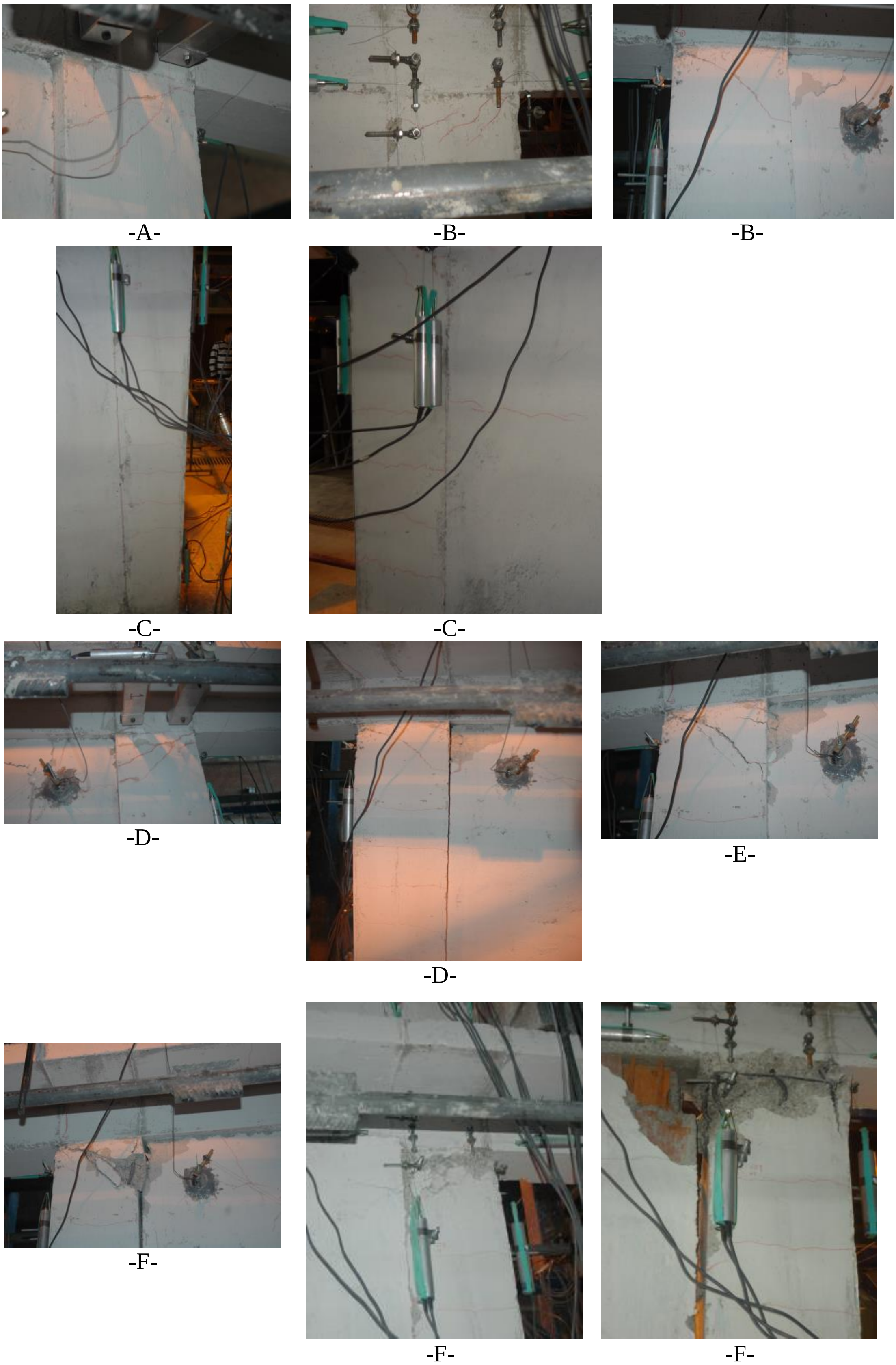


Figure 4.8 Observed damages related to D2 and D3 earthquake (infilled frame)

While the infill walls increased the stiffness of the frame, they also resulted in an increase in the base shear demand. The maximum base shear was measured as 77 kN during the bare frame test, whereas the maximum base shear was 189 kN during the infilled frame test (Figure 4.10). In the D3 motion, the first story column end rotations were significantly higher than those measured in the second story (Table 4.2). This unbalanced distribution of column end rotations denoted the formation of a soft story upon failure of the infill wall.

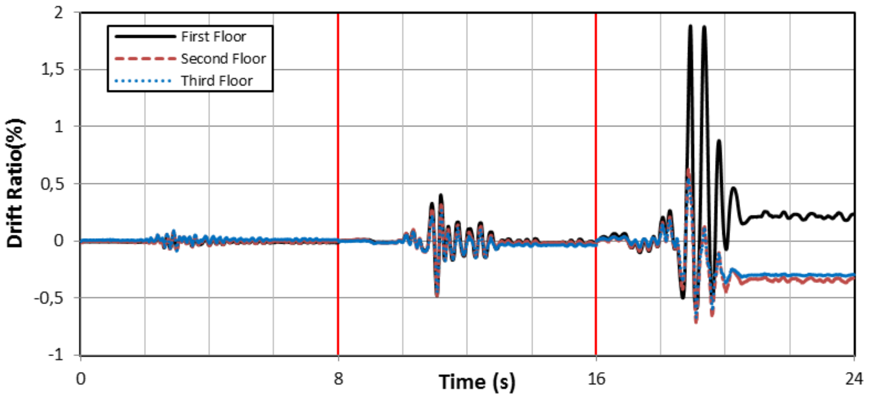


Figure 4.9 Inter story drift ratio time history (infilled frame)

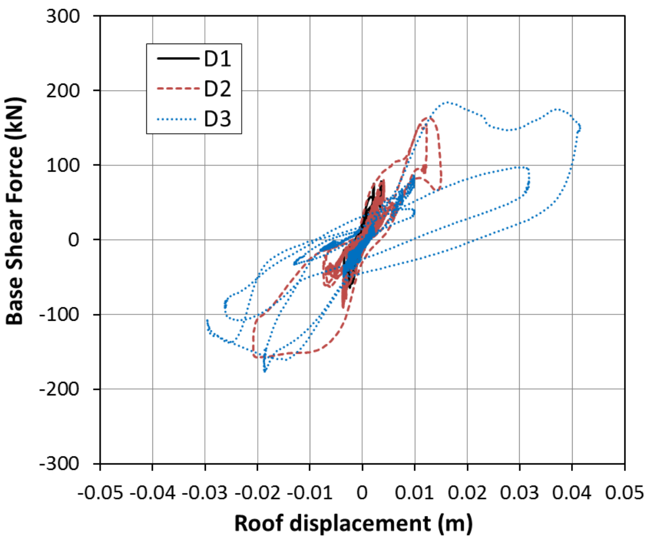


Figure 4.10 Base shear vs. roof displacement curves (infilled frame)

Table 4.2 Maximum column end rotations of infilled frame

| | 1st Story | | 2nd Story | |
|---|---|---|---|---|
| | Bottom | Top | Bottom | Top |
| D1 | 0.00053 | 0.00073 | 0.00060 | 0.00076 |
| D2 | 0.00425 | 0.00551 | 0.00341 | 0.00357 |
| D3 | 0.02038 | 0.02609 | 0.00757 | 0.00495 |

### 4.2.3 Strengthened frame

This specimen was strengthened by means of ECC panels attached to the brick infill wall. The D1 Earthquake caused 3.7 mm maximum roof displacement and 0.09% maximum drift ratio (Figure 4.11). Boundary cracks were observed between the ECC panels and surrounding structural elements (Figure 4.12). The specimen displayed elastic behavior during this ground motion with no visible damage.

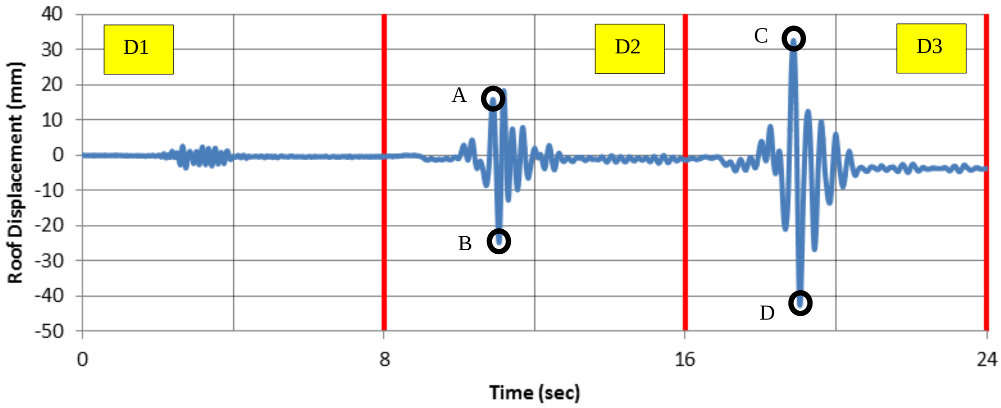


Figure 4.11 Roof displacement time history (strengthened frame)

ECC panels were effective in eliminating infill cracking at small deformation demands. The D2 earthquake caused 24 mm roof displacement. Maximum drift ratios of the first, second and third floors were 0.50%, 0.60% and 0.53%, respectively. The main damage was the flexural cracks on columns and cracks in anchorage regions of the bottom corner panels (Figure 4.13). The ECC panels did not sustain any damage, thereby proving the strength and stiffness enhancement obtained by the proposed strengthening technique. The column flexural cracks became widespread and crack widths increased. At the base of the infill wall cracks widened and a sliding behavior was observed during D3 ground motion (Figure 4.14).

Figure 4.12 Observed damages related to D1 earthquake (strengthened frame)

- A and B-

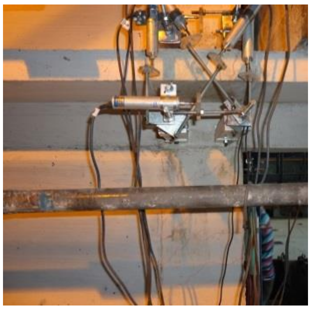

- A and B-

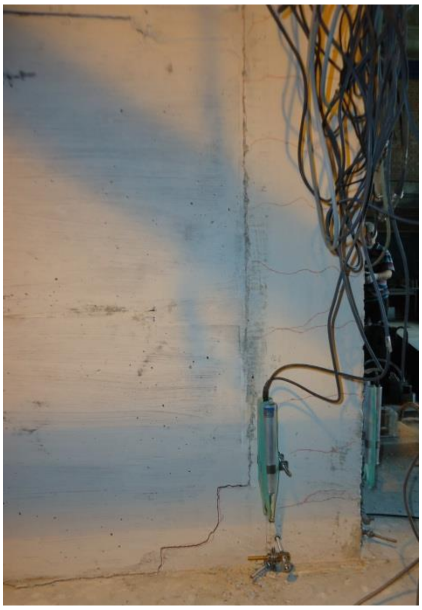

- A and B -

- A and B -

Figure 4.13 Observed damages related to D2 earthquake (strengthened frame)

- C -

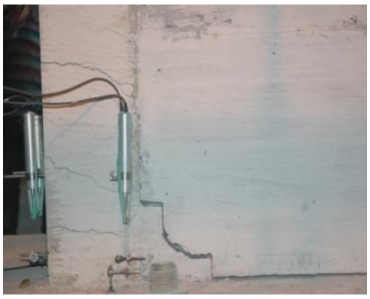

- C -

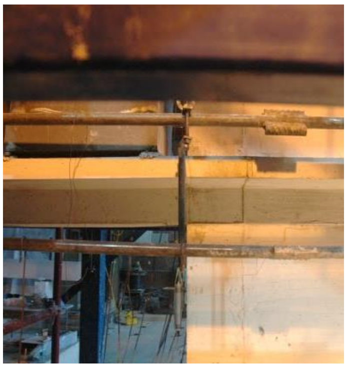

- D -

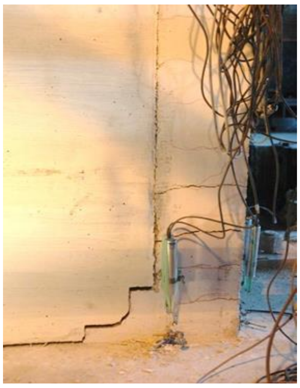

- D -

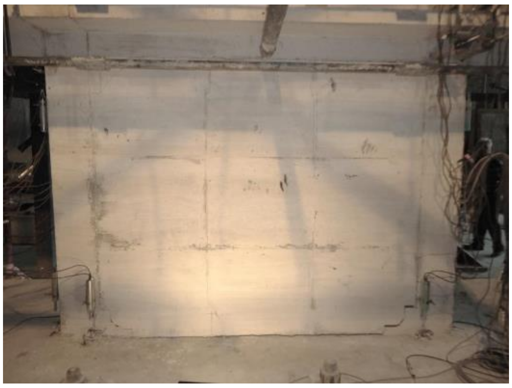

- D -

-C-

Figure 4.14 Observed damages related to D3 earthquake (strengthened frame)

The D3 motion resulted in an increase of the roof displacement to 41 mm and drift ratio to 0.86% at first story. The second and third story drift ratios were 0.99% and 0.91% (Figure 4.15). Despite the corner anchorage failures of panels, struts of the retrofitted wall increased the base shear capacity of the frame. The base shear force reached to 243 kN as can be observed in Figure 4.16. No strength decrease was observed even at the D3 earthquake level. It can be stated that ECC panels provided good deformation control, strength increase and were able to sustain inelastic deformations without loss of lateral strength. Moreover, the strengthening method reduced the peak column end rotations as shown in Table 4.3. It can be stated that ECC panel retrofit was successful in reducing the story displacement and column end rotation demands while increasing the base shear capacity of the system.

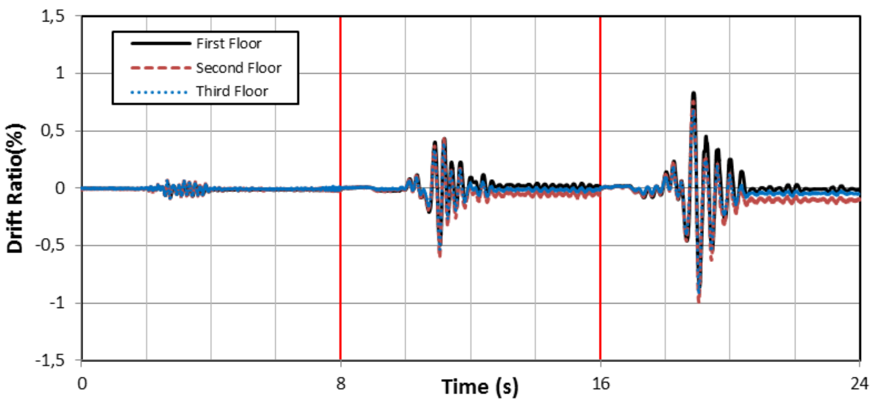


Figure 4.15 Inter story drift ratio time history (strengthened frame)

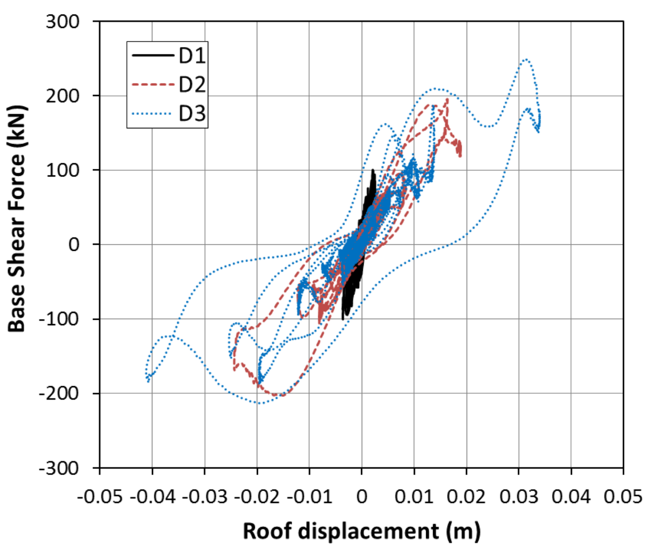


Figure 4.16 Base shear vs. roof displacement curves (infilled frame)

Table 4.3 Maximum column end rotations of strengthened frame

| | 1st Story | | 2nd Story | |
|---|---|---|---|---|
| | Bottom | Top | Bottom | Top |
| D1 | 0.00076 | 0.00119 | 0.00090 | 0.00099 |
| D2 | 0.00820 | 0.00279 | 0.00201 | 0.00295 |
| D3 | 0.01356 | 0.00412 | 0.00303 | 0.00559 |

### 4.3 Plastic column end rotations

Calculated plastic column end rotations have been represented in the bar charts for first and second story columns of each specimen (Figure 4.17). Excessive bottom end rotations were measured for the first story of the bare frame. Furthermore, large lateral displacements increased the second story plastic column end rotations. Infill walls limited the plastic column end rotations as compared to the bare frame. Shear demands during D3 ground motion increased the top column end plastic rotations for interior columns of the infilled frame. ECC panel application on infill walls decreased all column end plastic rotations. However, corner failure of the panels caused limited plastic rotations the interior columns bottom ends at the first story for the strengthened frame.

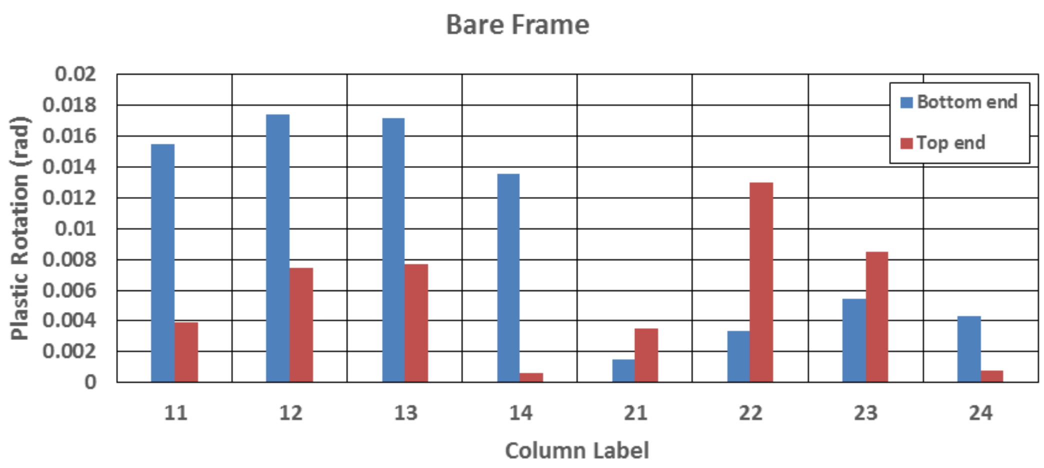


Figure 4.17 Plastic end rotations of first and second story columns (cont'd)

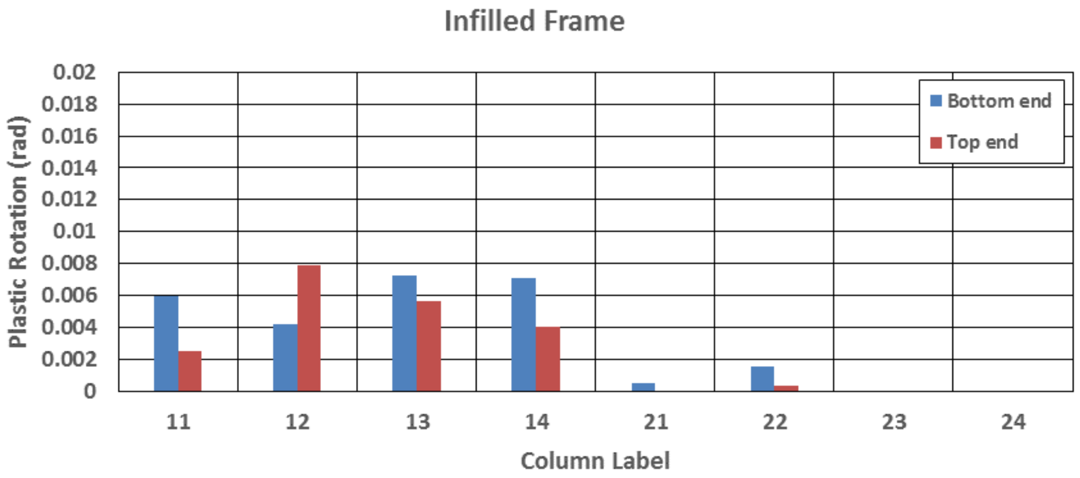


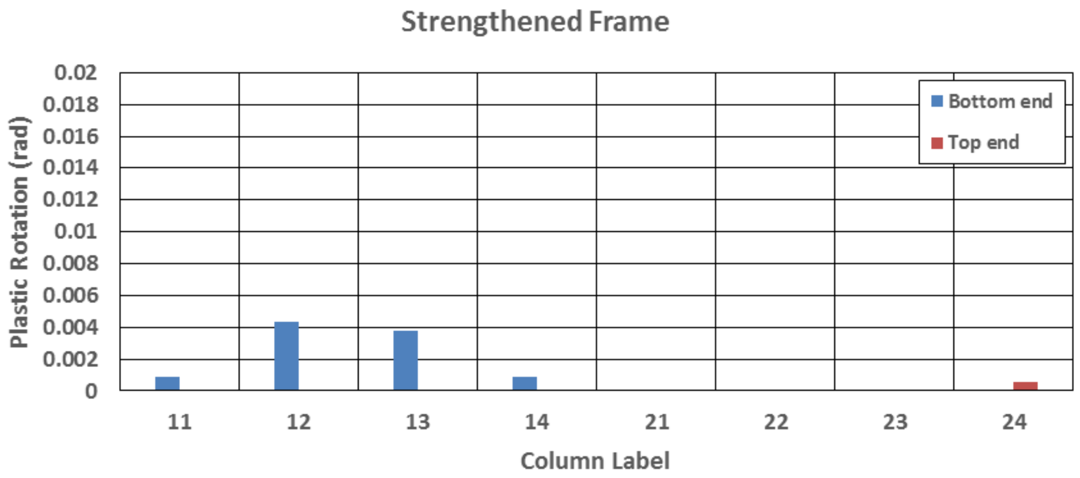


Figure 4.17 Plastic end rotations of first and second story columns (cont'd)

### 4.4 Force transducer results

Force transducers were assembled at the exterior column bases to attain moment, shear and axial forces. As a result, interaction and moment curvature diagrams were obtained for each column. Due to similar trends for each column, only one of the transducer results was evaluated. As seen in Figure 4.18, the axial force of the exterior columns varied between 8% and 12% during bare frame tests. Furthermore, the moment curvature diagram indicated the extreme deformation and plastic hinging at the base of exterior column during the D3 ground motion. The infilled frame axial force varied between 9% and 14%. Moreover, the moment curvature diagram shows the permanent deformation at the end of the D3 ground motion (Figure 4.18). The strengthened frame axial force changed between 9% and 15% for exterior columns during the strengthened frame tests. However, the curvatures remained limited. No excessive drift ratio was observed during D3 ground motion unlike for the bare and infilled frames.

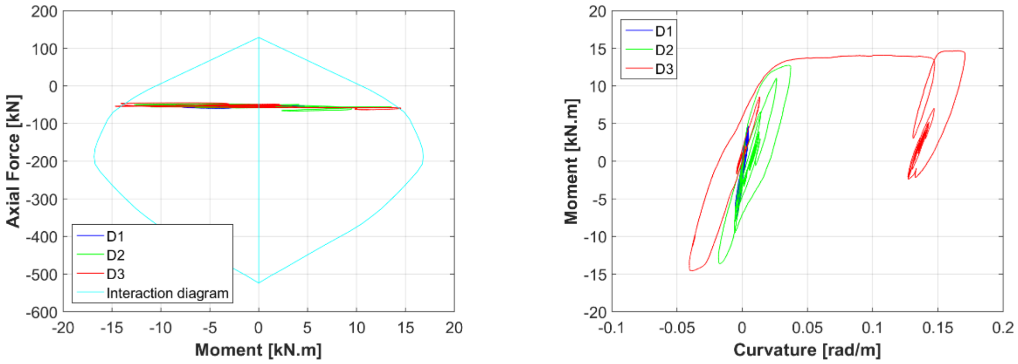

Bare frame

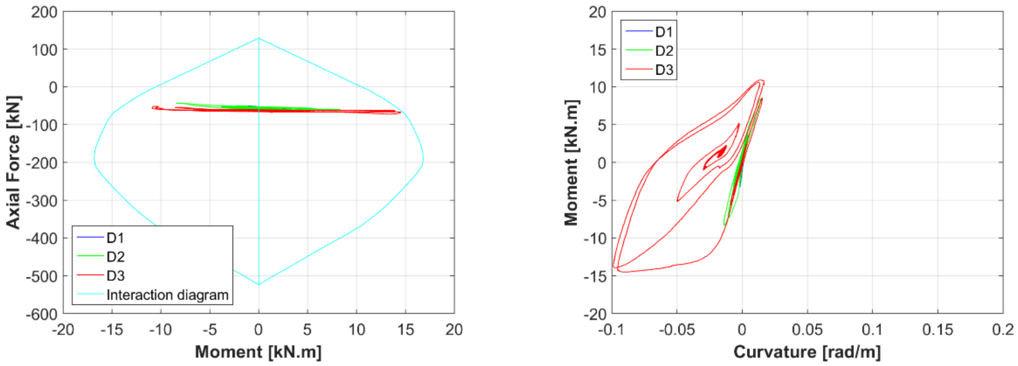

Infilled frame

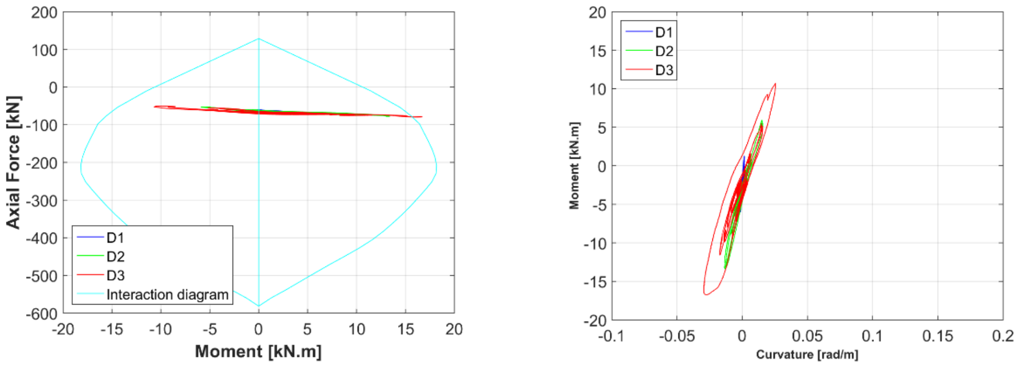

Strengthened frame

Figure 4.18 Column base responses

## 4.5 Energy Dissipation

The energy dissipation of the specimens is demonstrated in Figure 18. Cumulative dissipated energy was calculated by integration of the load measured from the servo-controlled actuator vs. story displacement curve. The bare frame dissipated more energy at the first story compared to other specimens. Excessive flexural column deformations and joint rotations increased the energy dissipation of the bare frame. The infill wall enhanced the lateral force capacity of the frame and also excessive shear damages cause more energy consumption, when total energy dissipation is considered. Damages concentrated on the first floor for the bare and infilled frames, therefore energy consumptions were more than the strengthened frame (Figure 4.19).

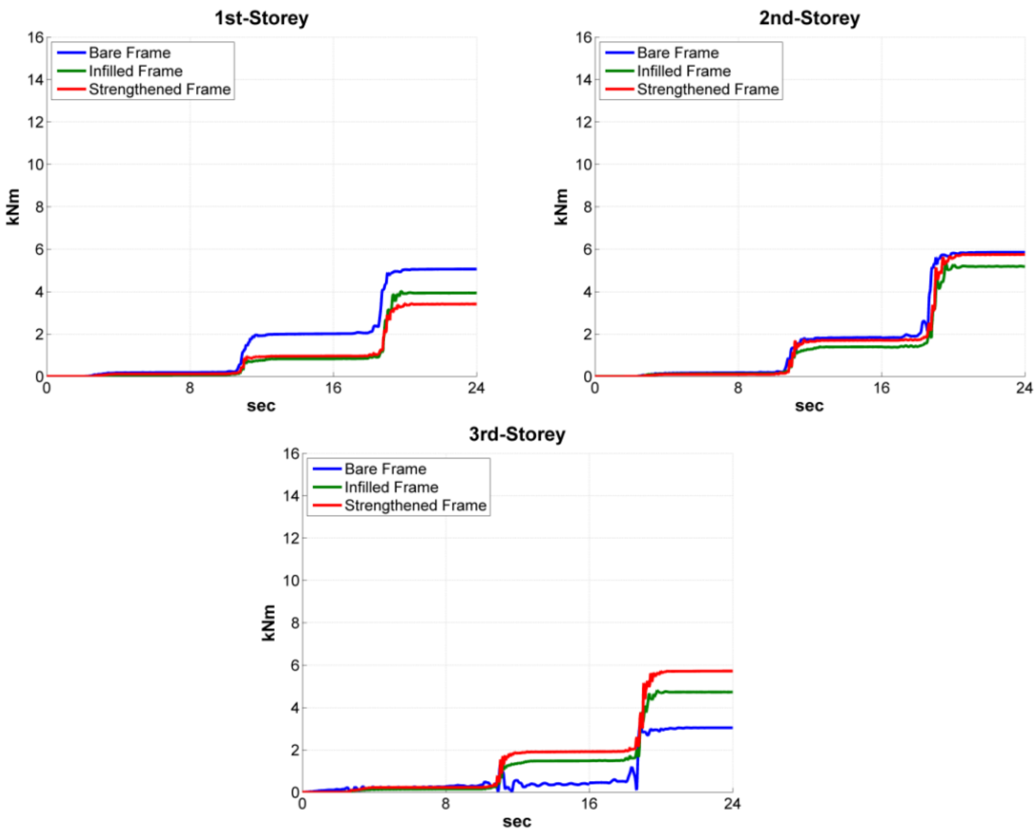


Figure 4.19 Energy dissipation curves for 1$^{st}$, 2$^{nd}$ and 3$^{rd}$ story

Bare, infilled and strengthened specimens reached 4.23 kNm, 3.71 kNm, 4.59 kNm energy levels for the D2 ground motion and 13.97 kNm, 13.85 kNm, 14.89 kNm for the D3 ground motion (Figure 4.20). Although the energy dissipation capacity of the bare frame and infilled frame were similar at the end of the experiment, the strengthened frame had the highest energy dissipation capacity at the end of both the D2 and D3 ground motions. The ECC panel application in infill walls improved the energy dissipation characteristics of the specimens.

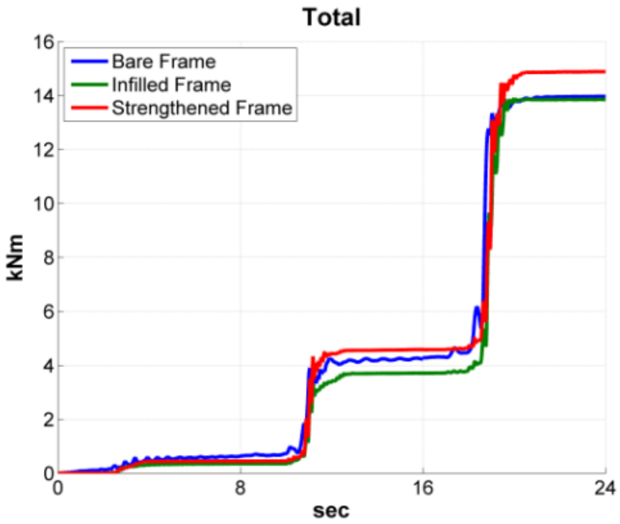


Figure 4.20 Total energy dissipation curves

### 4.6 Discussion of Test Results

A summary of the test results is presented in Table 4.4. A comparison of the specimens indicated that the infilled specimen and strengthened specimen experienced similar displacement demands under the D1 and D2 earthquakes. However, ECC panels helped to avoid the cracking damage observed in the infill walls. It can be stated that ECC panel application was quite successful in keeping the structure undamaged and in eliminating the needs of repair under small to moderate motions.

All stories of the bare frame exhibited at least 2% residual drift after the D3 earthquake. The presence of the brick infill wall limited the drift ratio demands of the upper stories during the D3 earthquake. However, the first floor drift ratio reached to a maximum value of around 2% level following the corner crushing of the infill wall. Strengthening of the infill walls with ECC panels positively affected the drift ratio demands by keeping them below the 1% level. The most important beneficial effect was the relatively uniform drift ratio distribution through stories upon retrofitting with the ECC panels. Furthermore, ECC panels helped the infill wall to remain intact even during the D3 earthquake, and consequently residual drifts of strengthened frame were limited during the D3 earthquake. Moreover, contrary to the presence of observed shear cracks on columns of infilled frame, no column shear crack was observed in strengthened frame. Columns and infill walls with ECC panels acted together as an integral unit which increased the deformability without loss of lateral strength.

The maximum plastic rotations of columns were obtained with the assumed plastic hinge length, which is half of the section depth. No plastic rotations were observed for the specimens during D1 earthquake. The highest plastic rotation demand was measured for the bare frame during the D2 and D3 motions. Excessive roof displacement of the bare frame resulted in increased ductility demand. The ductility demands of the infilled and strengthened frame were similar. The envelope response curves (Figure 4.21) also demonstrate the ductility range of each specimen.

The base shear capacity of the strengthened frame was about 30% higher than that of the infilled frame due to the panel application on the infill wall. It can be also observed that shear deformations of the infill wall were significantly reduced as a result of the ECC panel application (Table 11).

The cumulative dissipated energy was calculated by integration of the load vs. story displacement curve. The ECC panel application improved the energy dissipation characteristics of the specimen. Although, all specimens showed similar energy dissipation characteristics, the strengthened frame dissipated the energy with much higher displacement demands.

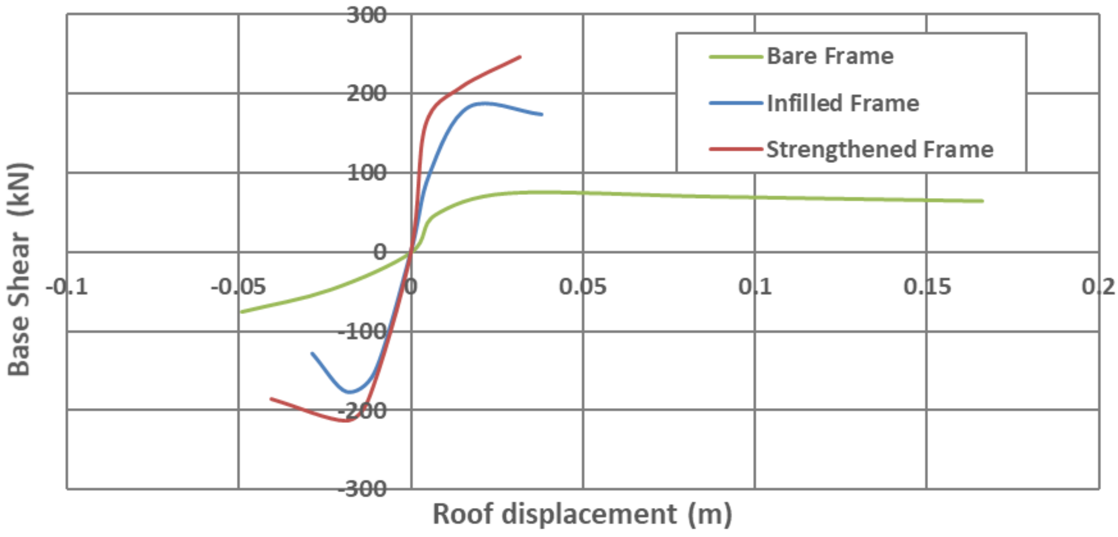


Figure 4.21 Envelope response curves of specimens

Table 4.4 Summary of test results

| Specimen | EQ | IDRmax (%) | Roof Disp. (mm) | Max Base Shear (kN) | Ductility Demand | Max Column Plastic Rotation (rad) | Max Infill Shear Def (mm) | Observed Damage |
|---|---|---|---|---|---|---|---|---|
| BF | D1 | 0.27 | 9.39 | 36.60 | 0.7 | - | - | Flexural cracks |
| | D2 | 1.31 | 47.46 | 66.59 | 3.7 | 0.00309 | - | Flexural and Joint cracks |
| | D3 | 4.65 | 190.28 | 76.71 | 19.0 | 0.01742 | - | Flexural and Joint cracks |
| IF | D1 | 0.10 | 3.61 | 63.68 | 0.4 | - | 0.24 | Flexural cracks |
| | D2 | 0.48 | 20.87 | 168.31 | 2.1 | 0.00035 | 1.13 | Shear cracks on wall |
| | D3 | 1.88 | 41.52 | 189.40 | 3.2 | 0.00786 | 14.20 | Shear cracks on wall and columns |
| SF | D1 | 0.09 | 3.69 | 72.06 | 0.3 | - | 0.20 | Flexural cracks |
| | D2 | 0.60 | 24.35 | 208.47 | 2.0 | 0.00185 | 0.46 | Flexural cracks |
| | D3 | 0.99 | 41.18 | 242.85 | 3.4 | 0.00430 | 0.66 | Flexural cracks |

The following conclusions were based on the results of tests:

- The deficient bare frame attained a maximum inter-story drift ratio of above 4% with a residual deformation of above 2%. This specimen experienced cracking damage under low to moderate motions leaving the structure in need of repair.

- The infilled frame, although experienced a stiffer response compared to BF, experienced cracking under the D2 motion. This suggests that reinforced concrete frames with infill walls are expected to be in need of repair under small to moderate motions. Upon failure of the infill wall, first story columns, the column rotation demands in the first story increased significantly. This result exhibits the change of structural frame response upon sudden failure of the infill walls.

- Upon retrofit with ECC panels, the following important structural benefits were obtained: i- no visible damage under low to moderate motions, ii- reduced interstory drift ratios up to 50%, iii- increased base shear capacity up to 30%, iv- a more uniform distribution of inter-story drift deformation demands, v- Intact nature of the retrofitted infill wall being less susceptible to out of plane collapse.

# CHAPTER 5

# ANALYTICAL MODELLING

## 5.1 Introduction

The Open System for Earthquake Engineering Simulation (Opensees) platform, developed at the Pacific Earthquake Engineering Research Center (PEER), was used for modeling the test frames. Opensees is capable of simulating the seismic response of structural and geotechnical systems. The nonlinear response of a system can be explored utilizing different types of material models, elements, and solution algorithms. Opensees is an open – source code which is advantageous for the user to analyze the structural system. Time history analyses were conducted for all models namely bare, infilled and strengthened frames.

## 5.2 Numerical modeling

### 5.2.1 Analytical model of the bare frame

The bare frame model was the basic model for the infilled and strengthened frames. The infill wall and ECC was adapted on to the bare frame model. The bare frame nonlinear model was composed of two parts essentially. The first part of the model was the description of the frame, and the second part was the identification of time history analyses for three different levels of synthetic ground motions.

The simulation of the bare frame was idealized as a 2-D problem with three degrees of freedom for each node. The nodal point system was generated in accordance with the test specimen and structural element lengths. Fixed-end boundary constraints were assigned for the supports (Figure 5.1). Node naming coincided with the coordinate system. For instance, “34” was second story level fourth column axis. Element naming follows “element type – story – coordinate system”. For instance, element name “132” stands for: “column element – third story – second axis”.

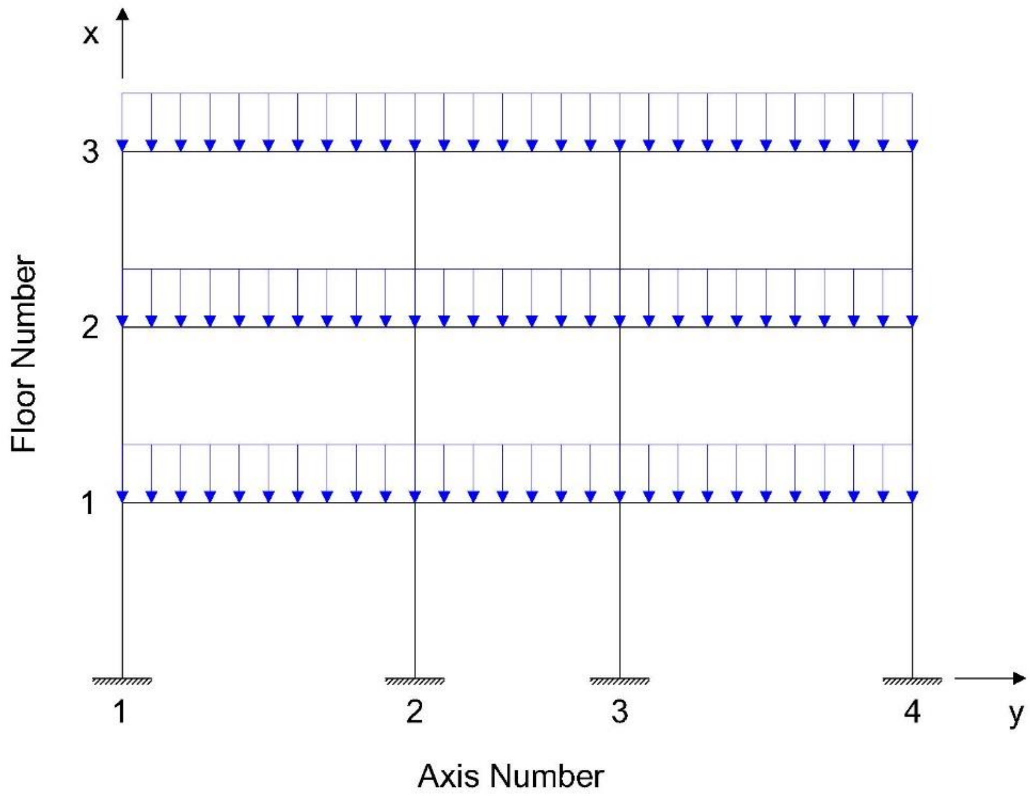


Figure 5.1 Finite element model (bare frame)

After setting of the nodal points system, material properties were specified for concrete and reinforcement. *Concrete01* material model (Kent and Park, 1971) was selected for concrete with zero tensile strength and degraded linear unloading/reloading stiffness as proposed by Karsan and Jirsa (1969). The same material model was used for confined and unconfined concrete (Figure 5.2). Concrete material model parameters are listed in Table 5.1, Table 5.2, and Table 5.3.

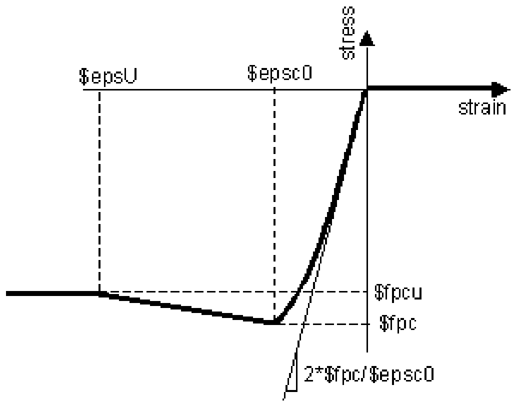


*$fpc*: Concrete compressive strength at 28 days

*$epsc0*: Concrete strain at maximum strength

*$fpcu*: Concrete crushing strength ($fpc*0.2)

*$epsU*: Concrete strain at crushing strength

Figure 5.2 Material model for concrete (Opensees 2016)

Table 5.1 Concrete material model parameters (bare frame)

| **Column** | **1st story** | | **2nd story** | | **3rd story** | |
|---|---|---|---|---|---|---|
| | Confined | Unconfined | Confined | Unconfined | Confined | Unconfined |
| ***$fpc (MPa)*** | 14.83 | 14.00 | 12.53 | 11.70 | 10.93 | 10.10 |
| ***$epsc0*** | 0.002118 | 0.002 | 0.002141 | 0.002 | 0.002163 | 0.002 |
| ***$fpcu (MPa)*** | 2.97 | 2.80 | 2.51 | 2.34 | 2.19 | 2.02 |
| ***$epsU*** | 0.017812 | 0.012150 | 0.022793 | 0.017155 | 0.030693 | 0.025077 |
| **Beam** | **1st story** | | **2nd story** | | **3rd story** | |
| | Confined | Unconfined | Confined | Unconfined | Confined | Unconfined |
| ***$fpc (MPa)*** | 16.01 | 14.00 | 13.71 | 11.70 | 12.11 | 10.10 |
| ***$epsc0*** | 0.002287 | 0.002 | 0.002343 | 0.002 | 0.002398 | 0.002 |
| ***$fpcu (MPa)*** | 3.20 | 2.80 | 2.74 | 2.34 | 2.42 | 2.02 |
| ***$epsU*** | 0.029634 | 0.012150 | 0.034582 | 0.017155 | 0.042450 | 0.025077 |

Table 5.2 Concrete material model parameters (infilled frame)

| **Column** | **1st story** | | **2nd story** | | **3rd story** | |
|---|---|---|---|---|---|---|
| | Confined | Unconfined | Confined | Unconfined | Confined | Unconfined |
| ***$fpc (MPa)*** | 13.53 | 12.70 | 14.73 | 13.90 | 14.83 | 14.00 |
| ***$epsc0*** | 0.002130 | 0.002 | 0.002119 | 0.002 | 0.002118 | 0.002 |
| ***$fpcu (MPa)*** | 2.71 | 2.54 | 2.95 | 2.78 | 2.96 | 2.80 |
| ***$epsU*** | 0.020129 | 0.014479 | 0.017959 | 0.012298 | 0.017812 | 0.012150 |
| **Beam** | **1st story** | | **2nd story** | | **3rd story** | |
| | Confined | Unconfined | Confined | Unconfined | Confined | Unconfined |
| ***$fpc (MPa)*** | 14.71 | 12.70 | 15.91 | 13.90 | 16.01 | 14.00 |
| ***$epsc0*** | 0.002317 | 0.002 | 0.002289 | 0.002 | 0.002287 | 0.002 |
| ***$fpcu (MPa)*** | 2.94 | 2.54 | 3.18 | 2.78 | 3.20 | 2.80 |
| ***$epsU*** | 0.031934 | 0.014479 | 0.029780 | 0.012298 | 0.029634 | 0.012150 |

Table 5.3 Concrete material model parameters (strengthened frame)

| Column | 1st story | | 2nd story | | 3rd story | |
|---|---|---|---|---|---|---|
| | Confined | Unconfined | Confined | Unconfined | Confined | Unconfined |
| ***$fpc (MPa)*** | 15.83 | 15.00 | 16.63 | 15.80 | 14.63 | 13.80 |
| ***$epsc0*** | 0.002110 | 0.002 | 0.002105 | 0.002 | 0.002120 | 0.002 |
| ***$fpcu (MPa)*** | 3.17 | 3.00 | 3.33 | 3.16 | 2.93 | 2.76 |
| ***$epsU*** | 0.016546 | 0.010876 | 0.015742 | 0.010067 | 0.018110 | 0.012450 |
| **Beam** | **1st story** | | **2nd story** | | **3rd story** | |
| | Confined | Unconfined | Confined | Unconfined | Confined | Unconfined |
| ***$fpc (MPa)*** | 17.01 | 15.00 | 17.81 | 15.80 | 15.81 | 13.80 |
| ***$epsc0*** | 0.002268 | 0.002 | 0.002255 | 0.002 | 0.002291 | 0.002 |
| ***$fpcu (MPa)*** | 3.40 | 3.00 | 3.56 | 3.16 | 3.16 | 2.76 |
| ***$epsU*** | 0.028380 | 0.010876 | 0.027584 | 0.010067 | 0.029930 | 0.012450 |

Three different bar diameters were used in the specimens. *Steel02* material model was used for steel (Figure 5.3). Stress and strain values of steel were the same because reinforcing bars were taken from the same batch and assembled for each test frame. For no stress degradation the *R* parameter was selected 20. Strain hardening value was 0.01 as recommended by TEC 2007. Material model entries are listed in Table 5.4:

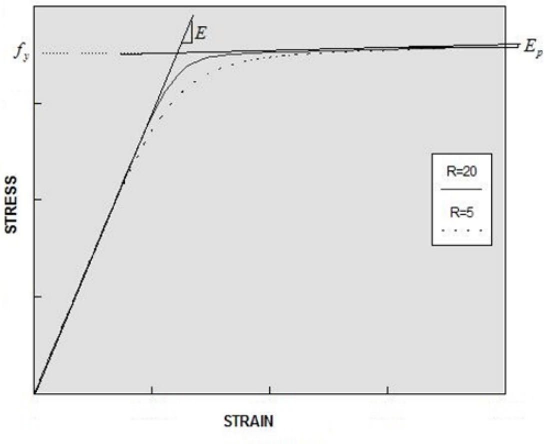


*$Fy*: Yield strength

*$E*: Initial elastic tangent

*$b*: Strain-hardening ratio

*$R0*, *$cR1*, *$cR2*: Parameters to control the transition from elastic to plastic branches. (Recommended value $R0=between 10 and 20, $cR1=0.925, $cR2=0.15 (Opensees 2016)

Figure 5.3 Material model for steel (Opensees 2016)

Table 5.4 Steel material model parameters

| **Bar Diameter** | **8 mm** | **10 mm** |
|---|---|---|
| ***$Fy (MPa)*** | 320 | 355 |
| ***$E (GPa)*** | 200 | 200 |
| ***$b*** | 0.01 | 0.01 |
| ***$R0*** | 20 | 20 |
| ***$R1*** | 0.925 | 0.925 |
| ***$R2*** | 0.15 | 0.15 |

Structural elements, beams and columns, were described with *nonlinearbeamcolumn* command which computes plasticity with an iterative force – based formulation. The Gauss-Lobatto integration method was selected for integration points. Five integration points were defined on each element and the fiber section model was adopted on each integration point. The number of fibers was 20 in the y – direction in local coordinates at the core concrete of the columns. Similarly, the cover concrete was divided in 20 fibers in the y – direction with a single layer on each side of the column section. A second – order P – Delta effect was considered in the columns. The number of fibers was 15 in the y – direction in local coordinates at the core concrete of beams. Besides that, the same divisions with a single layer on each side of the beam section were used for cover concrete. Moreover, flanges of the beams were modelled with 6 fibers in the y – direction (Figure 5.4). The nonlinear beam-column element ignores shear deformations. Weights of block masses on test specimen were defined as uniformly distributed load on the beam elements. Moreover, the mass of reinforced concrete elements was taken into account. Node recorders were defined for roof displacement; drift ratios for each story, base and story shear forces. Also, element recorders were considered at the column ends for curvature, rotation, and strain values. Stories were not modelled as rigid diaphragms because of damage observed on joint regions during testing. Time history analysis was conducted on the model to represent the PsD testing of Frames. Rayleigh damping was assumed with %5 damping value for the time history analysis. The Krylov-Newton time-stepping algorithm was used to better capture strength degradations (Scott and Fenves, 2010).

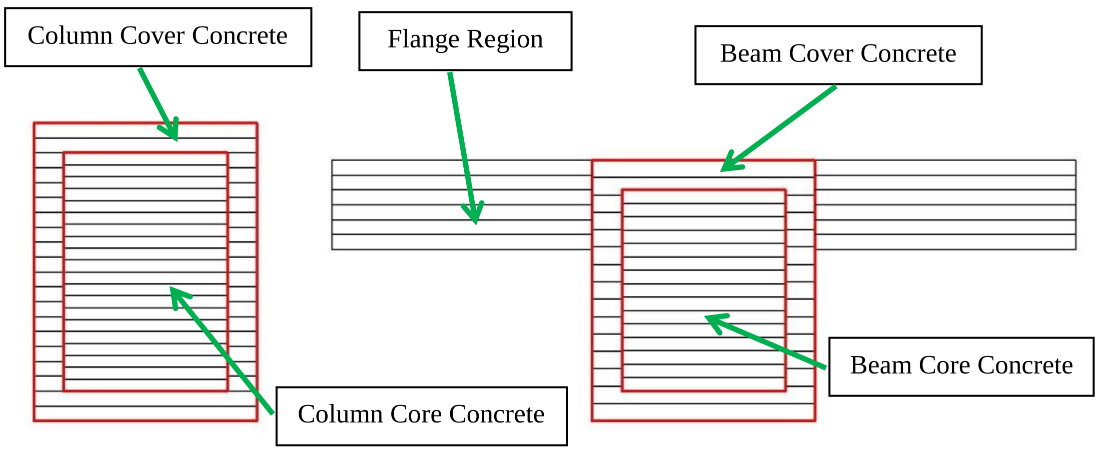


Figure 5.4 Fiber Section model

### 5.2.2 Infilled frame model

The bare frame model with truss elements, which represented the infill walls at mid bays for each story, was employed for infilled frame model (Figure 5.5). The same material models were used. Only concrete compressive stress and strain values were changed according to new uniaxial compressive stress values for the infilled frame. Moreover, the location of the steel blocks was changed in the infilled frame specimen.

Infill wall elements were considered as truss elements according to ASCE/SEI-41 (2007) and FEMA 356 Guidelines. The width of the truss element (*a*) was calculated from Eq. 5.3 and Eq. 5.4.

$$a = 0.175(\lambda_1 h_{col})^{-0.4} r_{inf} \quad (5.3)$$

$$\lambda_1 = \left[\frac{E_{ms}(t_{in}+t_p)\sin 2\theta}{4E_c I_{col} h_{inf}}\right]^{1/4} \quad (5.4)$$

$h_{col}$ : Column height between center lines of beams (mm)

$rinf$ : Diagonal length of infill panel (mm)

$\lambda_1$ : Coefficient used to determine equivalent width of infill strut

$\theta$ : Angle whose tangent is the infill height to length ratio (rad)

$E_c$ : Modulus of elasticity of frame material (MPa)

$E_{ms}$ : Modulus of elasticity of infill material (plaster and infill wall)

$h_{inf}$ : Height of infill wall (mm)

$I_{col}$ : Moment of inertia of column ($mm^4$)

$L_{inf}$ : Length of infill panel (mm)

$t_{in}$ : Thickness of brick unit (mm)

$t_p$ : Thickness of plaster (mm)

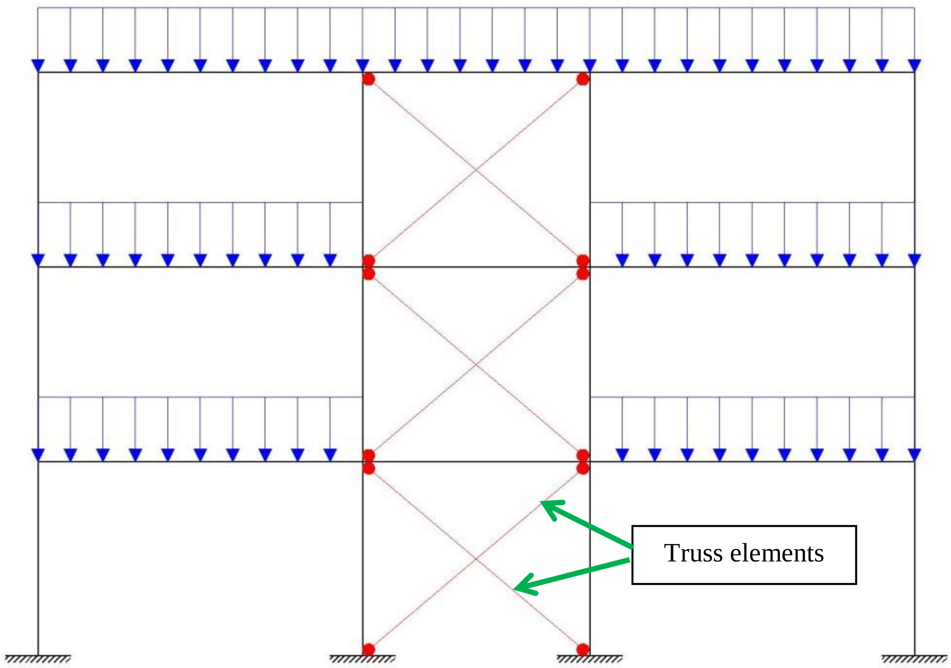


Figure 5.5 Infilled frame model

To calculate width of the truss element (a), elastic modulus of composite infill wall, including plaster and brick unit, was calculated according to Eq.5.5. The Turkish Earthquake Code (2007) and ACI 318-05 (2005) recommend different equations (Eq. 5.6 and Eq 5.7) to calculate the elastic modulus of plaster.

$$E_{ms} = \frac{E_{in}t_{in} + E_m t_p}{t_{in} + t_p} \tag{5.5}$$

$$E_c = 3250\sqrt{f_c} + 14000 \qquad \text{(TEC, 2007)} \tag{5.6}$$

$$E_c = 4700\sqrt{f_c} \qquad \text{(ACI 318-05, 2005)} \tag{5.7}$$

$E_{in}$ : Elastic modulus of brick unit (MPa)
$E_m$ : Elastic modulus of plaster (MPa)

The Turkish Earthquake Code (2007) recommends values for the elastic modulus of manufactured hollow brick as 1000 MPa. However, ASCE/SEI-41 (2007) proposed 4437 MPa (1.3×550×900psi) for good quality standard masonry wall. TEC (2007) and ASCE/SEI-41 (2007) recommended approximate values for sliding shear strength of the filling wall which were 0.25MPa and 0.24MPa (1.3×27psi) respectively. The compressive strength of the truss element was calculated with Eq. 5.8 and Eq. 5.9.

$$V_{ss} = f_{mv}L\left(t_{in} + t_p\right) \tag{5.8}$$

$$f_{cm} = V_{ss}/\left[a\cos\theta\left(t_{in} + t_p\right)\right] \tag{5.9}$$

$V_{ss}$ : Total shear resistance along the wall length
$f_{mv}$ : Shear strength of bed mortar/plaster mix.
$L$ : Length of the infill wall
$f_{cm}$ : Compressive strength of the strut
$E_{st}$ : Elastic Modulus of strut

*Concrete04* type material model was used for the truss element. Popovic's equation (1973) was employed for the compressive stress-strain behaviour of the infill struts as proposed by Madan et al. (1997). The strain at peak compressive stress was taken as 0.002 and ultimate strain was 0.004 (Figure 5.6). Tensile stresses were excluded in the material model. The compressive strength of the strut and elastic modulus of infill wall were selected as 3.1 MPa and 6.0 GPa, respectively. The strut area was taken as 0.02 m2 appropriate according to Table 5.5 and Table 5.6.

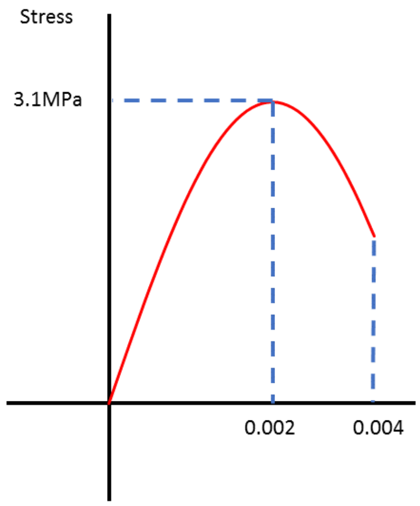


Figure 5.6 *Concrete04* type material model for infill (infilled frame)

Table 5.5 Strut properties of infill wall with respect to TEC (2007)

| Infilled Frame | $f_{cm}$ (MPa) | Strut Area ($m^2$) | $E_{ms}$ (MPa) |
|---|---|---|---|
| Story – 1 | 3.07 | 0.020 | 4783 |
| Story – 2 | 3.06 | 0.020 | 4737 |
| Story – 3 | 3.06 | 0.020 | 4718 |

Table 5.6 Strut properties of infill wall with respect to ACI 318-05 (2005)

| Infilled Frame | $f_{cm}$ (MPa) | Strut Area ($m^2$) | $E_{ms}$ (MPa) |
|---|---|---|---|
| Story – 1 | 3.15 | 0.019 | 6034 |
| Story – 2 | 3.13 | 0.019 | 5968 |
| Story – 3 | 3.13 | 0.019 | 5940 |

### 5.2.3 Strengthened frame model

The strengthened frame model was composed of the infilled frame model and additional truss elements for the ECC panel (Figure 5.7). The same material models were used for ECC. Only concrete compressive stress and strain values were changed according to new uniaxial compressive stress values for the strengthened frame. The strut width, compressive strength and elastic modulus of strut element were calculated once more for strengthened frame infill wall. They are summarized in Table 5.7 and Table 5.8. The compressive strength of the strut and the elastic modulus of the infill wall were calculated as 3.1 MPa and 6.0 GPa, respectively. 0.02 $m^2$ strut area was considered appropriate for strengthened frame infill wall.

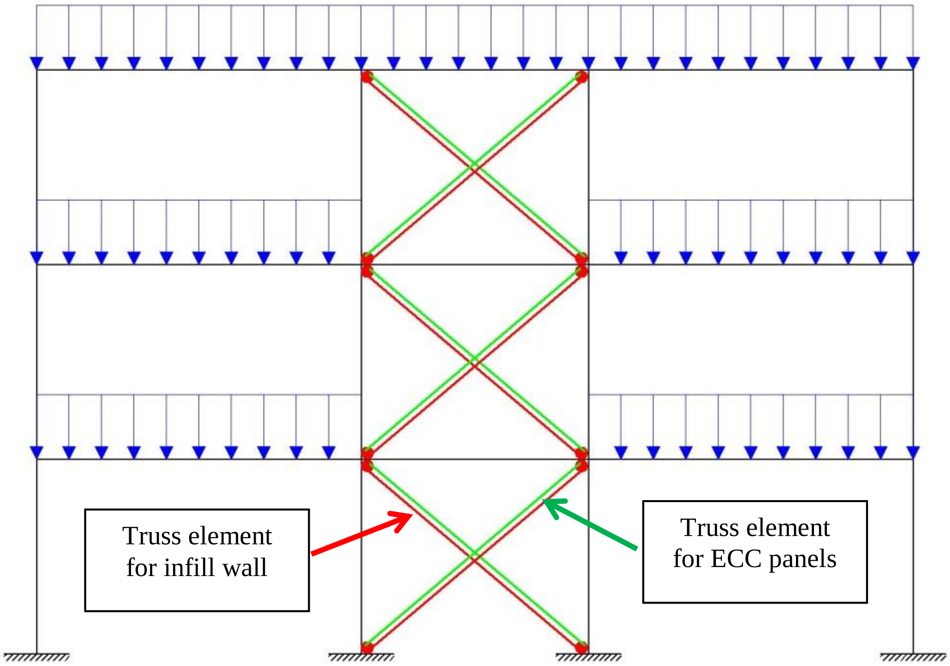


Figure 5.7 Strengthened frame model

Table 5.7 Strut properties of infill wall with respect to TEC (2007)

| Strengthened Frame | $f_{cm}$ (MPa) | Strut Area ($m^2$) | $E_{ms}$ (MPa) |
|---|---|---|---|
| Story – 1 | 3.06 | 0.020 | 4755 |
| Story – 2 | 3.06 | 0.020 | 4809 |
| Story – 3 | 3.06 | 0.020 | 4620 |

Table 5.8 Strut properties of infill wall with respect to ACI 318-05 (2005)

| Strengthened Frame | $f_{cm}$ (MPa) | Strut Area ($m^2$) | $E_{ms}$ (MPa) |
|---|---|---|---|
| Story – 1 | 3.12 | 0.019 | 5994 |
| Story – 2 | 3.12 | 0.019 | 6073 |
| Story – 3 | 3.12 | 0.019 | 5799 |

The ECC panel zone was considered as an infill wall with a different type of material. Equations were revised for the ECC material. The modulus of elasticity of infill material ($E_{ms}$) was taken as Modulus of elasticity of ECC in Eq. 5.4. Also the thickness of the wall element was assumed as the thickness of the ECC panel (25 mm). Suryanto et al. (2010) recommended a shear transfer model (Figure 5.8) for ECC, which was adopted for the normal strength concrete model (Li et al. 1989). The shear stress of ECC material was computed by Eq. 5.9 and Eq. 5.10. The parameter 0.25 (Eq 5.11) provides conformity for ECC including approximately 2% by volume of PVA fibers (Suryanto, 2009). The ratio of crack slip to crack opening ($\beta=\gamma/\omega$) value increases with increment of crack slip so that the shear strength of ECC (Vecc) reaches a constant value ($0.25f_{ecc}$) according to Eq. 5.11.

$$f_{ecc} = 3.8(f'_{ecc})^{1/3} \tag{5.10}$$

$$V_{ecc} = 0.25 f_{ecc} \frac{\beta^2}{1+\beta^2} \tag{5.11}$$

$f'_{ecc}$ : Compressive strength of the ECC

$f_{ecc}$ : Maximum shear stress of ECC that can be transferred across a crack

$V_{ecc}$ : Shear strength of ECC

$\beta$ : Ratio of crack slip to crack opening

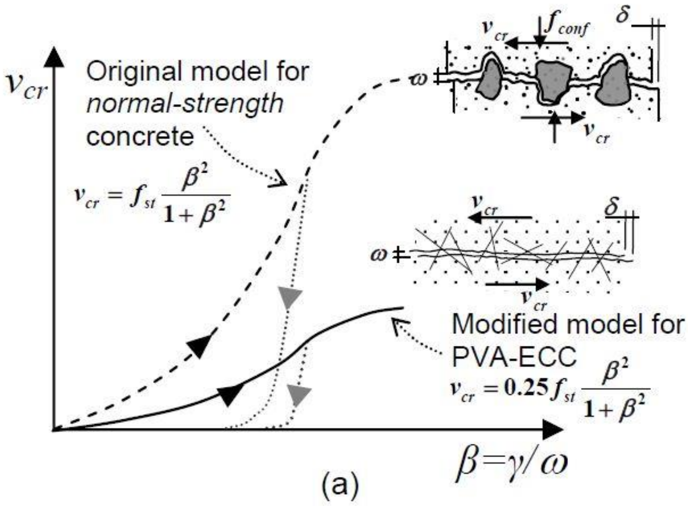


Figure 5.8 Basic model for average shear stress-strain relationship of cracked PVA-ECC (Suryanto et al. 2010)

Strut properties are summarized in Table 5.9 and Table 5.10 in accordance with TEC (2007) and ACI 318-05 (2005). The same material model, *Concrete04* was employed for ECC struts. The compressive strength of the ECC strut was determined as 39 MPa. The elastic modulus of ECC was established from elastic modulus tests. The peak Strain at tension/compression was taken as 0.037/-0.005, and the ultimate strain at tension/compression was assumed as 0.06/-0.012 (Fischer and Li, 2003) (Figure 5.10). Moreover, tension stress was selected as 4 MPa as recommended in the literature. The strut area was selected as 0.0043 $m^2$ to be appropriate.

Table 5.9 Strut properties of infill wall with respect to TEC (2007)

| ECC Panel | $f_{ecc}$ (MPa) | Strut Area ($m^2$) | $E_{ecc}$ (MPa) |
|---|---|---|---|
| Story – 1 | 38.12 | 0.0043 | 15.000 |
| Story – 2 | 38.07 | 0.0044 | 15.000 |
| Story – 3 | 38.19 | 0.0043 | 15.000 |

Table 5.10 Strut properties of infill wall with respect to ACI 318-05 (2005)

| ECC Panel | $f_{ecc}$ (MPa) | Strut Area ($m^2$) | $E_{ecc}$ (MPa) |
|---|---|---|---|
| Story – 1 | 39.59 | 0.0042 | 15.000 |
| Story – 2 | 39.48 | 0.0042 | 15.000 |
| Story – 3 | 39.75 | 0.0042 | 15.000 |

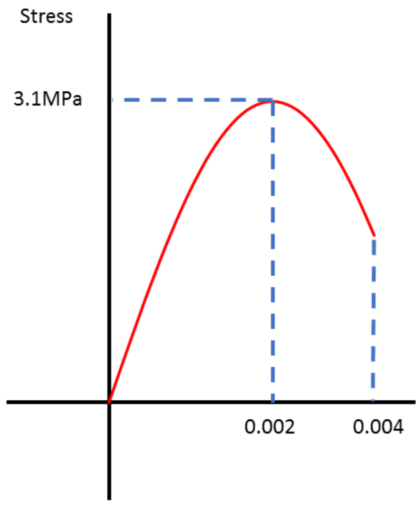


Figure 5.9 *Concrete04* type material model for infill (strengthened frame)

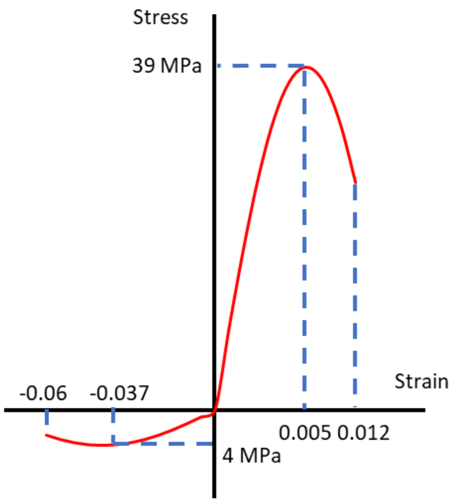


Figure 5.10 *Concrete04* type material model for ECC (strengthened frame)

### 5.3 Analysis results

Time history analysis results of the Opensees models for each specimen were compared with the real pseudo – dynamic experimental results. Roof displacements, story drift ratios, base and story shear forces, and curvature of the first story columns time histories were examined to get the differences between the analytical and experimental results.

#### 5.3.1 Bare frame

The bare frame experimental results were compared with analysis results. Roof displacement time histories are demonstrated in Figure 5.11. The inter-story drift ratio time history comparisons are shown in Figure 5.12. Base and Story Shear force time histories are represented in Figure 5.13. Finally, column bottom and top curvature time histories are given in Figure 5.14 and Figure 5.15.

It was observed that the maximum drift ratios in the experiment and in the model were close to each other during the D2 earthquake. However, the error rate of drift ratios during the D3 earthquake increased. The model drift ratios were found to be low for the second and third floors (Figure 5.12). Nevertheless, the first story maximum drift ratio of the model approached to the test results for the D2 and D3 earthquake (Table 5.12). In the model, the drift was concentrated on the first floor. This damage concentration forces both frames to have a soft story behavior. A more uniform damage distribution was observed at every story level during the pseudo-dynamic testing.

The analytical prediction error increases excessively especially during the D3 earthquake. This discrepancy was attributed to the extensive damage in the joints of the top story due to inadequate bond. Experimental and analytical roof displacements were close to each other during the D1 and D2 ground motions. Since introduction of damage to the analytical model is extremely complicated, the divergence of analytical and experimental behavior looks exaggerated . Table 5.11 summarizes the peak roof displacement results.

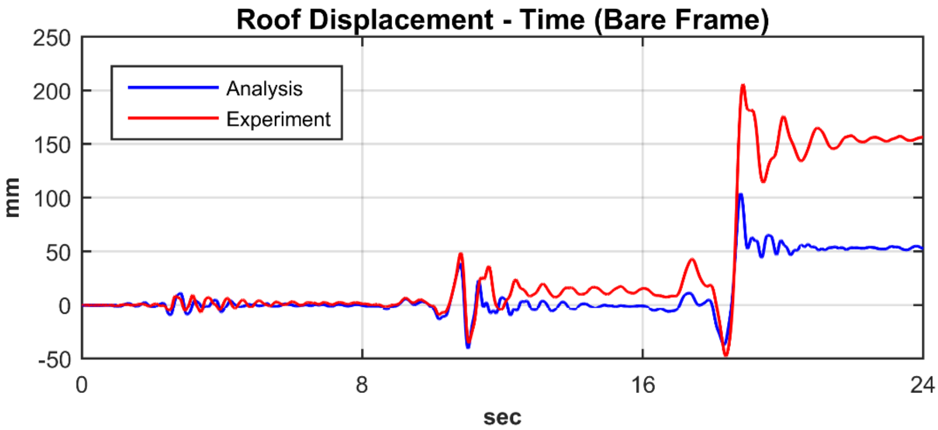

Figure 5.11 Roof displacement time history (bare frame)

Base shear forces were close to the experimental values for the model (Figure 5.13). Nevertheless, the error increased in the second and third stories (Table 5.13). Extensive differences were observed at the third story. However, story shear forces were calculated close to experimental results at the second story for the bare frame model under the D2 ground motion.

Peak top and bottom column end curvatures calculated analytically in the analysis coincide with experimental curvatures up to 18.5 sec (Figure 5.14 and Figure 5.15). However, after that second experimental values of peak first story column curvatures were lower than those of the model. This also indicates the soft story behavior of the analysis. Although there is difference between the column curvatures, residual curvatures approach at the column bottom end for the experimental and bare frame model. Measured bottom curvatures are greater than top curvatures during the D3 ground motion due to more flexural damage. The same behavior can be seen in the analytical model.

Generally, column rotations and joint damages compensated the lateral demands during the experiment. The peak lateral displacement demands during the D3 ground motion caused more column curvatures than shown in the experiment, because the analysis could not include the joint rotations.

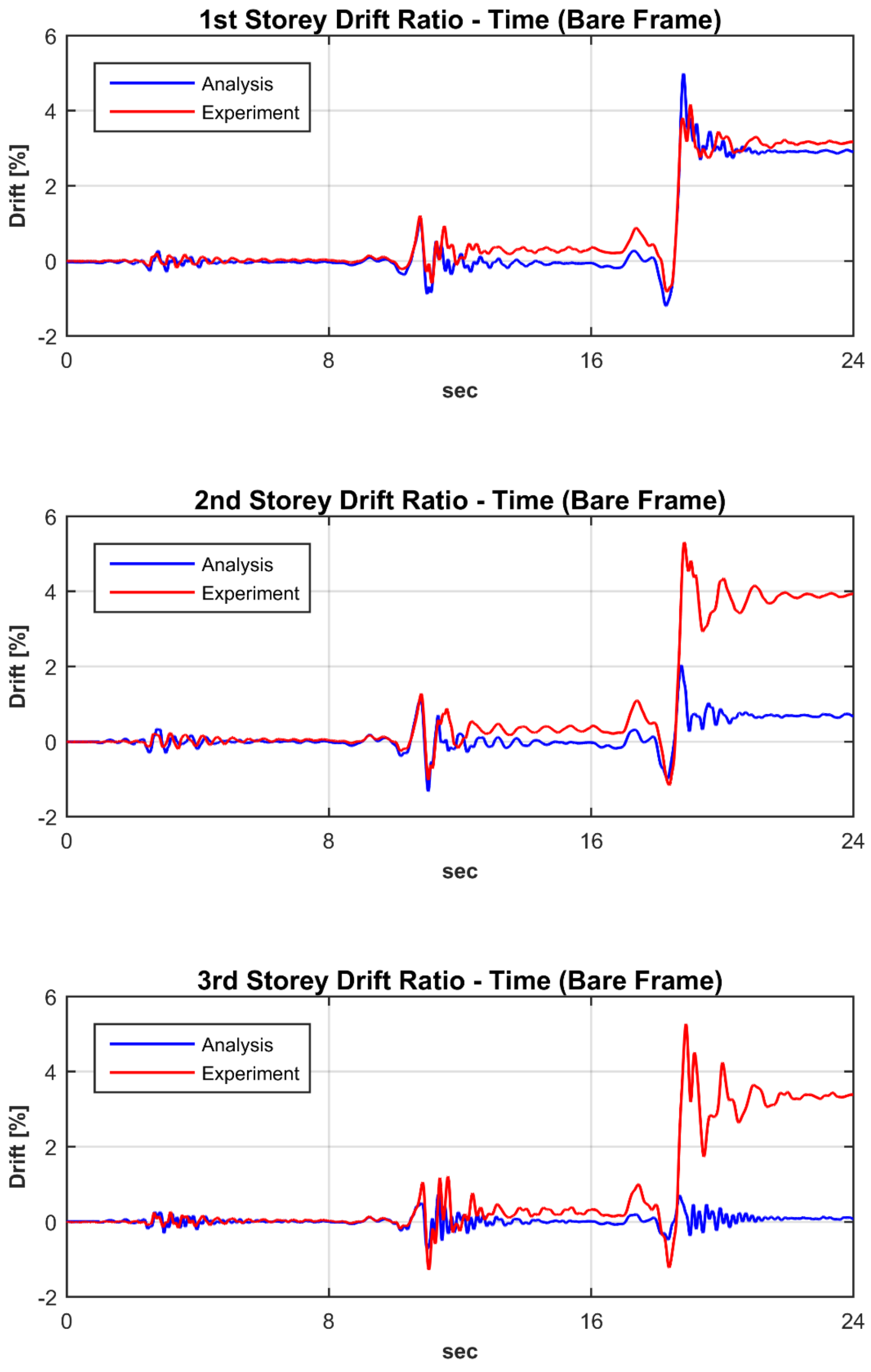


Figure 5.12 Inter-story drift ratio time history (bare frame)

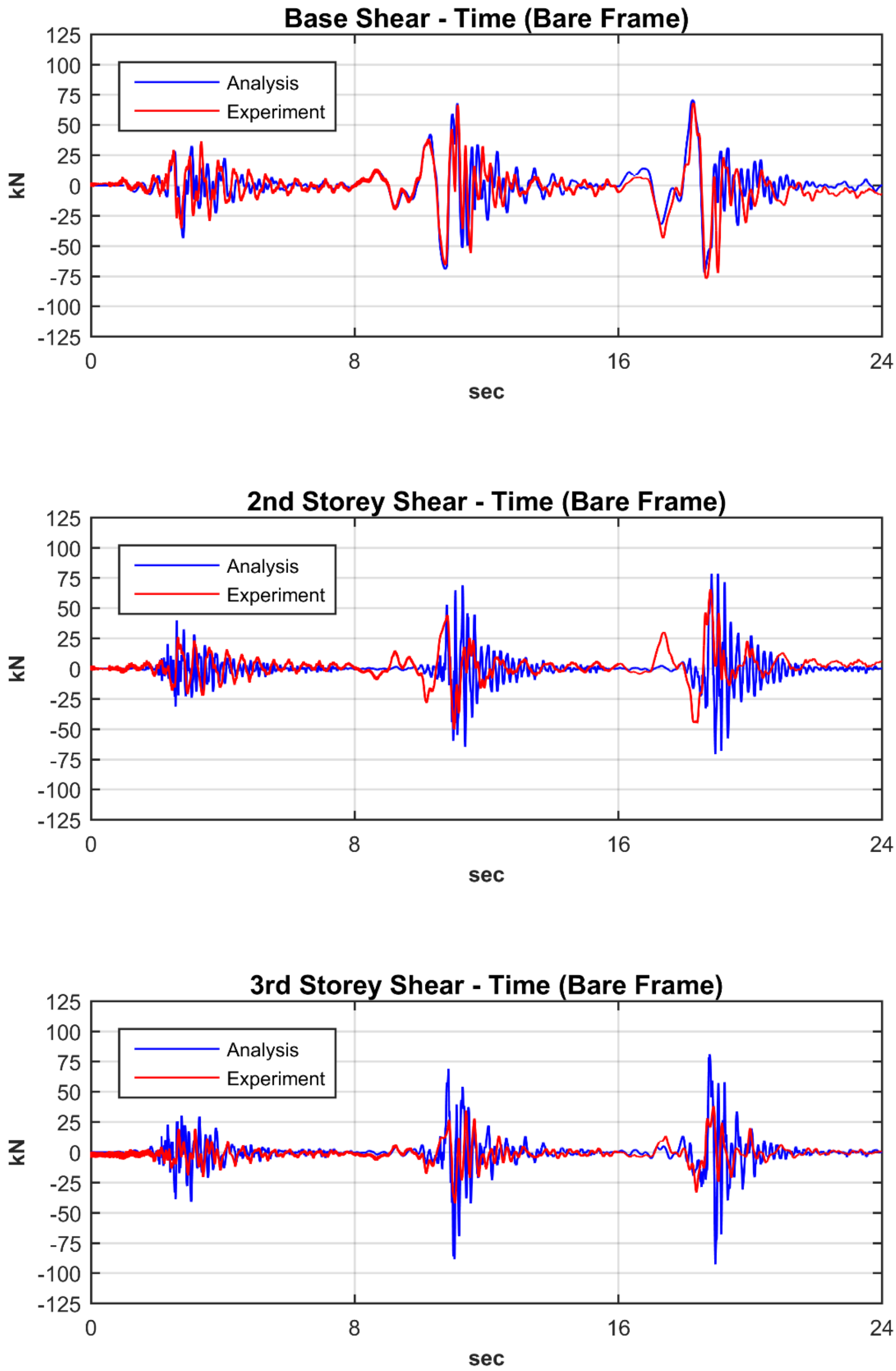


Figure 5.13 Story shear force time history (bare frame)

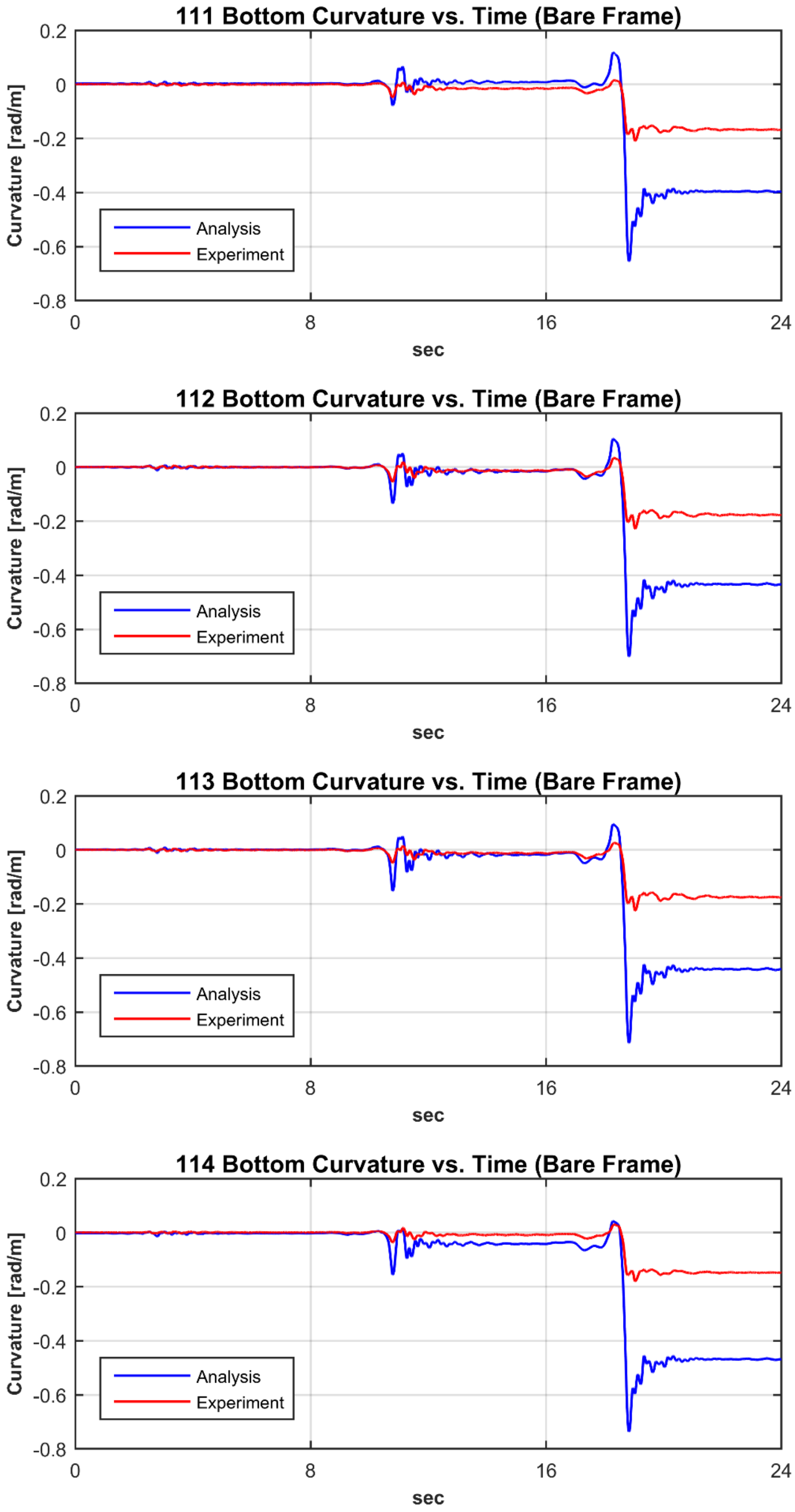


Figure 5.14 Bottom end curvatures of 1st story columns (bare frame)

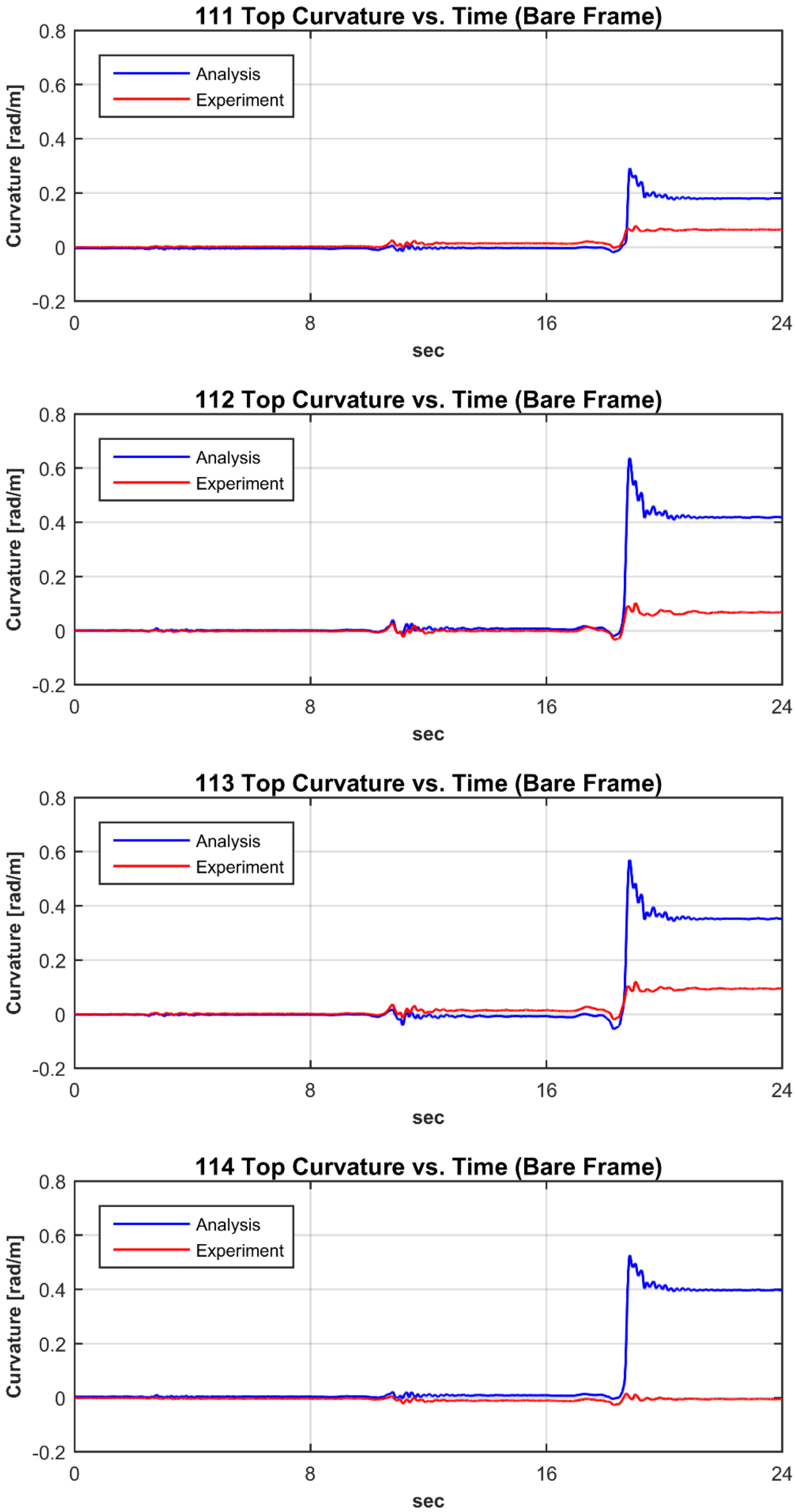


Figure 5.15 Top end curvatures of 1st story columns (bare frame)

Table 5.11 Peak roof displacement comparisons (bare frame)

| Ground Motion | Maximum Roof Displacement (mm) | | Error (%) |
|---|---|---|---|
| | Experiment | Analysis | Analysis |
| D1 | 9.39 | 11.35 | 20.87 |
| D2 | 47.46 | 40.68 | -14.29 |
| D3 | 190.28 | 103.94 | -45.38 |

Table 5.12 Peak inter-story drift comparisons (bare frame)

| Story | Ground Motion | Maximum Inter-Story Drift (%) | | Error (%) |
|---|---|---|---|---|
| | | Experiment | Analysis | Analysis |
| 1st | D1 | 0.21 | 0.29 | 38.10 |
| 1st | D2 | 1.18 | 1.13 | -4.24 |
| 1st | D3 | 3.47 | 5.00 | 44.09 |
| 2nd | D1 | 0.24 | 0.35 | 45.83 |
| 2nd | D2 | 1.25 | 1.33 | 6.40 |
| 2nd | D3 | 4.54 | 2.04 | -55.07 |
| 3rd | D1 | 0.27 | 0.30 | 11.11 |
| 3rd | D2 | 1.31 | 0.74 | -43.51 |
| 3rd | D3 | 4.65 | 0.71 | -84.73 |

Table 5.13 Peak story shear error (bare frame)

| Story | Ground Motion | Maximum Base Shear (kN) | | Error (%) |
|---|---|---|---|---|
| | | Experiment | Analysis | Analysis |
| 1st | D1 | 36.60 | 43.36 | 18.47 |
| 1st | D2 | 66.59 | 69.05 | 3.69 |
| 1st | D3 | 76.71 | 71.63 | -6.62 |
| 2nd | D1 | 26.30 | 39.89 | 51.67 |
| 2nd | D2 | 50.03 | 68.81 | 37.54 |
| 2nd | D3 | 65.53 | 78.69 | 20.08 |
| 3rd | D1 | 20.48 | 40.84 | 99.41 |
| 3rd | D2 | 42.12 | 88.52 | 110.16 |
| 3rd | D3 | 42.12 | 92.77 | 120.25 |

### 5.3.2 Infilled frame

The experimental and OpenSees model results of the infilled frame are discussed at in this section. Roof displacement time histories are shown in Figure 5.16. The inter-story drift ratio time history comparisons are demonstrated in Figure 5.17. Base and Story Shear force time histories are displayed in Figure 5.18. Finally, column bottom and top curvature time histories are represented in Figure 5.19 and Figure 5.20.

The infilled wall model could not capture the peak roof displacements under the D1 ground motion (Figure 5.16). But the accuracy of the model increased during the D2 and D3 ground motions (Table 5.14). The infill wall in the specimen and similarly truss members in the analytical model restricted roof displacements and residual displacements as compared to the bare frame.

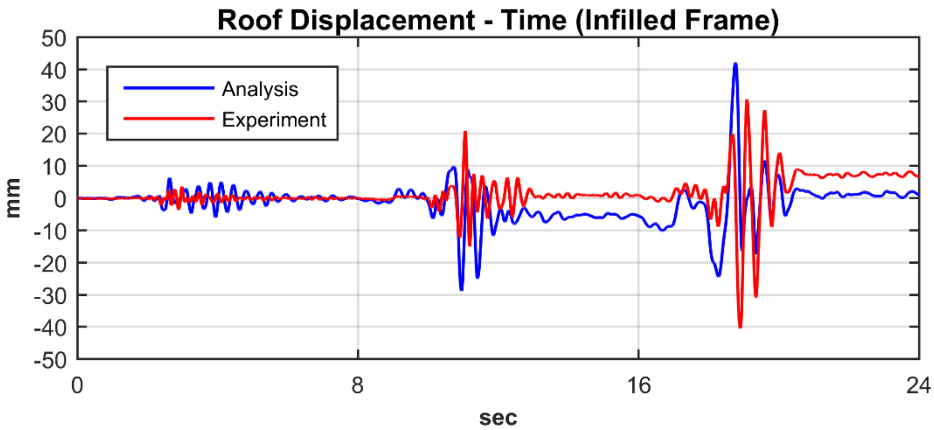


Figure 5.16 Roof displacement time history comparisons (infilled frame)

Table 5.14 Peak roof displacement error (infilled frame)

| Ground Motion | Maximum Roof Displacement (mm) | | Error (%) |
|---|---|---|---|
| | Experiment | Analysis | Analysis |
| D1 | 3.61 | 6.24 | 72.85 |
| D2 | 20.87 | 28.74 | 37.71 |
| D3 | 41.52 | 41.75 | 0.55 |

The model did not predict inter – story drift ratios well during the D1 ground motion. Also, the drift ratio error increased under the D2 ground motion for the first story (Table 5.15). The D3 earthquake forced first story drifts to its limits both in the model and in the experiment. (Figure 5.17). The infilled frame model also reflected the damage state of the frame. However, drift ratios of the second and third story remained limited during the D2 and D3 ground motion.

Table 5.15 Peak inter-story drifts error (infilled frame)

| Story | Ground Motion | Maximum Inter-Story Drift (%) | | Error (%) |
|---|---|---|---|---|
| | | Experiment | Analysis | Analysis |
| 1st | D1 | 0.07 | 0.14 | 100.00 |
| 1st | D2 | 0.48 | 1.21 | 152.08 |
| 1st | D3 | 1.88 | 2.49 | 32.45 |
| 2nd | D1 | 0.09 | 0.19 | 111.11 |
| 2nd | D2 | 0.48 | 0.67 | 39.58 |
| 2nd | D3 | 0.72 | 0.60 | -16.67 |
| 3rd | D1 | 0.10 | 0.17 | 70.00 |
| 3rd | D2 | 0.44 | 0.32 | -27.27 |
| 3rd | D3 | 0.66 | 0.37 | -43.94 |

The base shear prediction of the model was lower than the experimental results (Figure 5.18). The error decreased for the second and third story shear forces (Table 5.16). The base shear capacity of the test (Infilled) frame was preserved during the D2 and D3 ground motion despite excessive damages on neighboring column ends and the infill wall.

Experimental results show that the infill wall limited the bottom and top curvatures at the first story columns (Figure 5.19 and Figure 5.20). However, there was a variation between the experiment and analytical results during the D3 ground motion. Peak curvatures reach approximately 0.4 rad/m at the bottom and top column ends. Non-ductile flexural (no shear) behaviors could not be captured completely by the OpenSees model which uses flexural elements for beam columns.

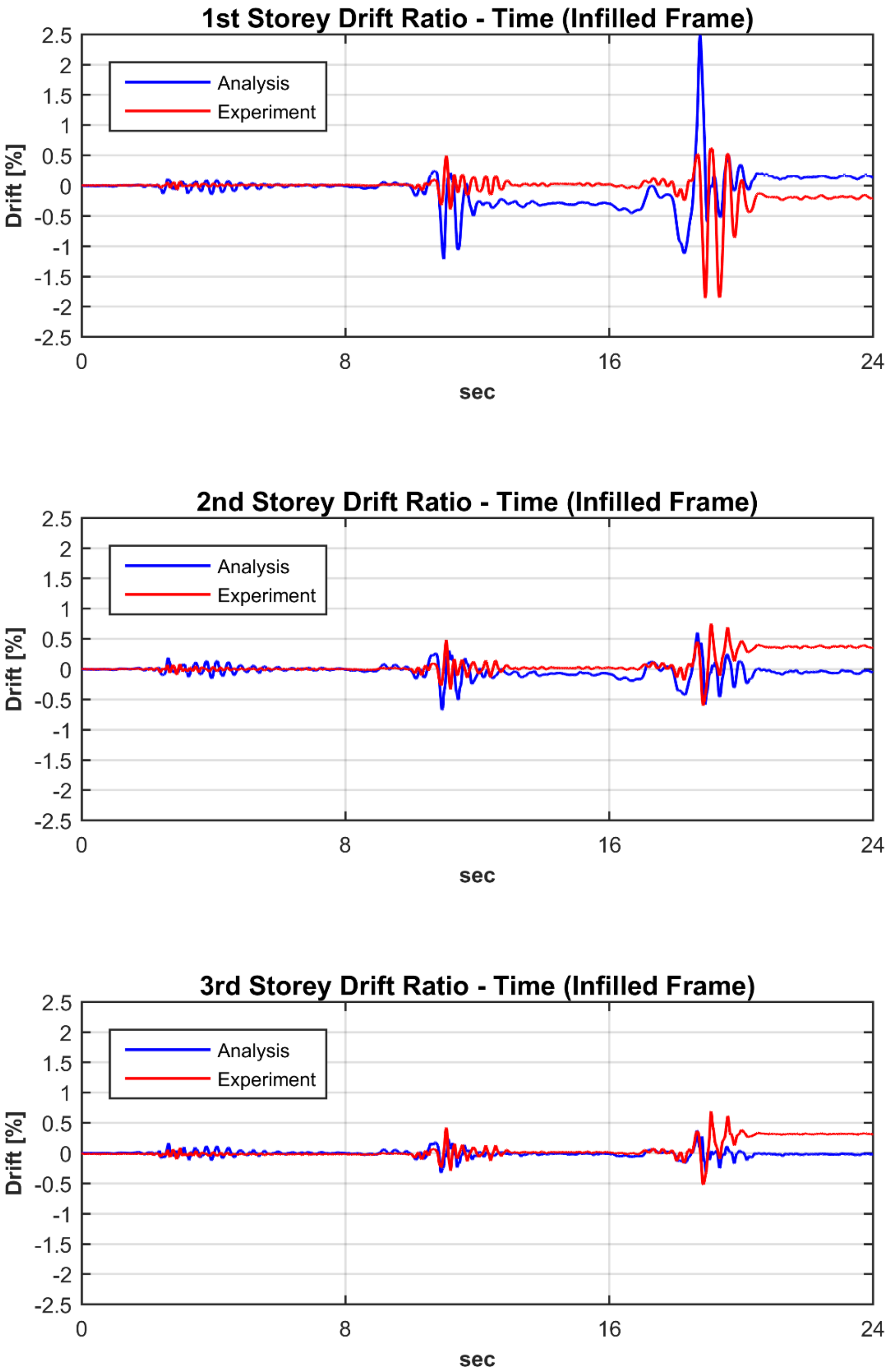


Figure 5.17 Inter-story drift ratio time history comparisons (infilled frame)

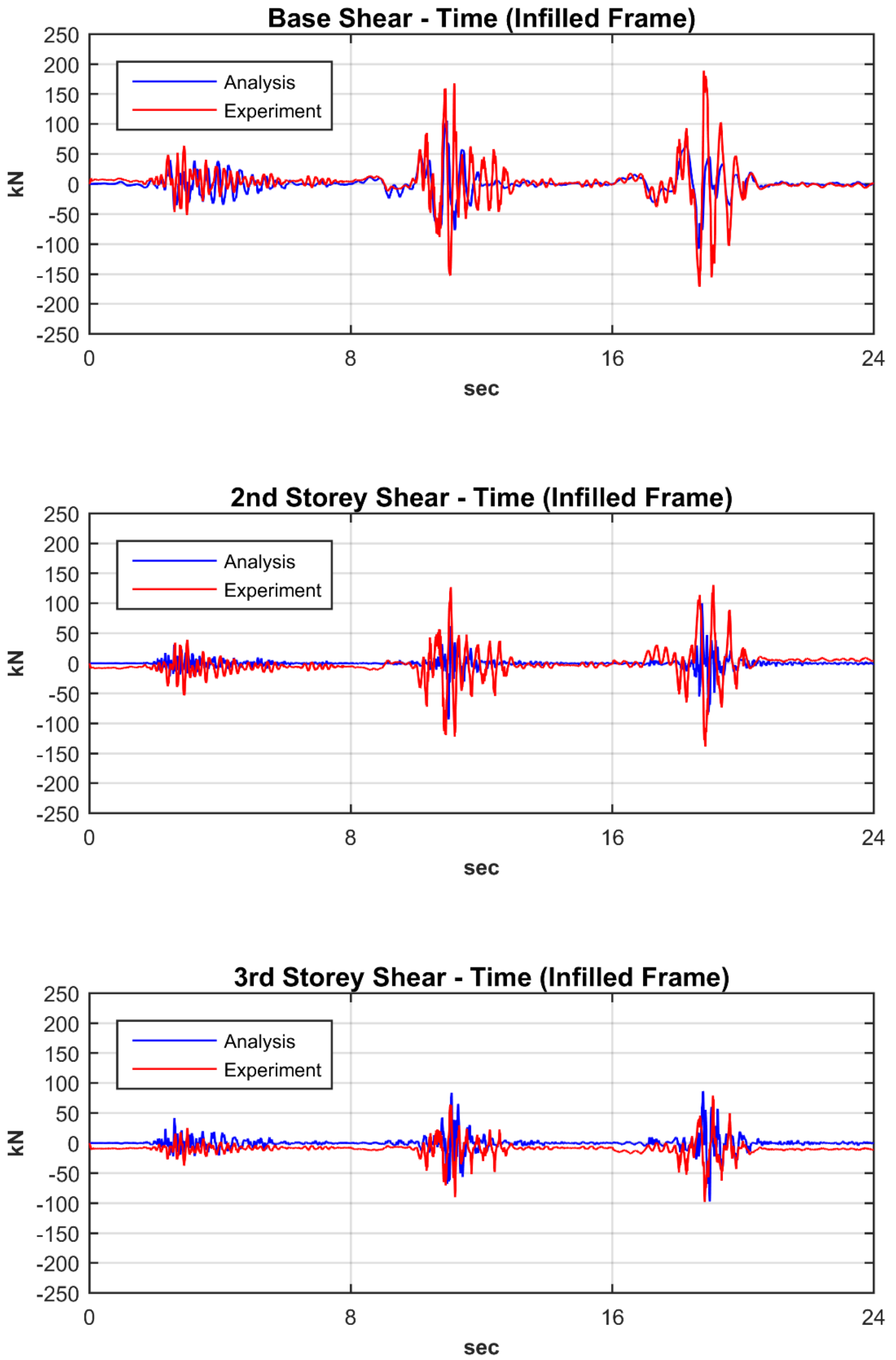


Figure 5.18 Story shear force time history comparisons (infilled frame)

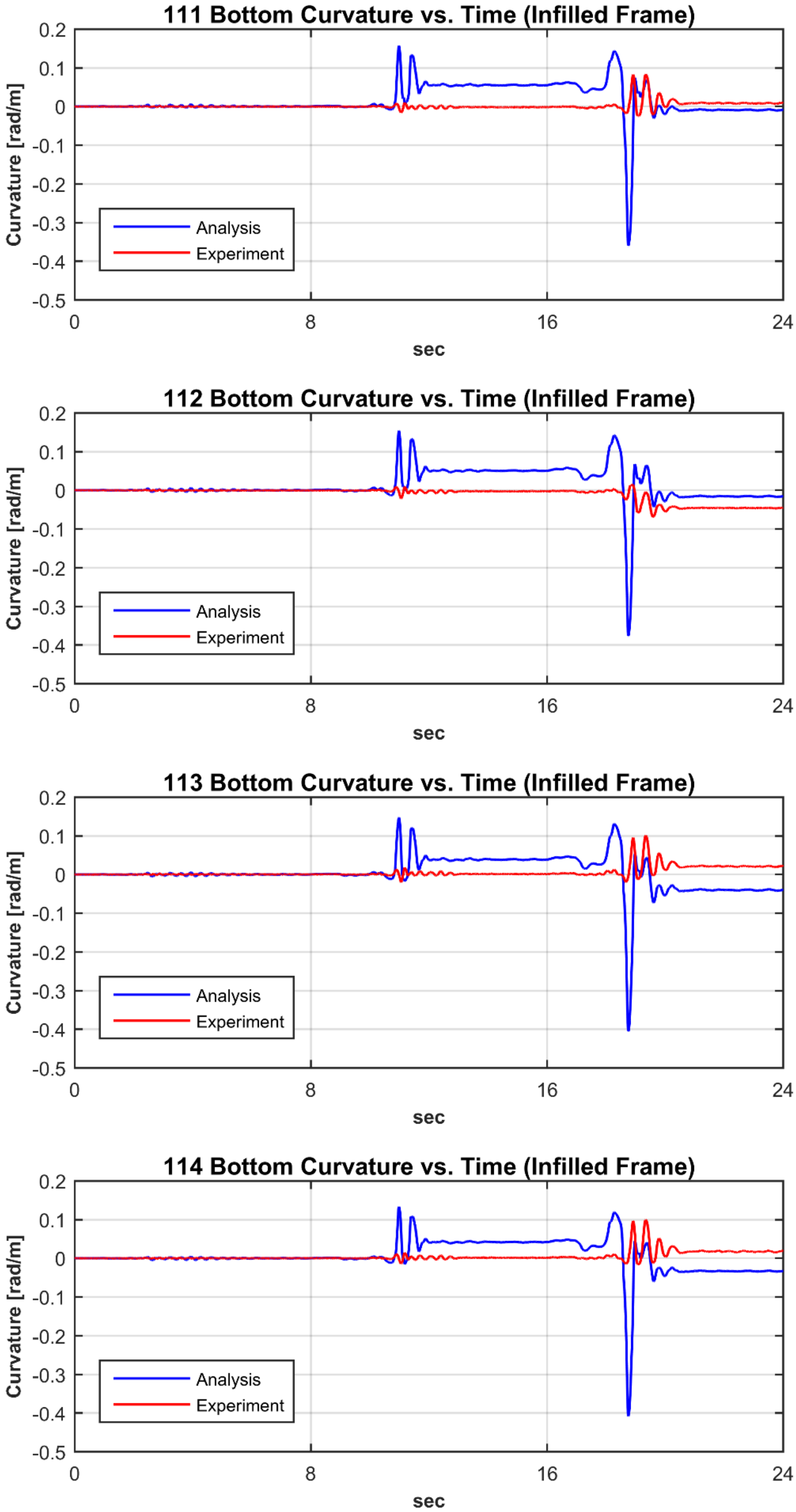


Figure 5.19 Bottom end curvatures of 1st story columns (infilled frame)

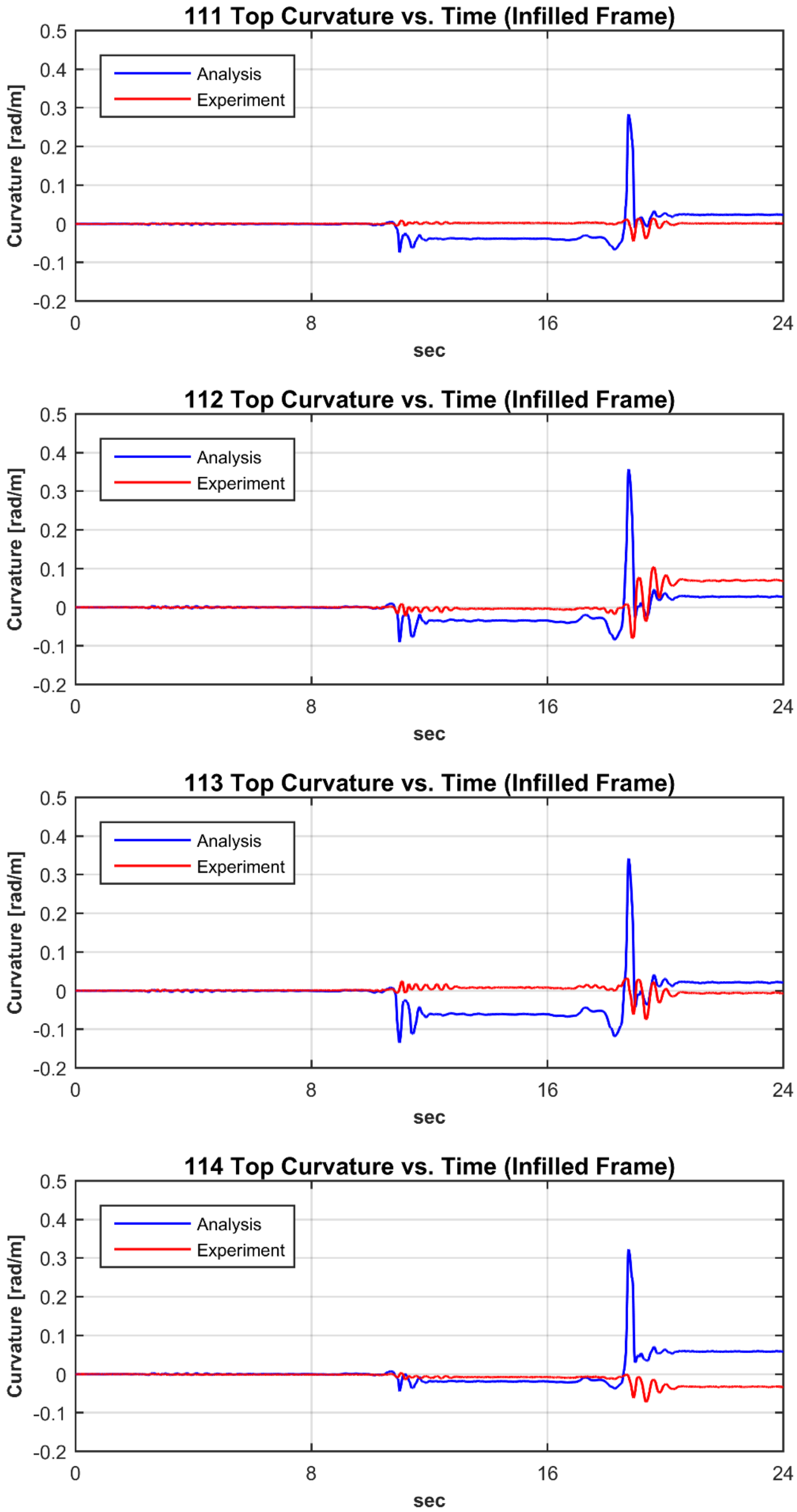


Figure 5.20 Top end curvatures of 1st story columns (infilled frame)

Table 5.16 Peak story shear error (infilled frame)

| Story | Ground Motion | Maximum Base Shear (kN) | | Error (%) |
|---|---|---|---|---|
| | | Experiment | Analysis | Analysis |
| 1st | D1 | 63.68 | 42.40 | -33.42 |
| 1st | D2 | 168.31 | 105.50 | -37.32 |
| 1st | D3 | 189.40 | 107.62 | -43.18 |
| 2nd | D1 | 53.24 | 30.98 | -41.81 |
| 2nd | D2 | 126.84 | 93.13 | -26.58 |
| 2nd | D3 | 138.21 | 99.82 | -27.78 |
| 3rd | D1 | 37.52 | 41.60 | 10.87 |
| 3rd | D2 | 90.19 | 84.18 | -6.67 |
| 3rd | D3 | 98.04 | 97.22 | -0.84 |

### 5.3.3 Strengthened frame

The experimental results and OpenSees model of the strengthened frame are explained in this section. Generally, the existence of strengthened material on infill walls reduced the displacement demand of the frame and increased the lateral force demand during the D1, D2 and D3 ground motions. The effect of strengthening ACC panel on the infill wall was captured by inserting additional truss elements on the wall truss elements.

Roof displacement time histories are shown in Figure 5.21. The inter-story drift ratio time history comparisons are demonstrated in Figure 5.22. Base and Story Shear force time histories are displayed in Figure 5.23. Finally, column bottom and top curvature time histories are represented in Figure 5.24 and Figure 5.25.

The infilled frame and strengthened frame test results are similar from the roof displacement point of view during all D1, D2, and D3 earthquakes. Analytical results of the strengthened frame match the experimental results acceptably well during the D2 earthquake (Table 5.17). The difference, however increases during the D3 earthquake. While experimental measurements give 43 mm maximum roof displacement during the D3 earthquake, the peak value is calculated as 51 mm in the Opensees analysis (Figure 5.21).

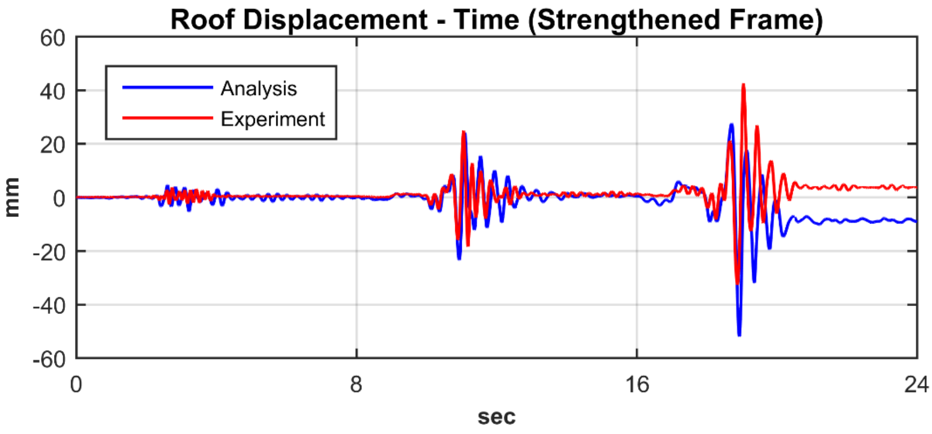


Figure 5.21 Roof displacement time history comparisons (strengthened frame)

Table 5.17 Peak roof displacement error (strengthened frame)

| Ground Motion | Maximum Roof Displacement (mm) | | Error (%) |
|---|---|---|---|
| | Experiment | Analysis | Analysis |
| D1 | 3.69 | 5.27 | 42.82 |
| D2 | 24.35 | 23.99 | -1.48 |
| D3 | 41.18 | 51.90 | 26.03 |

Generally, the error between the analytical and experimental inter-story drift ratios is lower than that of the Bare frame and infilled frame results for the strengthened frame (Table 5.18). Measured and analysis drift ratio values were limited to 1.41%. This indicates the close relationship between the damage level and drift ratio. Although, analytical displacements are out-of-phase with the experimental results during the D3 earthquake after 18.5 sec., the peak roof displacement and drift ratios were estimated closely (Figure 5.22).

Pseudo-dynamic testing showed that application of ECC panels on the infill wall increased the lateral load capacity of the infilled frame. This positive effect was captured in the analytical model by additional truss elements for ECC panels (Figure 5.23). The base shear prediction of strengthened model was better than for the infilled wall model. However, the second story shear prediction was poorer than other stories in the strengthened model (Table 5.19).

Bottom and top end curvatures decreased with the application of ECC panels (Figure 5.24 and Figure 5.25). The strengthened frame model displayed a similar behavior. There was a difference between the model and experiment for the bottom and ends of exterior column curvatures. Furthermore, these variations decreased at the top end exterior column curvatures.

Table 5.18 Peak inter-story drifts error (strengthened frame)

| Story | Ground Motion | Maximum Inter-Story Drift (%) | | Error (%) |
|---|---|---|---|---|
| | | Experiment | Analysis | Analysis |
| 1st | D1 | 0.08 | 0.10 | 25.00 |
| 1st | D2 | 0.50 | 0.66 | 32.00 |
| 1st | D3 | 0.86 | 1.41 | 63.95 |
| 2nd | D1 | 0.09 | 0.14 | 55.56 |
| 2nd | D2 | 0.60 | 0.64 | 6.67 |
| 2nd | D3 | 0.99 | 1.22 | 23.23 |
| 3rd | D1 | 0.09 | 0.13 | 44.44 |
| 3rd | D2 | 0.53 | 0.59 | 11.32 |
| 3rd | D3 | 0.91 | 0.98 | 7.69 |

Table 5.19 Peak story shear error (strengthened frame)

| Story | Ground Motion | Maximum Base Shear (kN) | | Error (%) |
|---|---|---|---|---|
| | | Experiment | Analysis | Analysis |
| 1st | D1 | 72.06 | 56.49 | -21.61 |
| 1st | D2 | 208.47 | 158.48 | -23.98 |
| 1st | D3 | 242.85 | 179.67 | -26.02 |
| 2nd | D1 | 48.24 | 34.94 | -27.56 |
| 2nd | D2 | 162.48 | 79.98 | -50.78 |
| 2nd | D3 | 199.95 | 100.48 | -49.75 |
| 3rd | D1 | 36.10 | 43.23 | 19.76 |
| 3rd | D2 | 112.87 | 98.54 | -12.70 |
| 3rd | D3 | 125.32 | 105.51 | -15.81 |

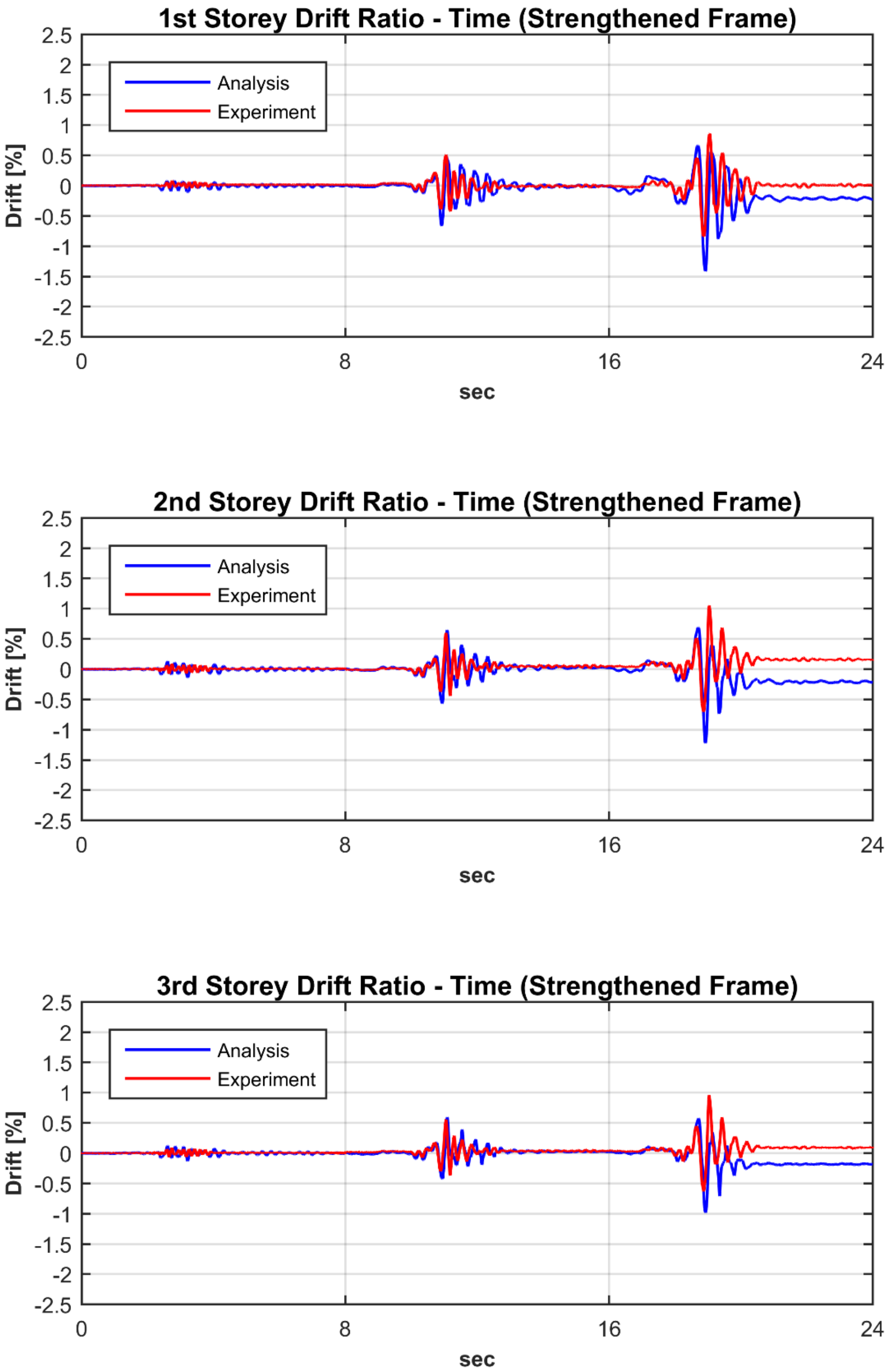


Figure 5.22 Inter-story drift ratio time history comparisons (strengthened frame)

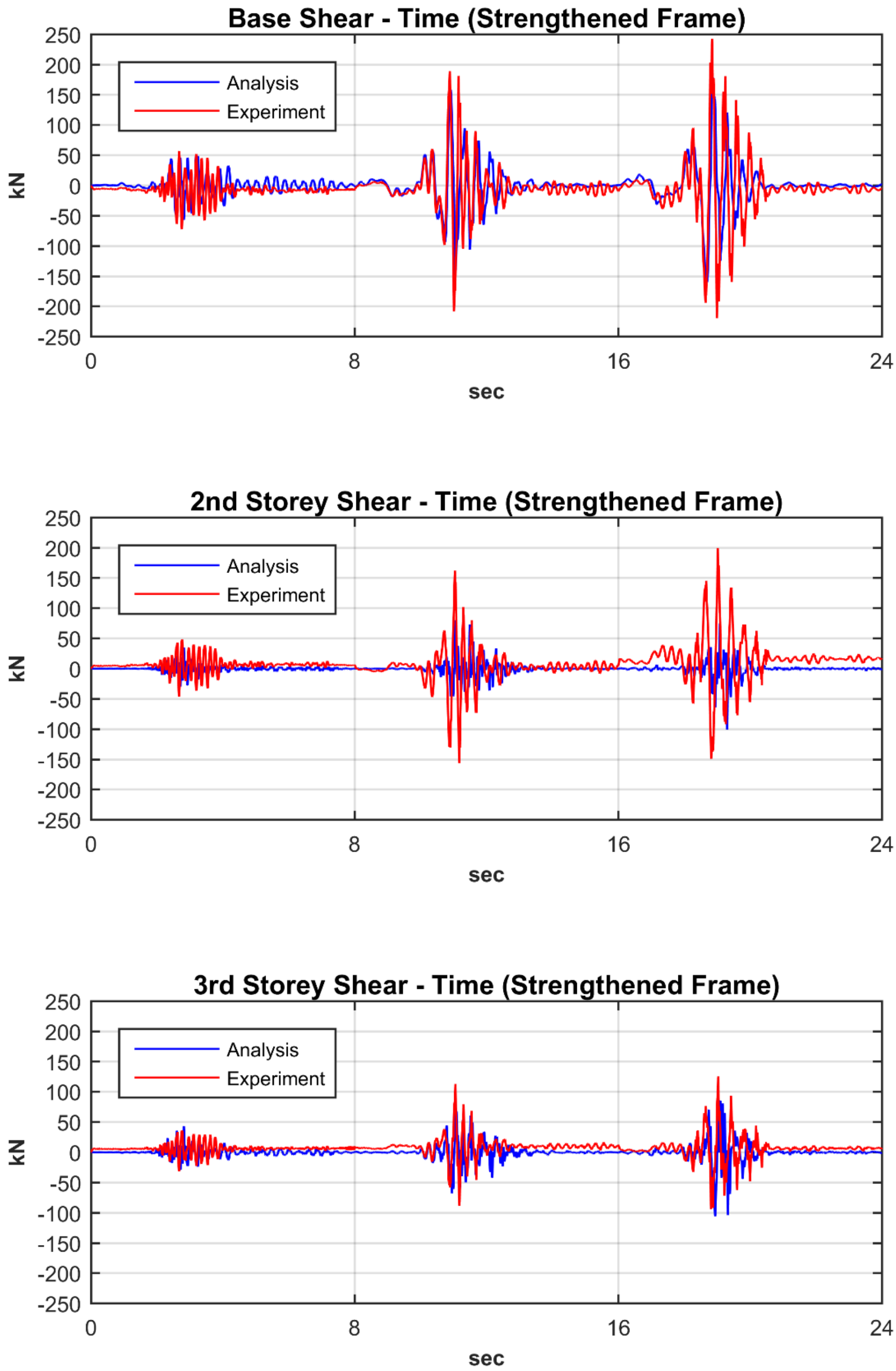


Figure 5.23 Story shear force time history comparisons (strengthened frame)

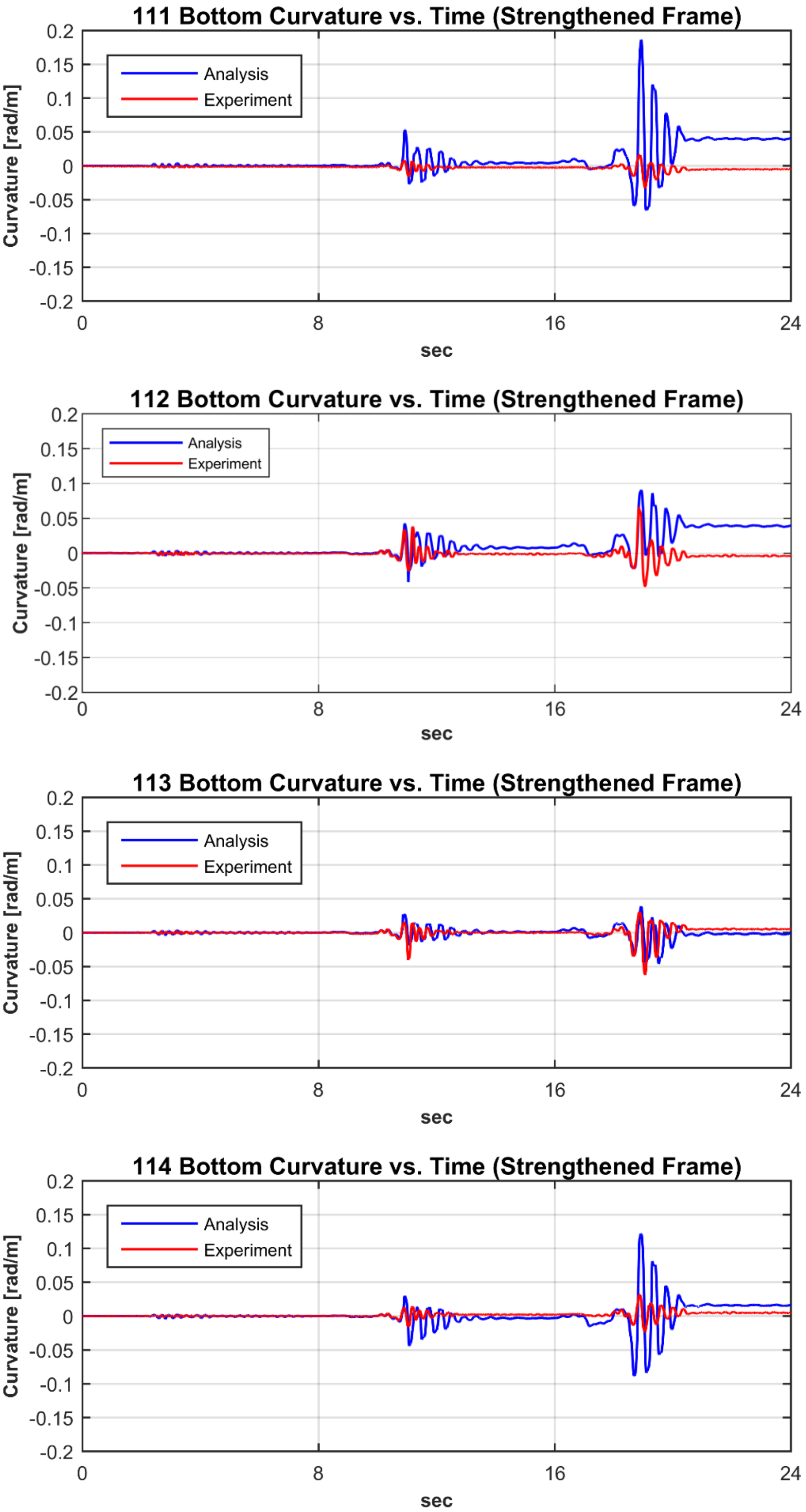


Figure 5.24 Bottom end curvatures of 1st story columns (strengthened frame)

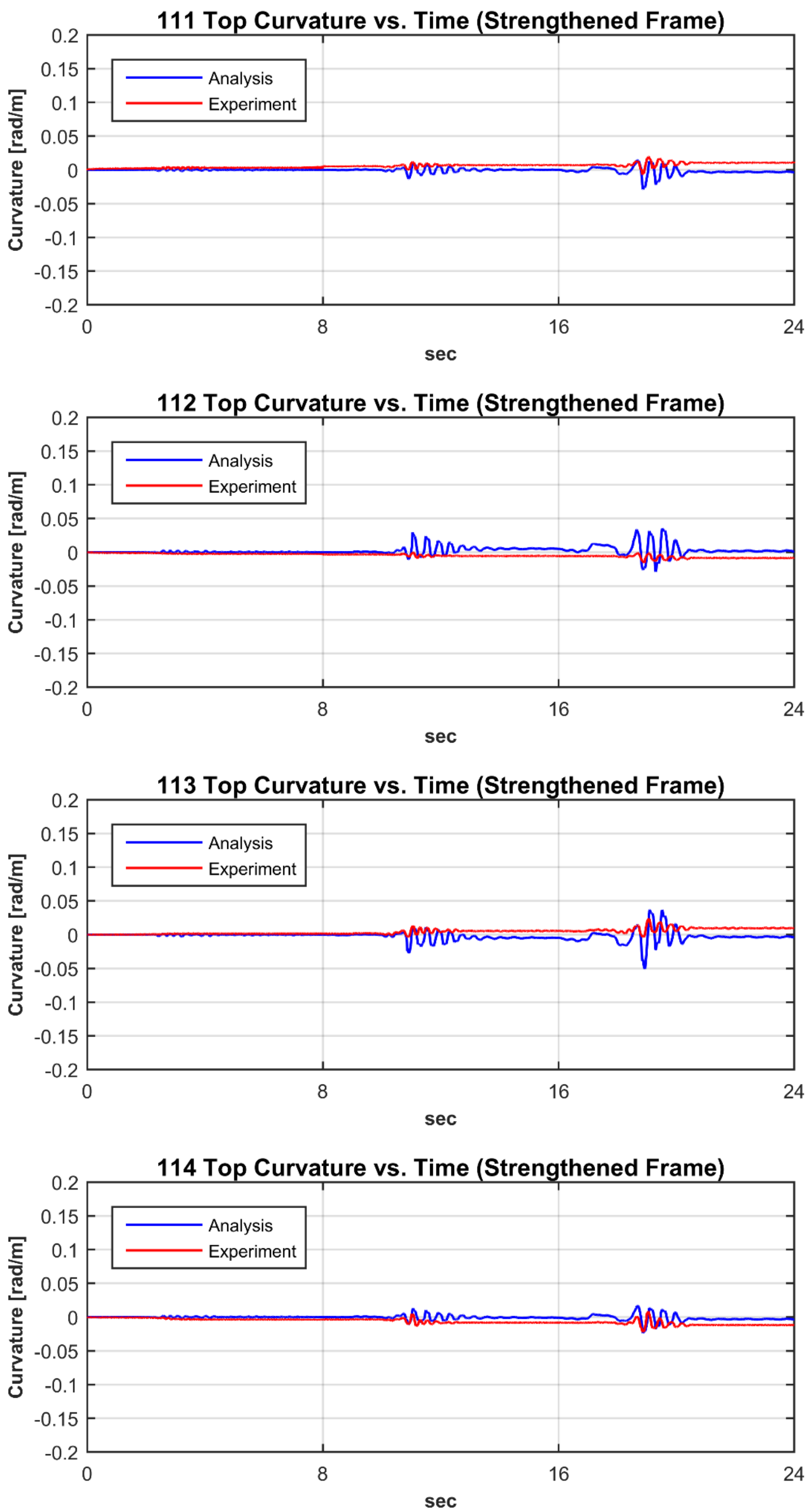


Figure 5.25 Top end curvatures of 1st story columns (strengthened frame)

### 5.4 Performance evaluation of test frames

Strain – based damage state limits given in TEC 2007 and the rotation-based performance limits given in ASCE/SEI 41-06 were used for the evaluation of the performance levels of columns. Pseudo – dynamic test results and Opensees analysis results were explored by utilizing the first and second story column strains and rotation values.

TEC 2007 characterizes three damage state limits for performance evaluations, which are Minimum Damage (MD), Safety Limit (SL), and Collapse Limit (CL), for ductile members. The strain limits of TEC 2007 are given in Table 5.21 for longitudinal reinforcement and concrete in compression. The volume of existing confining steel to volume of required confining steel ratio ($\rho_s/\rho_{sm}$) was calculated as 0.33 due to deficient type column design. Therefore, strain limits were determined as 0.0035, 0.0068 and 0.0086 (Table 5.20).

Table 5.20 TEC 2007 damage state limits

| | Strain Limits | | |
|---|---|---|---|
| | MD | SL | CL |
| Longitudinal Reinforcement | 0.010 | 0.040 | 0.060 |
| Concrete (Compression) | 0.0035 | $0.0035+0.01(\rho_s/\rho_{sm})$ =0.0068 | $0.004+0.014(\rho_s/\rho s_m)$ =0.0086 |

Three performance limits are identified for ductile members according to ASCE/SEI 41-06. These are Immediate Occupancy (IO), Life Safety (LS), and Collapse Prevention (CP). Plastic rotation limits for the columns are linearly interpolated from the axial load and shear reinforcement factor limits in ASCE/SEI 41-06's Table 6-8. Classification Criteria for columns were taken *condition ii* because of reinforcement deficiency of closed hoops with 90$^o$ hooks and plastic shear capacity of the column, and shear demand at flexural yielding of the plastic hinges. Plastic rotation limits were calculated for inner and outer columns for each specimen. Performance limits are summarized in Table 5.21.

Table 5.21 ASCE column damage state limits

| **Bare Frame** | **Plastic Rotation Limits [rad]** | | |
|---|---|---|---|
| | IO | LS | CP |
| Inner | 0.0041 | 0.0087 | 0.0134 |
| Outer | 0.0046 | 0.0094 | 0.0143 |
| **Infilled Frame** | Plastic Rotation Limits [rad] | | |
| | IO | LS | CP |
| Inner | 0.0033 | 0.0077 | 0.0122 |
| Outer | 0.0065 | 0.0129 | 0.0194 |
| **Strengtehend Frame** | Plastic Rotation Limits [rad] | | |
| | IO | LS | CP |
| Inner | 0.0037 | 0.0082 | 0.0128 |
| Outer | 0.0067 | 0.0135 | 0.0202 |

Limits taken from TEC (2007) and ASCE/SEI 41-06 were used to assess the experimental results and analysis results for each specimen. Figure 5.26 associates the relation between the standards as damage regions. The damage regions are Minimum Damage (MD), Significant Damage (SD), Heavy Damage (HD), Collapse (CP)

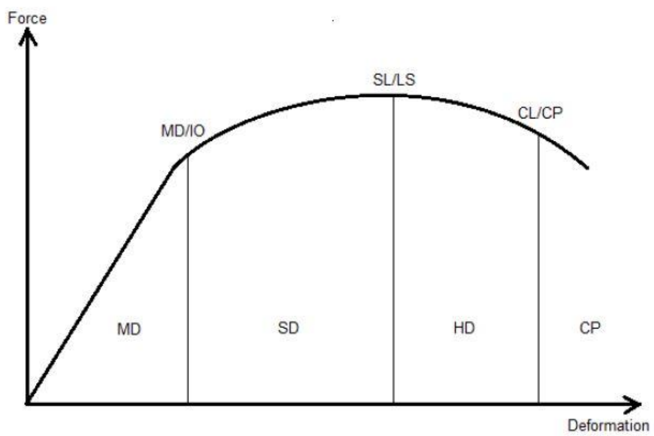


Figure 5.26 Damage/performance limits and performance levels

### 5.4.1 Performance evaluation of bare frame

The D1 ground motion caused minimum damage on columns based on both experimental and analytical results. Consequently, the damage results related to the D1 ground motion are not presented. Experiment and analysis results were given in the same figure for bare, infilled and strengthened specimens.

Performance evaluations of the bare frame columns are represented in Figure 5.27 according to TEC (2007) damage levels. Damages concentrated at the bottom ends of the first story columns during the D2 ground motion. Extensive damage indicates the inelastic deformation of columns during the D3 ground motion. Comparable results were obtained for the bare frame model. Most of the columns reached collapse limit during the D3 ground motion for bare frame model. The D3 ground motion forced the system to collapse. Strain limits passed the collapse prevention limits.

There was no significant damage according to ASCE/SEI 41-06 during the D3 ground motion for the experiment (Figure 5.28). However, in the bare frame model, similar to TEC, high damage (HD) zones were observed at the bottom of the first story columns according to ASCE evaluation. As mentioned before, large flexural cracks in the column and beam ends, and shear cracking in the joint regions were observed during the experiment. Moreover, inter story drift ratios and large residual story level displacements indicated that the system was in a state of collapse.

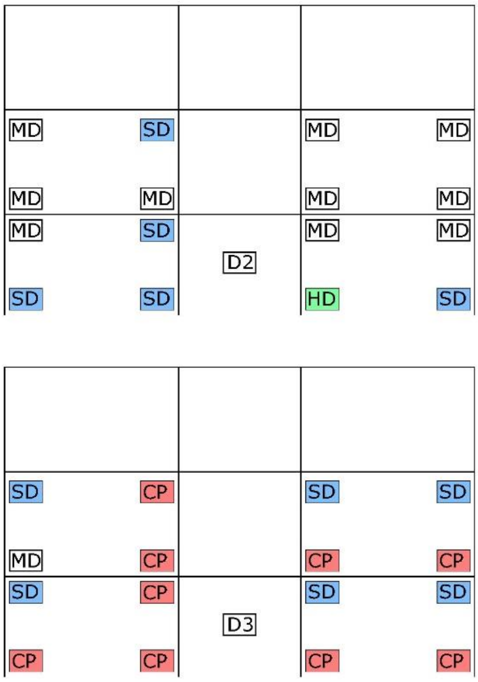


Experiment

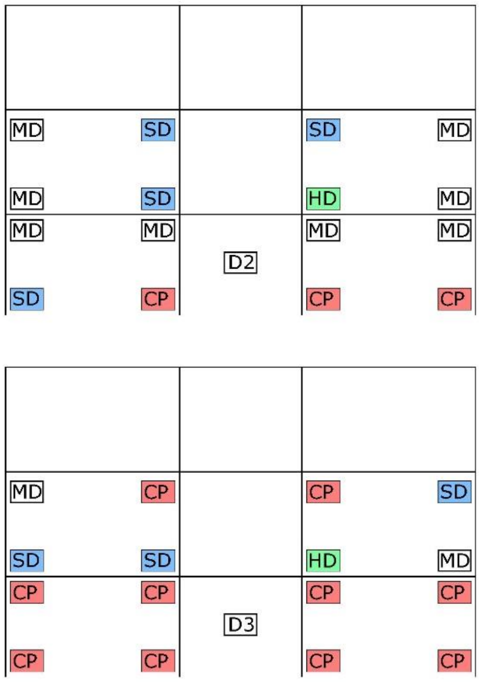


Analysis

First story interior column bottom end

First story exterior column bottom end

First story exterior column

Exterior columns

Figure 5.27 Damage levels of bare frame w.r.t. TEC and observed damages

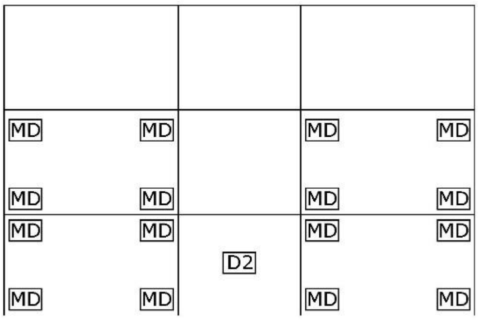


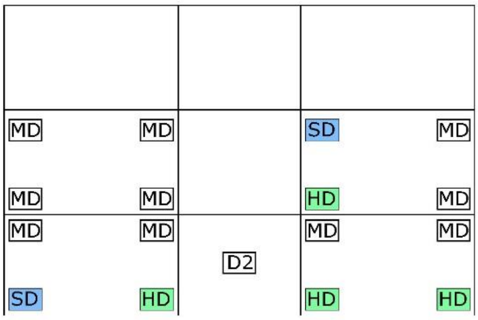


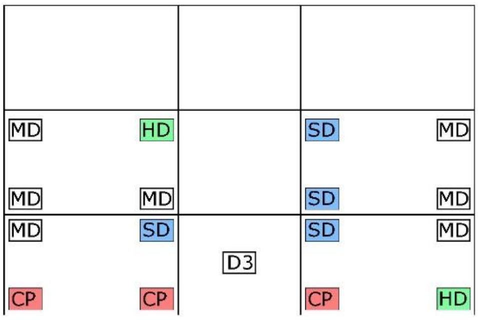


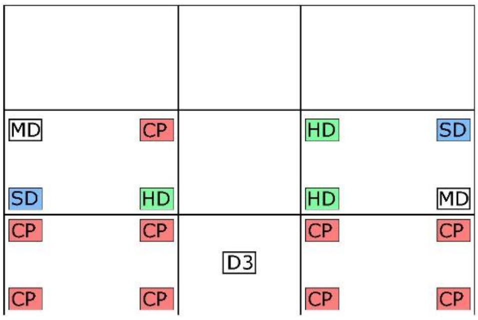


Experiment

Analysis

First story interior column bottom end

Second story exterior column top end

First story exterior column bottom end

Interior columns

Figure 5.28 Damage levels of bare frame w.r.t. ASCE and observed damages

### 5.4.2 Performance evaluation of infilled frame

The presence of the infill wall reduced the damage levels during D2 ground motion (Figure 5.29). There were three significant damage regions observed with respect to TEC (2007). The infilled frame model predicted more significant damage points for the first story column ends. The OpenSees model is composed of flexural type of structural elements. The additional truss elements to model infill walls reduced element end rotations in the analysis; however, they could not capture the real behavior as infill walls actually restrict the whole column deformation. During the D2 earthquake testing of the infilled specimen, diagonal cracks formed first in walls which inclined towards column ends.

Diagonal cracks in first story infill wall penetrated later into the column ends and the D3 earthquake caused these cracks to reach a severe and significant level. Performance evaluation according to TEC (2007) illustrated this situation with collapse and high damage regions at the top end of the neighbor columns to infill wall for the first story (Figure 5.29). Time history analysis of the infilled frame gave convenient results related to strain based performance assessment.

All damage levels at column ends remained in the minimum damage region according to ASCE/SEI 41-06 during D2 ground motion for the infilled frame specimen (Figure 5.30). However, ASCE/SEI 41-06 performance evaluation assessed many significant damage regions in addition to high damage points for the infilled frame model.

Damages were due to shear cracks at infilled frame during the D3 ground motion. However, rotation based performance evaluation of the infilled frame experiment could not give accurate determination for shear type failures. Infilled frame model column end rotations were greater than experiment results. Consequently, most of the column end plastic rotations passed the collapse prevention limit except one exterior column end for the infilled frame model (Figure 5.30).

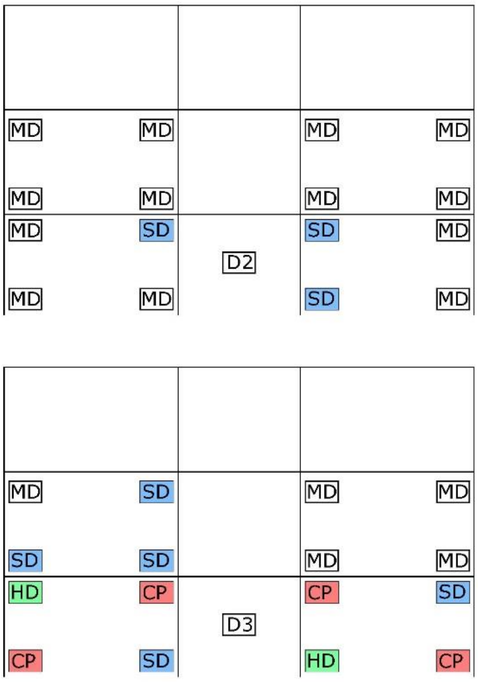


Experiment

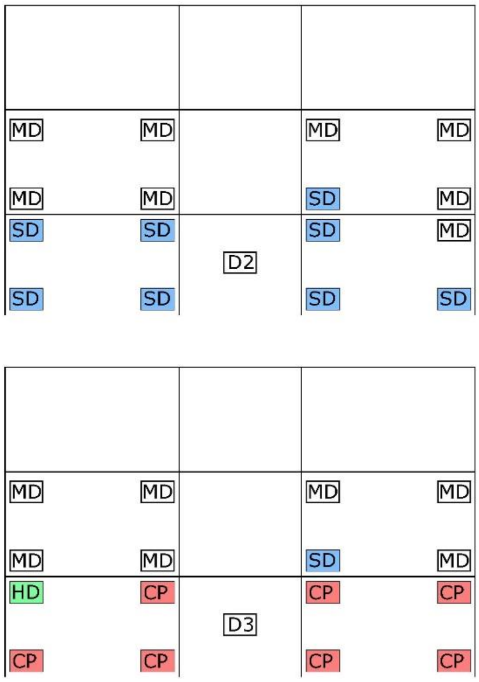


Analysis

First story interior column top end

First story interior column top end

First story exterior column bottom end

First story exterior column top end

Figure 5.29 Damage levels of infilled frame w.r.t. TEC and observed damages

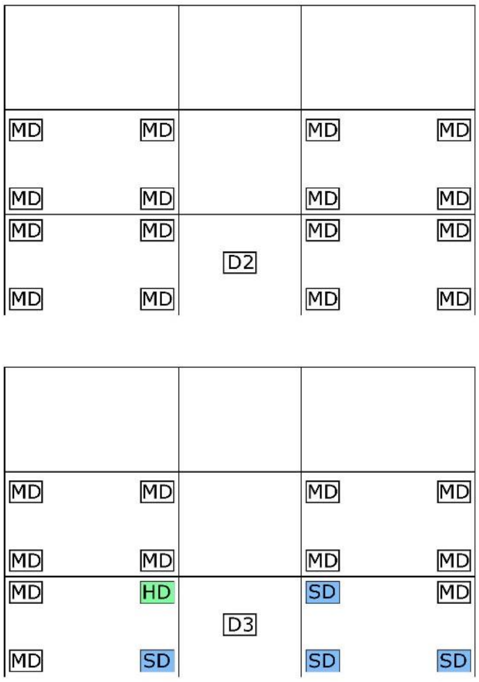


Experiment

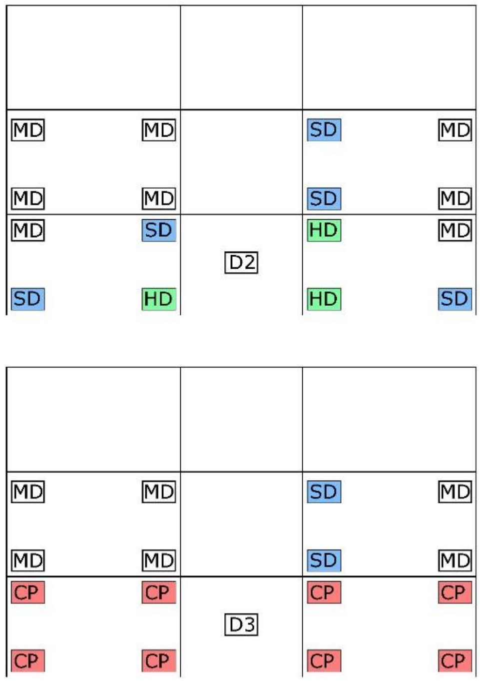


Analysis

First story interior column top end

First story exterior column bottom end

First story interior column top end

Interior columns

Figure 5.30 Damage levels of infilled frame w.r.t. ASCE and observed damages

### 5.4.3 Performance evaluation of strengthened frame

Experimental observations showed that implementing ECC panels on infill walls minimized the damage on the structural elements. Flexural damages were recognized on the columns. Tensile stresses on ECC panels caused loss of integration between panels and neighboring first story columns during D2 ground motion. Performance evaluation of column w.r.t TEC (2007) presents this situation in Figure 5.31. Most of columns remained in the minimum damage state except the bottom ends of second story middle columns during the D2 ground motion. The analytical model of the strengthened frame represented a similar behavior with experiment. The D3 ground motion caused dilation of flexural cracks at the bottom end of the inner columns and spreading corner disintegration at the first story ECC panels.

Strain levels of the strengthened frame model were higher than the experimental values; as a result significant damage existed especially at the bottom ends of first story columns with respect to performance evaluation of TEC (2007) (Figure 5.31)

ASCE/SEI 41-06 assessments showed that all columns stayed in minimum damage condition during the D2 ground motion for the strengthened frame specimen (Figure 5.32). Two significant damage points at the bottom end of the first story interior columns indicate the disintegration of the panels.

Additional truss application in the strengthened frame model reduced the damages states according to ASCE/SEI 41-06. The rotation levels of the model column elements were higher than the experiment values. As a result more significant and high damage state points were obtained for the strengthened frame model (Figure 5.32).

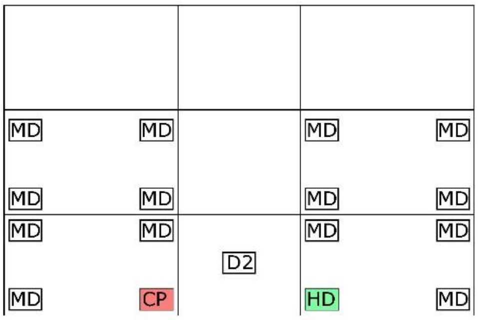


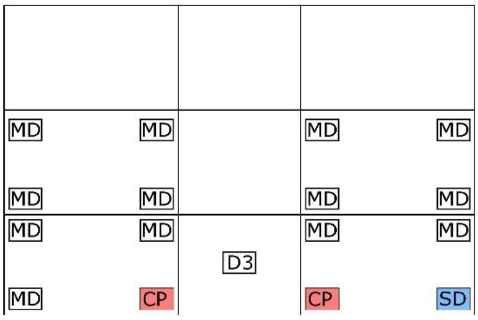


Experiment

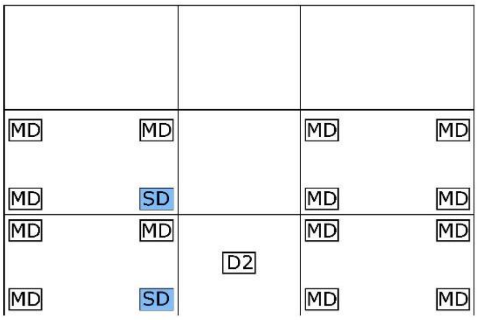


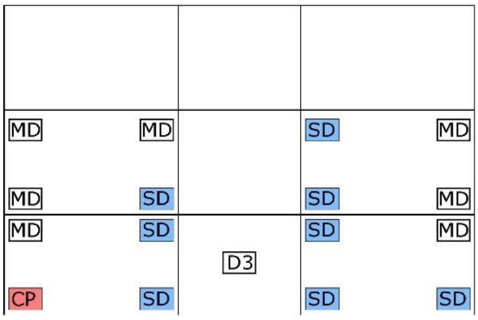


Analysis

First story interior column bottom end

First story interior column bottom end

First story exterior column top end

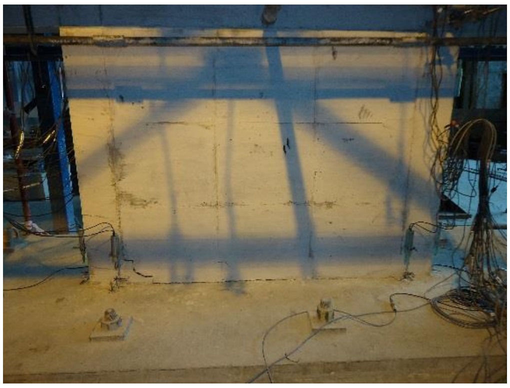

First story interior columns

Figure 5.31 Damage levels of strengthened frame w.r.t. TEC and observed damages

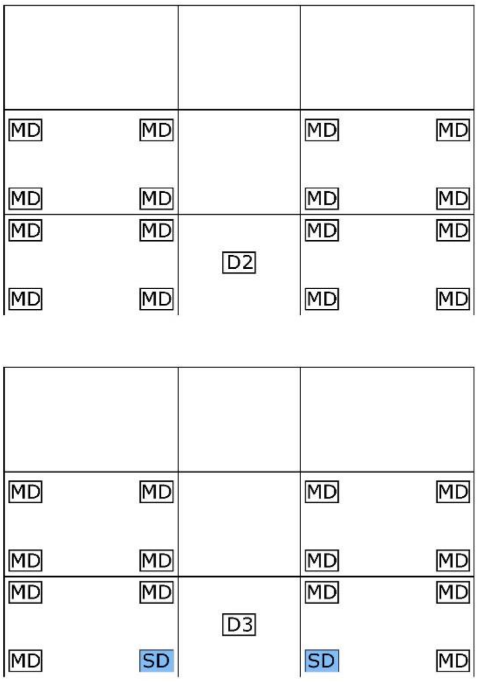


Experiment

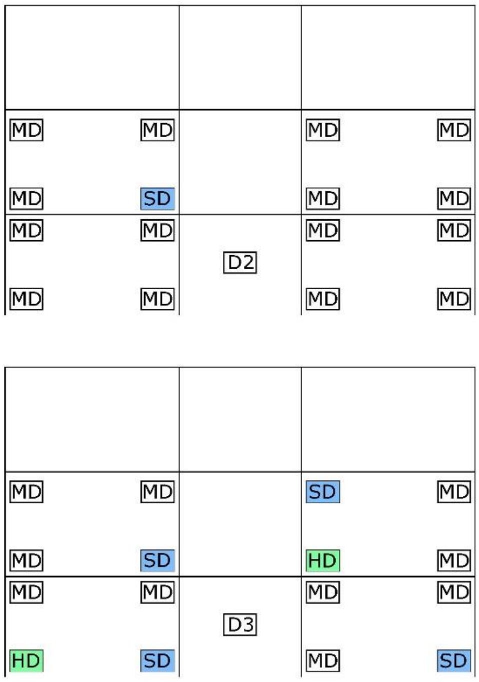


Analysis

First story interior column bottom end

First story interior column bottom end

First story exterior column top end

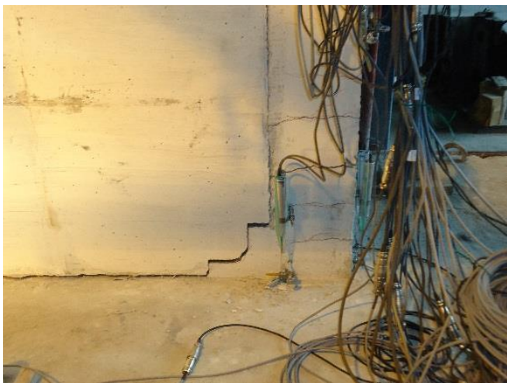

First story interior column bottom end

Figure 5.32 Damage levels of strengthened frame w.r.t. ASCE and observed damages

# CHAPTER 6

# CONCLUSIONS

## 6.1 Summary

The aim of this study was to strengthen the masonry infill walls in RC structures by means of Engineered Cementitious Composite (ECC) panels. Within the scope of this study, Pseudo-dynamic tests were performed on half scale, three-story, three-bay deficient RC frames. Deficiencies were inadequate steel reinforcement, low material strength and plain bar usage. The test series consisted of three specimens namely a bare frame, an infilled frame, and a strengthened frame. Continuous pseudo-dynamic testing was employed for all specimens using synthetic ground motions compatible with the site-specific earthquake spectra developed for the city center of Düzce. Three synthetic ground motions were generated to represent earthquakes with an exceedance probability of 50% in 50 years for local site class Z1/rock (D1), 10% in 50 years for Z1/rock (D2), and 10% in 50 years for Z3/soft soil (D3). Nonlinear time history analyses were performed in the OpenSees platform. Test results and analytical modeling results have been presented in this thesis. Additionally, performance evaluation was conducted on the first and second story columns of the specimens with respect to TEC (2007) and ASCE/SEI 41-06. The effect of masonry infill walls on deficient frame behavior and the effectiveness of the application of ECC panels as a strengthening method were reviewed.

## 6.2 Conclusions

- Comparison of the bare and infilled frame tests indicated that hollow clay tile infill increases the strength and stiffness of the frame substantially. The presence of an infill wall increased the base shear capacity of the frame while restricting the story displacements. However, infill walls transfer shear forces to the adjacent columns due to diagonal compression strut action. Consequently, infill walls cause shear damage on column ends during earthquake excitation. The effect of infill walls should be taken into account at the design stage to prevent brittle type failure modes of structural elements.

- In the course of the main project, a new effective and economical strengthening technique was developed which will minimize disturbance of the occupants of a building. For this purpose, Engineered Cementitious Composite (ECC) panels were produced in reasonable size and weight, which make their application simple and feasible. ECC panels behave in a ductile manner due to their composition, physical properties and high compressive strength.

- The proposed strengthening technique improved the lateral strength, base shear, and energy dissipation capacity of the frame substantially while limiting inter-story drift ratios. Additionally, ECC panel application reduced damage levels.

- With the application of ECC panels on fill walls, the shear type of failure of columns due to diagonal strut action of infill walls was transformed to uniform flexural cracks along columns. Moreover, no damage was monitored on the infill wall and ECC panels during testing.

- In the infilled frame test, bricks broke and fell during D3 ground motion. Despite that, ECC panel application on the infill wall strengthened the infill wall and kept the wall intact. In this way, damages and deaths due to wall fall-over can be avoided during earthquakes.

- The modeling of deficient frames is a demanding process due to nonlinear material behavior, and replacing 3-dimensional real members with 1-dimensional frame elements makes it difficult to get the real behavior especially at joints and to get the damage distribution in the structure. Despite this fact, the general behavior of the specimens was caught acceptably with nonlinear time history analysis in peak roof displacements, inter-story drift ratios, and base shear. Both infill walls and ECC panels were modeled separately with diagonal truss elements.

- The performance evaluation of infilled and strengthened frame columns shows that damage distribution of analysis was higher than observed in the experiment. Also, analysis evaluations gave more conservative results than experiments. Therefore, analysis can be employed to assess the performance of the structure.

- Strain-based damage state limits given in TEC 2007 and rotation-based performance limits given in ASCE/SEI 41-06 were used for the evaluation of the performance levels of columns. Pseudo-dynamic test results and Opensees analysis results were examined within this scope. Generally, TEC 2007 assessments were found to be more conservative than ASCE/SEI 41-06 performance evaluation results.

# REFERENCES


Aktan, H. M. (1986). Pseudo-dynamic testing of structures. Journal of engineering mechanics, 112(2), 183-197.

Altin, S., Ersoy, U., & Tamkut, T. (1992). Hysteretic response of reinforced-concrete infilled frames. Journal of Structural Engineering, 118(8), 2133-2150.

Altin, S., Anil, Ö., Kara, M. E., & Kaya, M. (2008). An experimental study on strengthening of masonry infilled RC frames using diagonal CFRP strips. Composites Part B: Engineering, 39(4), 680-693.

American Society of Civil Engineers (ASCE), 2000. Prestandard and Commentary for the Seismic Rehabilitation of Buildings, Report No. FEMA 356, Reston, VA.

American Society of Civil Engineers (ASCE), 2007. Seismic Rehabilitation of Existing Buildings, Report No. ASCE/SEI 41-06, Reston, VA, 428 pp.

Anil, Ö., & Altin, S. (2007). An experimental study on reinforced concrete partially infilled frames. Engineering Structures, 29(3), 449-460.

Aykaç, B., Özbek, E., Babayani, R., Baran, M., & Aykaç, S. (2017). Seismic strengthening of infill walls with perforated steel plates. Engineering Structures, 152, 168-179.

Bae, B., Park, B., Choi, H., & Choi, C. (2010). Performance enhancement effect of unreinforced masonry walls using sprayable ECC. Fracture Mechanics of Concrete and Concrete Structures, May 23-28, 1817-1823

Canbay, E., Ersoy, U., & Ozcebe, G. (2003). Contribution of reinforced concrete infills to seismic behavior of structural systems. ACI Structural Journal, 100(5), 637-643.

Canbay, E., Ersoy, U., & Tankut, T. (2004). A three component force transducer for reinforced concrete structural testing. Engineering Structures, 26(2), 257-265

Chang, S. Y. (2002). Explicit pseudodynamic algorithm with unconditional stability. Journal of Engineering Mechanics, 128(9), 935-947.

Code, A. C. I. (2005). Building Code Requirements For Structural Concrete And Commentary (ACI 318M-05). American Concrete Institute, Farmington Hill, Michigan.

Dehghani, A., Nateghi-Alahi, F., & Fischer, G. (2015). Engineered cementitious composites for strengthening masonry infilled reinforced concrete frames. Engineering Structures, 105, 197-208.

Fenerci, A., Binici, B., Ezzatfar, P., Canbay, E., & Ozcebe, G. (2016). The effect of infill walls on the seismic behavior of boundary columns in RC frames. Earthquakes and Structures, 10(3), 539-562.

Fiorato, A. E., Sozen, M. A., & Gamble, W. L. (1970). An investigation of the interaction of reinforced concrete frames with masonry filler walls. University of Illinois Engineering Experiment Station. College of Engineering. University of Illinois at Urbana-Champaign.

Fischer, G., & Li, V. C., 2003. Deformation Behavior of FRP Reinforced ECC Flexural Members under Reversed Cyclic Loading Conditioned. ACI Structural Journal, V. 100, No. 1, Jan.-Feb., pp. 25-35.

Govindan, P., Lakshmipathy, M., & Santhakumar, A. R. (1986, July). Ductility of lnfilled Frames. In Journal Proceedings (Vol. 83, No. 4, pp. 567-576).

Hashemi, S. A. (2007). Seismic evaluation of reinforced concrete buildings including effects of masonry infill walls. University of California, Berkeley.

Kadysiewski, S., & Mosalam, K. M. (2009). Modeling of unreinforced masonry infill walls considering in-plane and out-of-plane interaction (Vol. 70). Berkeley, CA: Pacific Earthquake Engineering Research Center.

Kakaletsis, D. J., & Karayannis, C. G. (2008). Influence of masonry strength and openings on infilled R/C frames under cycling loading. Journal of Earthquake Engineering, 12(2), 197-221.

Kanda, T., & Li, V. C. (1998). Interface property and apparent strength of high-strength hydrophilic fiber in cement matrix. Journal of materials in civil engineering, 10(1), 5-13.

Karsan, I. D., & Jirsa, J. O. (1969). Behavior of concrete under compressive loadings. Journal of the Structural Division.

Kent, D. C., & Park, R. (1971). Flexural members with confined concrete. Journal of the Structural Division.

Keskin S. B. (2014). Dimensional Stability Of Engineered Cementitious Composites. Phd. Thesis. Middle East Technical University.

Kewalramani, M. A., Mohamed, O. A., & Syed, Z. I. (2017). Engineered cementitious composites for modern civil engineering structures in hot arid coastal climatic conditions. Procedia engineering, 180, 767-774.

Koutromanos, I., Kyriakides, M., Stavridis, A., Billington, S., & Shing, P. B. (2012). Shake-table tests of a 3-story masonry-infilled RC frame retrofitted with composite materials. Journal of Structural Engineering, 139(8), 1340-1351.

Kurt, E. G., Binici, B., Kurç, Ö., Canbay, E., & Özcebe, G. (2011). Seismic performance of a deficient reinforced concrete test frame with infill walls. Earthquake Spectra, 27(3), 817-834.

Kurt, E., Kurc, O., Binici, B., Canbay, E., & Ozcebe, G. (2011). Performance examination of two seismic strengthening procedures by pseudodynamic testing. Journal of Structural Engineering, 138(1), 31-41.

Kyriakides, M. A., & Billington, S. L. (2013). Cyclic response of nonductile reinforced concrete frames with unreinforced masonry infills retrofitted with engineered cementitious composites. Journal of Structural Engineering, 140(2), 04013046.

Li, B. (1989). Contact density model for stress transfer across cracks in concrete. Journal of the Faculty of Engineering, the University of Tokyo, (1), 9-52.

Li, V. C. (1993). From micromechanics to structural engineering-the design of cementitous composites for civil engineering applications.

Li, V. C. (2003). On engineered cementitious composites (ECC). Journal of advanced concrete technology, 1(3), 215-230.

Li, V. C. (2008). Engineered cementitious composites (ECC) material, structural, and durability performance.

Li, V. C., Horii, H., Kabele, P., Kanda, T., & Lim, Y. M. (2000). Repair and retrofit with engineered cementitious composites. Engineering Fracture Mechanics, 65(2-3), 317-334.

Li, V. C., & Kanda, T. (1998). Innovations forum: engineered cementitious composites for structural applications. Journal of Materials in Civil Engineering, 10(2), 66-69.

Maalej, M., & Li, V. C. (1994). Flexural/tensile-strength ratio in engineered cementitious composites. Journal of Materials in Civil Engineering, 6(4), 513-528.

Maalej, M., Lin, V. W. J., Nguyen, M. P., & Quek, S. T. (2010). Engineered cementitious composites for effective strengthening of unreinforced masonry walls. Engineering Structures, 32(8), 2432-2439.

Madan, A., Reinhorn, A. M., Mander, J. B., & Valles, R. E. (1997). Modeling of masonry infill panels for structural analysis. Journal of structural engineering, 123(10), 1295-1302.

Mahin, S. A., & Shing, P. S. B. (1985). Pseudodynamic method for seismic testing. Journal of Structural Engineering, 111(7), 1482-1503.

Mahin, S. A., Shing, P. S. B., Thewalt, C. R., & Hanson, R. D. (1989). Pseudodynamic test method—Current status and future directions. Journal of Structural Engineering, 115(8), 2113-2128.

Marjani, F., & Ersoy, U. (2002). Behaviour of Brick Infilled R/C Frames under Reversed Cyclic Loading. In ECAS 2002 International Symposium on Structural and Earthquake Engineering, METU Publication.

Mehrabi, A. B., Benson Shing, P., Schuller, M. P., & Noland, J. L. (1996). Experimental evaluation of masonry-infilled RC frames. Journal of Structural engineering, 122(3), 228-237.

Misir, I. S., Ozcelik, O., Girgin, S. C., & Yucel, U. (2016). The behavior of infill walls in RC frames under combined bidirectional loading. Journal of Earthquake Engineering, 20(4), 559-586.

Molina, F. J., Verzeletti, G., Magonette, G., Buchet, P. H., & Geradin, M. (1999). Bi-directional pseudodynamic test of a full-size three-storey building. Earthquake Engineering & Structural Dynamics, 28(12), 1541-1566.

Nakashima, M. (1990). Integration techniques for substructure pseudo-dynamic test. In 4th US National Conference on Earthquake Engineering, 1990. 5.

Negro, P., & Verzeletti, G. (1996). Effect of infills on the global behaviour of R/C frames: energy considerations from pseudodynamic tests. Earthquake engineering & structural dynamics, 25(8), 753-773.

Ockleston, A. J. (1955). Load tests on a three storey reinforced concrete building in Johannesburg. The Structural Engineer, 33, 304-322.

Ozcelik, R., Binici, B., & Kurc, O. (2012). Pseudo dynamic testing of an RC frame retrofitted with chevron braces. Journal of Earthquake Engineering, 16(4), 515-539.

Peek, R., & Yi, W. H. (1990). Error analysis for pseudodynamic test method. I: Analysis. Journal of engineering mechanics, 116(7), 1618-1637.

Polyakov, S. V. (1956). Masonry in framed buildings. Gosudarstvennoe izdatel'stvo Literatury postroitel'stvu i arkhitekture.

Popovics, S. (1973). A numerical approach to the complete stress-strain curve of concrete. Cement and concrete research, 3(5), 583-599.

Read, J. B. (1965). Testing to destruction of full-size portal frames. Cement and Concrete Association.

Rivero, C.E, Walker, W. H. (1982), "An analytical study of the interaction of frames and infill masonry walls", Civil Engineering Studies, SRS-502.

Saatcioglu, M., Mitchell, D., Tinawi, R., Gardner, N. J., Gillies, A. G., Ghobarah, A., ... & Lau, D. (2001). The August 17, 1999, Kocaeli (Turkey) earthquake damage to structures. Canadian Journal of Civil Engineering, 28(4), 715-737.

Şahmaran, M., Bilici, Z., Ozbay, E., Erdem, T. K., Yucel, H. E., & Lachemi, M. (2013). Improving the workability and rheological properties of Engineered Cementitious Composites using factorial experimental design. Composites Part B: Engineering, 45(1), 356-368.

Scott, M. H., & Fenves, G. L. (2009). Krylov subspace accelerated Newton algorithm: application to dynamic progressive collapse simulation of frames. Journal of Structural Engineering, 136(5), 473-480.

Sevil, T., Baran, M., Bilir, T., & Canbay, E. (2011). Use of steel fiber reinforced mortar for seismic strengthening. Construction and Building Materials, 25(2), 892-899.

Shing, P. B., Nakashima, M., & Bursi, O. S. (1996). Application of pseudodynamic test method to structural research. Earthquake spectra, 12(1), 29-56.

Smith, B. S. (1962). Lateral stiffness of infilled frames. Journal of the Structural Division, 88(6), 183-226.

Sucuoğlu, H., & Siddiqui, U. A. (2014). Pseudo-dynamic testing and analytical modeling of AAC infilled RC frames. Journal of Earthquake Engineering, 18(8), 1281-1301.

Suryanto, B. (2009). Mechanics of high performance fiber reinforced cementitious composite (HPFRCC) under principal stress rotation (Doctoral dissertation, Thesis (PhD), University of Tokyo).

Suryanto, B., Nagai, K., & Maekawa, K. (2010). Modeling and analysis of shear-critical ECC members with anisotropic stress and strain fields. Journal of Advanced Concrete Technology, 8(2), 239-258.

Takanashi, K., Udagawa, K., Seki, M., Okada, T., & Tanaka, H. (1975). Nonlinear earthquake response analysis of structures by a computer-actuator on-line system. Bulletin of Earthquake Resistant Structure Research Center, 8, 1-17.

Turkish Earthquake Code (2007). Specifications for structures to be built in seismic areas. Ministry of Public Works and Settlement, Ankara, Turkey.

Žarnić, R., & Tomaževič, M. (1985). Study of the behaviour of masonry infilled reinforced concrete frames subjected to seismic loading.

Zhou, J., Qian, S., Ye, G., Copuroglu, O., van Breugel, K., & Li, V. C. (2012). Improved fiber distribution and mechanical properties of engineered cementitious composites by adjusting the mixing sequence. Cement and Concrete Composites, 34(3), 342-348.

# CURRICULUM VITAE

Surname, Name: Ayatar, Mehmet Engin

Nationality: Turkish (TC)

Date and Place of Birth: 23 June 1982, Ankara

Marital Status: Married

Phone: +90 555 452 88 44

email: meayatar@gmail.com

## EDUCATION

| Degree | Institution | Year of Graduation |
|---|---|---|
| MS | İTU, Civil Engineering | 2009 |
| BS | METU, Civil Engineering | 2006 |
| High School | Sincan Süleyman Demirel Anadolu Lisesi, Ankara | 2000 |

## WORK EXPERIENCE

| Year | Place | Enrollment |
|---|---|---|
| 2012-Present | İller Bankası A.Ş. | Technical Expert |
| 2010-2012 | METU | Project Engineer |
| 2009-2010 | Atılım University | Research Asistant |
| 2008-2009 | PROTEK Project | Civil Engineer |
| 2007-2008 | Kayı Construction | Civil Engineer |

## FOREIGN LANGUAGES

Fluent English

## PUBLICATIONS

M. B. Mutlu, M.E. Ayatar, B. Binici, O. Kurç, E. Canbay, H. Sucuoglu, G. Ozcebe (2011). “Üç Katlı Betonarme Bir Çerçevenin Dinamik Benzeri Deneyleri ve Sayısal Simülasyonları”. 1. Türkiye Deprem Mühendisliği ve Sismoloji Konferansı ODTÜ – ANKARA

M.E. Ayatar, E. Canbay, B. Binici (2015). “Yapıların Çimento Esaslı Kompozit Panellerle Güçlendirilmesi”. 3. Türkiye Deprem Mühendisliği ve Sismoloji Konferansı, 14-16 Ekim 2015 – DEÜ – İZMİR